arXiv:1512.04027v1 [quant-ph] 13 Dec 2015

REVIEW ARTICLE

Quantum systems under frequency modulation

M P Silveri[1,2], J A Tuorila[1], E V Thuneberg[1], G S Paraoanu[3]

[1]Department of Physics, University of Oulu, P.O. Box 3000, FI-90014, Finland
[2]Department of Physics, Yale University, New Haven, Connecticut 06520, USA
[3]Department of Applied Physics, Aalto University School of Science, Aalto University, P.O. Box 15100, FI-00076 AALTO, Finland

December 15, 2015

Abstract. We review the physical phenomena that arise when quantum mechanical energy levels are modulated in time. The dynamics resulting from changes in the transition frequency is a problem studied since the early days on quantum mechanics. It has been of constant interest both experimentally and theoretically since, with the simple two-level model providing an inexhaustible source of novel concepts. When the transition frequency of a quantum system is modulated, several effects appear: transitions to higher levels by Landau-Zener-Stückelberg-Majorana interference, motional averaging and narrowing and the formation of dressed states with the appearance of sidebands in the spectrum. Adiabatic changes result in the accumulation of geometric phases, which can be used to create topological states. In recent years, an exquisite experimental control in time domain over the parameters entering the Hamiltonian, and high-fidelity readout schemes allowed the state of the system to be monitored nondestructively. These developments happened in the field of quantum devices, especially superconducting qubits, as a well as in atomic physics, in particular in ultracold gases, and as a result of these advances, it became possible to demonstrate these fundamental effects. The purpose of this review is to present some of these developments: from examples on two-level atoms and harmonic oscillators to multilevel and many-particle systems.

PACS numbers: PACS

Keywords: min three and max seven keywords

Contents

1 Introduction **3**

2 Background **5**
2.1 Time-dependent Hamiltonian 5
2.2 Perturbation theory in the interaction picture 7

3 Two state system **9**
3.1 Probe spectrum 10
3.2 Coherent modulation 11
3.2.1 Static coupling and Floquet approach 14
3.2.2 Dynamic Stark effect and basis dependence of RWA 19
3.2.3 Steady state population 20
3.3 Discretized periodic time-evolution 21
3.3.1 Landau-Zener transition probability 23
3.3.2 Validity of the LZ-formula 25
3.3.3 Sudden approximation 25
3.3.4 Multi-level Landau-Zener 26
3.3.5 Dynamic and geometric phases via control of detuning 26
3.4 Incoherent modulation 27
3.4.1 Generating function 28
3.4.2 Gaussian modulation 29
3.4.3 Increasing the dephasing time of qubits by motional narrowing . . 30
3.4.4 Random telegraph noise and motional effects 32

4 Harmonic oscillator **34**
4.1 Squeezing by sudden frequency modulations 35
4.2 Dephasing by stochastic frequency changes 38

5 Coupled systems **39**
5.1 Modulated Jaynes-Cummings Hamiltonian 39
5.1.1 Spectrum of the Jaynes-Cummings Hamiltonian 40
5.1.2 Modulation of the atom frequency 41
5.1.3 Modulation of the cavity frequency 42
5.1.4 The simulated ultrastrong coupling by frequency modulation . . . 44
5.2 Modulated radiation pressure Hamiltonian 44

6 Many-body systems **46**
6.1 Motional averaging with hot atomic gases 46
6.2 Three-level systems 47
6.3 Topological transitions 48
6.4 Cold atomic gases 52

7 Conclusions **54**

1. Introduction

The year 1932 can be perhaps considered as the year of birth of the two-level model: almost simultaneously, Lev Landau [1, 2], Clarence Zener [3], Ernst Stückelberg [4], and Ettore Majorana [5], solved the problem of the transition rate between the energy levels of a spin-1/2 particle under a nondiabatic sweep across the avoided level crossing. It was already then realized that a phase difference between the two levels will appear at the end of this process, and if the passage is reversed then the resulting occupation probability will be an oscillatory function. This phase is typically referred to as the Stückelberg phase. The corresponding population oscillations are conceptually similar to the interference pattern in a Mach-Zehnder interferometer, with the two states playing the role of the interferometer paths travelled by the photons. In many natural phenomena, the basic physics can indeed be described by a two-level model. For example in atomic collisions, the incoming atoms in the ground state make transitions to a higher excited states as they approach each other. In inelastic scattering processes, Stückelberg interference has been seen already since the 1960's in several experiments as oscillations in the atomic collisional crosssection as a function of the scattering angle [6].

In a parallel theoretical development, the issue of what happens when a system is subjected to noise that shifts its energy levels became a paradigmatic problem in the theory of dephasing. Several theoretical approaches can be followed, depending on the structure of the noise power spectrum. For a two-level system, the so-called spin-boson model consists of a qubit coupled to a bath of harmonic oscillators, with an interaction Hamiltonian of the type $\sum_j \sigma_z(a_j + a_j^\dagger)$, where σ_z is the Pauli matrix of the qubit and a_j and $a_j^\dagger$ are the annihilation and creation operators for the j'th harmonic oscillator. The bath is assumed in equilibrium at a certain temperature, and thus thermal fluctuations in the position of the harmonic oscillators will produce dephasing in the off-diagonal matrix elements.

Equally important, the driving of a two-level system via σ_x or σ_y coupling is a topic that bears similarities to frequency modulation. The excitation of a quantum system by an oscillating magnetic field was observed for the first time in 1939 in the experiments of Isidor Rabi with molecular beams aiming at measuring nuclear magnetic moments [7]. When this type of driving is resonant, the population oscillates between the ground state and the first excited state with a frequency (called Rabi frequency) which is determined by the effective coupling between the system and the field. This result was already obtained in a general form in the paper by Majorana [5] as well as in the early theoretical works by Rabi [8]. In a further development, stimulated by the need to understand the geometric mapping of quantum states introduced by Majorana [9], Felix Bloch wrote the standard Bloch equations used widely in NMR and introduced the sphere representation for spin 1/2 [10].

It is only a recent experimental achievement that the two-level physics was realized

in single quantum systems, with well-characterized qubits and full control of external parameters. An important precusor to modern experiments has been the observation in the early 90's of Stückelberg interference with thermal Rydberg atoms driven by short microwave pulses [11]. For example in experiments on mesoscopic systems, it became possible to drive the Landau-Zener transitions and at the same monitor the time evolution of its quantum state. It is also possible to create artificial noise and input it in the system, thus realizing the situation of fluctuating energy levels and study its behavior under various types of noise.

Certainly a major driving force for these has been the possibility of using two-level systems as elements of quantum computers or quantum simulators. Improvements in gate and measurement fidelities as well as increasing the coherence times are essential if this goal were to be achieved. Naturally, since a quantum processor consists of many qubits, this raises the question of the role of dephasing in a many-body system. Several experimental inroads have been made here; this direction has just opened, and more will be done in the following years.

This review aims at presenting the phenomena that arise when the quantum mechanical energy levels are modulated in prototype one- and many-body systems. We do not aim to give a comprehensive review of the Landau - Zener - Stückelberg - Majorana interference, spin-boson model or tunneling, for which authoritative reviews already exist, see *e.g.* [12–14], but we will introduce some of the key results in such a way that our presentation is self-consistent. In this sense, our review complements the standard results with relatively recent developments, especially triggered by advances in experiment. Sometimes this brings a fresh view on classical results as well. For example, let us look at a spin-1/2 system under frequency modulation. By simply changing the basis through a $\pi/2$ rotation around the y-axis the frequency modulation will transform into a Rabi-type drive, with coupling to the σ_x operator. Although extremely simple, this connection has only recently been studied systematically [15] and observed experimentally using a nitrogen-vacancy spin in diamond [16]. Another example is the strongly nonadiabatic regime of frequency modulation, where the Landau-Zener transition formula is no longer valid [17–19]. In this case, even for sudden modulations, Stückelberg interference appears but the formalism for calculating the interference maxima and minima has to be modified accordingly [20].

The paper is organized as follows. We start in section 2 with a brief introductory material on the perturbation theory in the interaction picture. This allows us to derive rather general expressions for the transition probability under a perturbation that shifts the energy levels of a multilevel system, and to calculate the corresponding transition rates. Then we continue toward analyzing specific quantum systems and we discuss the corresponding experimental realizations. First in section 3 we review modulation effects in two-level systems: we consider coherent and incoherent modulations and introduce the concepts of sidebands, dynamical localization, Landau-Zener-Stückelberg interference, dephasing, and effects of motional narrowing and averaging. We also discuss the experimental observation of the Berry phase in a superconducting circuit. In section

4, we move to the harmonic oscillator. We consider here the creation of squeezed states by parametric modulation and continue discussion on dephasing effects due to random variations in the frequency. In section 5 we move on to discussing the effects in coupled systems: the paradigmatic model for such a system is the qubit-resonator system (Jaynes-Cummings model), where we show that a certain combination of modulations can be used to to create two-qubit gates, or bring the system into the ultrastrong coupling regime. Finally, section 6 deals with complex quantum systems: these includes non-harmonic multilevel artificial atoms, many-qubit systems with fixed or tunable couplings, as well as atomic systems. Several recent experiments demonstrate the fertility of ideas related to frequency modulation, which has enabled the simulation of topological transitions both with superconducting circuits and with ultracold gases, and the observation of the effects of motional averaging with thermal atoms as well as with a logical qubit relayed between several physical qubits. Section 7 summarizes the results and presents future prospects.

With a history as old as quantum mechanics itself, the problem of frequency modulation in quantum systems still remains an invaluable source of theoretical insights. The beautiful blend between theory and experimental techniques will likely continue to yield interesting results.

2. Background

2.1. Time-dependent Hamiltonian

We study quantum system where the Hamiltonian $\hat{H}(t)$ depends explicitly on time t. Due to the time-dependence, the instantaneous eigenbasis $\{|\psi_n(t)\rangle\}$ of the Hamiltonian consists of the so-called *adiabatic eigenstates*:

$$\hat{H}(t)|\psi_n(t)\rangle = E_n(t)|\psi_n(t)\rangle. \tag{1}$$

For simplicity, we assume here that the spectrum of the Hamiltonian is discrete and non-degenerate. In the adiabatic basis, the solution of the time-dependent Schrödinger equation can be written as the linear combination

$$|\Psi(t)\rangle = \sum_n c_n(t)|\psi_n(t)\rangle. \tag{2}$$

The key-point that separates time-dependent quantum systems from the time-independent ones is that the former can experience *transitions* between the energy eigenstates. By a transition, we mean the following. Assuming that the system starts from one of the eigenstates, i.e. $|\Psi(0)\rangle = |\psi_n(0)\rangle$, the transition probability from n to m is defined as

$$p_{n\to m}(t) = |c_m(t)|^2 = |\langle\psi_m(t)|\Psi(t)\rangle|^2 = |\langle\psi_m(t)|\hat{U}(t,0)|\psi_n(0)\rangle|^2, \tag{3}$$

where $\hat{U}(t,0)$ is the time-evolution operator. Thus, the transition probabilities can be found once the instantaneous eigenvalue problem for the Hamiltonian has been solved,

and the unitary time-evolution is known. For a time-independent system, the transition probabilities $p_{n\to m} = \delta_{nm}$ since the corresponding basis is formed by stationary states.

A typical problem in *quantum dynamics* is to find the transition probabilities $p_{n\to m}(t)$. When the time-evolution is slow, i.e. [21]

$$\left| \frac{\langle \psi_m(t)|\dot{\hat{H}}_1(t)|\psi_n(t)\rangle}{E_m(t) - E_n(t)} \right| \ll \frac{|E_m(t) - E_n(t)|}{\hbar}, \tag{4}$$

one can show that the system will follow the instantaneous eigenstate in time. This is called *adiabatic* time-evolution. Accordingly, the transitions are again suppressed and the system gathers only the phase

$$\phi_n(t) = i\int_0^t \left\langle \psi_m(\tau)|\dot{\psi}_m(\tau)\right\rangle d\tau = \frac{1}{\hbar}\int_0^t E_n(\tau)d\tau + \gamma_n(t), \tag{5}$$

where $t = 0$ defines the initial time of the problem. In the last form the phase is expressed as the sum of the dynamic phase and a geometric phase γ_n, which only depends on the travelled path [22].

If the adiabatic approximation (4) does not hold, the population can "leak out" from the initial state, resulting in general in $p_{n\to m}(t) \neq \delta_{nm}$. Based on Eq. (4), the strongest deviations from adiabaticity occur between such states n and m that are close in energy, i.e. $E_n(t) \approx E_m(t)$. Often, one can restrict the discussion of the dynamics to the subspace spanned by such two (nearly) degenerate states.

For a major part of this review we restrict to study systems that have a time-dependent Hamiltonian of the following form,

$$\hat{H} = \hat{H}_0 + \hat{H}_C + \hat{H}_P, \tag{6}$$

$$\hat{H}_0 = \hbar\sum_i [\omega_i + \xi_i(t)]|i\rangle\langle i|, \tag{7}$$

$$\hat{H}_C = \hbar\sum_{i,j} \Delta_{ij}|i\rangle\langle j|. \tag{8}$$

Here $|i\rangle$ is a set of orthonormal states with index $i = 1, 2, \ldots, N$. The first term $\hat{H}_0$ gives that their energies fluctuate $E_i(t) = \hbar[\omega_i + \xi_i(t)]$ because of time dependent classical modulation $\xi_i(t)$. The coupling term $\hat{H}_C$ describes possible static couplings between the states with constant coupling amplitudes Δ_{ij}. The probe term $\hat{H}_P$ describes the effect of a sinusoidal field that is used to study the properties of the Hamiltonian $\hat{H}_0 + \hat{H}_C$. The probe $\hat{H}_P$ is assumed to be a weak perturbation, but no such assumption is made concerning the modulation $\xi_i(t)$. For the probe we use

$$\hat{H}_P = \hbar g_P \cos(\omega t)\hat{V}, \tag{9}$$

where g_P and ω describe the strength and the angular frequency of the probe, and $\hat{V}$ is the hermitian operator that induces transitions between the states $|i\rangle$. Possible diagonal components in the probe do not cause transitions between the states, and can thus be safely included in $\hat{H}_0$. On top of the Hamiltonian (6), we sometimes assume a weak coupling to environment, which allows the system to relax.

2.2. Perturbation theory in the interaction picture

In this section we derive a formula [Eq. (18)] for the transition rate caused by the probe. Here we neglect the coupling term H_C (8). The case of a finite H_C will be addresses later in Sec. 3.2.1. The standard procedure to calculate the effect of a weak perturbation [23] is to write the Hamiltonian in the interaction picture, where the diagonal part is removed. This can be achieved with the time-dependent unitary transformation $\hat{H} \to \hat{U}^\dagger \hat{H} \hat{U} + i\hbar(\partial_t \hat{U}^\dagger)\hat{U}$, where

$$\hat{U}(t) = e^{-i\int_0^t \hat{H}_0(\tau)d\tau/\hbar} = e^{-i\sum_i [\omega_i t + \zeta_i(t)]|i\rangle\langle i|}. \tag{10}$$

Here $\zeta_i(t) \equiv \int_0^t \xi_i(\tau)d\tau$ is the dynamical phase accumulated due to the modulations. This modulation phase turns out to be very important quantity when one determines the probe response of the modulated transition.

After the transformation, the Hamiltonian of the probed and modulated quantum system is

$$\hat{H}(t) = \frac{\hbar g_P}{2}\hat{U}^\dagger(t)\left(e^{i\omega t} + e^{-i\omega t}\right)\hat{V}\hat{U}(t). \tag{11}$$

Now, if the probe is weak compared to the transition energies ($g_P \ll |\omega_i - \omega_j|$), we can solve the time-dependent Schrödinger equation using the first order perturbation theory for the time-evolution operator $\hat{U}(t,0)$. We obtain in the first-order in the perturbation parameter g_P:

$$\hat{U}(t,0) = 1 - \frac{i}{\hbar}\int_0^t \hat{H}(t')dt' + O(g_P^2). \tag{12}$$

Let us first consider transitions from state $|n\rangle$. We find the amplitude of the transition into state $|m\rangle$ ($m \neq n$) as

$$\gamma_{n\to m}(t) \equiv \langle m|\hat{U}(t,0)|n\rangle = -\frac{i}{\hbar}\int_0^t \langle m|\hat{H}(t')|n\rangle dt' + O(g_P^2). \tag{13}$$

Substituting in the expressions (10) and (11) we find that the integrand consists of a sum oscillating terms. Out of these only the slowly oscillating terms (also called secular terms) lead to substantial transition probability. Therefore we make the *rotating wave approximation* (RWA), where we neglect the fast oscillating terms. In particular, looking at final states at energy $E_f \approx E_i + \hbar\omega$, where E_i is the initial state energy, we can neglect the term proportional to $e^{i\omega t}$ in (11). The error made here is small as long as we are not interested in the case $\omega \approx 0$. Note that both absorption ($E_f > E_i$) and emission ($E_f < E_i$) are included in this approximation, the latter case corresponding to negative ω [because of the $\omega \leftrightarrow -\omega$ symmetry of (11)].

The transition probability from arbitrary initial state $|\psi(0)\rangle = \sum_i c_i|i\rangle$ into the state $|m\rangle$ can be written as

$$\gamma_m(t) \equiv \sum_n c_n \gamma_{n\to m} \tag{14}$$

where we can include also the $n = m$ term when the probe is off-diagonal. Summing over all final states, the total transition probability to states with energy increase $\hbar\omega$ is

$$P_\omega(t) = \sum_m |\gamma_m(t)|^2 = \frac{g_P^2}{4}\int_0^t dt_1 \int_0^t dt_2\, e^{i\omega(t_1-t_2)} \left\langle \hat{V}(t_1)\hat{V}(t_2)\right\rangle + O(g_P^3), \quad (15)$$

where $\hat{V}(t) = \hat{U}^\dagger(t)\hat{V}\hat{U}(t)$ is the interaction picture version of $\hat{V}$ (9), and the expectation value is calculated with respect to the density matrix $\hat{\rho}_0 = |\psi(0)\rangle\langle\psi(0)| = \sum_{n,\ell} c_n c_\ell^* |n\rangle\langle\ell|$. We make change to new variables $\tau = t_1 - t_2$ and $T = (t_1 + t_2)/2$ and define

$$B(T) = \begin{cases} T & \text{if } T < t/2, \\ t - T & \text{if } T > t/2. \end{cases} \quad (16)$$

We get

$$P_\omega(t) = \frac{g_P^2}{4}\int_0^t dT \int_{-B(T)}^{B(T)} d\tau\, e^{i\omega\tau} \left\langle \hat{V}(T+\tau/2)\hat{V}(T-\tau/2)\right\rangle + O(g_P^3). \quad (17)$$

Next we assume the system is in stationary state and also that the system is large or coupled to a bath. This makes the correlation to decay for large τ. In the limit of large t the T integration gives linear growth in time and can define the transition rate

$$S(\omega) \equiv \frac{dP_\omega}{dt} = \frac{g_P^2}{4}\int_{-\infty}^{\infty} \left\langle \hat{V}(\tau)\hat{V}(0)\right\rangle e^{i\omega\tau} d\tau. \quad (18)$$

As stated above, positive ω corresponds to absorption and negative to emission [24]. We see that the transition rate in the modulated system is given by the Fourier transform of the stationary two-time correlation function of the probe Hamiltonian expressed in the interaction picture. In other words, the transition rate is given by the power spectral density of the probe operator evaluated in the unperturbed system. Notice that in the absence of modulation, the transition rate reduces to that given by Fermi's golden rule [23]:

$$S(\omega) = \frac{\pi g_P^2}{2}\sum_m |\langle m|\hat{V}|n\rangle|^2 \delta(\omega_m - \omega_n - \omega) \quad (19)$$

when $\hat{\rho}_0 = |n\rangle\langle n|$.

There is always some coupling of the studied system to the environment. Because of the coupling, the state of the system can no more described in terms of a single quantum state $|\psi\rangle$. Instead, the standard procedure is to introduce a density operator $\hat{\rho} = \sum_i p_i |\psi_i\rangle\langle\psi_i|$, where $|\psi_i\rangle$'s are some states and p_i's give the probabilities that the system is in this particular state. All the measurable information about the state of the system is contained in the density operator. The expectation value $\langle\hat{O}\rangle$ of operator $\hat{O}$, for example, is given by $\mathrm{Tr}(\hat{\rho}\hat{O})$. If the coupling to the environment is weak, one can derive the master equation, which gives the time development of the density matrix [25]. The explicit form of the master equation depends on the system and is given below when needed.

In the following, we calculate the spectrum (18) for coherent and incoherent modulations in a in two-state system and in a harmonic oscillator, and for some examples

in few- and many-body systems. In some cases, we will give a complementary explanation of the physics by calculating the transition rates directly from the master equation.

3. Two state system

In this section we consider the case that the relevant state space consists of only two basis states. This is often a good approximation in cases where the transition energy between the two states differs from the transition energies to other states. A two state system is also known as two level system, or a qubit, meaning a quantum bit. The two state model has a long history, in particular in NMR [26] and in optics [27]. As long as the upper state probability is small, the behaviour of a two-state system is identical to the two lowest levels of a harmonic oscillator. Difference arises when the third and higher levels of the harmonic oscillator are excited, whereas "saturation" takes place in the two-state system.

We study the effect modulation of the level spacing in a two state system. We apply the general Hamiltonian (6)-(9) but limit first to the case without the static coupling, $H_C = 0$. The Hamiltonian is

$$\hat{H}(t) = \frac{\hbar}{2}[\omega_0 + \xi(t)]\hat{\sigma}_z + \hbar g_P \cos(\omega t)\hat{\sigma}_x. \tag{20}$$

Here $\hat{\sigma}_i$'s denote the Pauli spin matrices with $i = x, y, z$. The eigenstates of $\hat{\sigma}_z$ are called diabatic states. The eigenstates corresponding to eigenvalues +1 and -1 are marked by $|\uparrow\rangle$ and $|\downarrow\rangle$, respectively. The first term in (20) gives that their time dependent energy difference is $\hbar\omega_0 + \hbar\xi(t)$. The second, probe term generates transitions between the diabatic states.

One way to visualize the state of the system is by mapping it onto a three dimensional surface called Bloch's sphere (figure 1). In this representation, the spin state is expressed by the expectation values of the $\hat{\sigma}_i$ operators, which give the coordinates of the state vector on three orthogonal axes corresponding to $i = x, y, z$. The modulation $\xi(t)$ in the transition energy leads into a rotation of and arbitrary state $|\psi\rangle$ around the $\langle\sigma_z\rangle$-axis by the azimuthal angle

$$\zeta(t) \equiv \int_0^t \xi(\tau)d\tau, \tag{21}$$

which is the time-dependent phase caused by the modulation. The Bloch's sphere has unit radius for a normalized, pure quantum state.

There are several ways to proceed from here. In the next section, we will discuss the response of the modulated transition to the probe in terms of time-dependent perturbation theory. In section 3.2, we apply the perturbative result to the case of coherent modulation. The problem of coherent continuous modulation will be discussed both in the case of weak and strong amplitude modulation. In the former case, the relevant equations are greatly simplified with the application of RWA but, in the latter, one has to introduce the so-called Floquet approach so that the contributions from the terms neglected in the RWA (so-called generalized Bloch-Siegert shifts) are properly

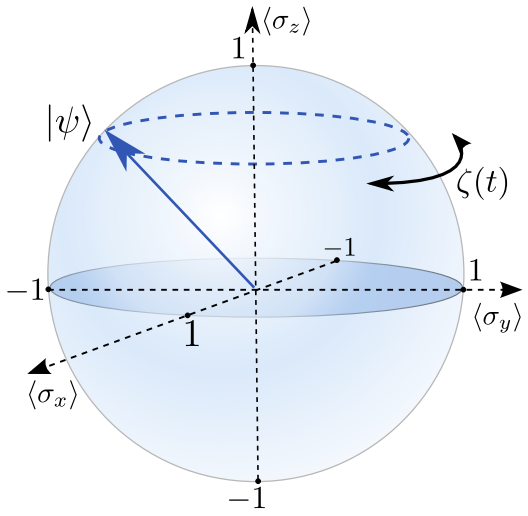

Figure 1. Bloch sphere representation of the state of a two-level system with modulated transition frequency.

included. Also, a complementary discussion in terms of discretized time-evolution will be given in section 3.3. Section 3.4 is devoted to the application of the perturbative result into the case of incoherent modulation.

3.1. Probe spectrum

We analyse the two-state Hamiltonian (20) in terms of time-dependent perturbation theory described in section 2.2. In a two-state system the unitary transformation (10) takes the form

$$\hat{U}(t) = e^{-i\hat{\sigma}_z[\omega_0 t+\zeta(t)]/2}. \tag{22}$$

It is useful to define qubit raising and lowering operators, $\hat{\sigma}_+ \equiv |\uparrow\rangle\langle\downarrow|$ and $\hat{\sigma}_- \equiv |\downarrow\rangle\langle\uparrow|$, respectively. In the interaction picture they get time dependence

$$\hat{\sigma}_\pm(t) = \hat{U}^\dagger\hat{\sigma}_\pm\hat{U} = e^{\pm i(\omega_0 t+\zeta(t))}\hat{\sigma}_\pm. \tag{23}$$

Corresponding to (11), the Hamiltonian (20) is transformed to

$$\hat{H}(t) = \hbar g_P \cos(\omega t)\left[A(t)e^{i\omega_0 t}\hat{\sigma}_+ + A^*(t)e^{-i\omega_0 t}\hat{\sigma}_-\right], \tag{24}$$

where $A(t) \equiv e^{i\zeta(t)}$ is the dynamical phase factor arising from the modulation. The transition rate can be adapted from equation (18):

$$S(\omega) = \frac{g_P^2}{4}\int_{-\infty}^{\infty} e^{i\omega t}\,\langle\hat{\sigma}_x(t)\hat{\sigma}_x(0)\rangle\,dt. \tag{25}$$

We concentrate here on the absorptive transitions, which allows us to write the absorption rate in the RWA as

$$S(\omega) = \frac{g_P^2}{4}\int_{-\infty}^{\infty} e^{i\omega t}\langle\hat{\sigma}_-(t)\hat{\sigma}_+(0)\rangle\,\mathrm{d}t. \tag{26}$$

In order to take into account coupling with the environment, we need the master equation (section 2.2). For a two state system the master equation takes the form [25]

$$\frac{\mathrm{d}\hat{\rho}}{\mathrm{d}t} = -\frac{\mathrm{i}}{\hbar}[\hat{H},\hat{\rho}] - \frac{\Gamma_\phi}{4}\left[\hat{\sigma}_z,[\hat{\sigma}_z,\hat{\rho}]\right] + \frac{\Gamma_1}{2}\left(2\hat{\sigma}_-\hat{\rho}\hat{\sigma}_+ - \hat{\sigma}_+\hat{\sigma}_-\hat{\rho} - \hat{\rho}\hat{\sigma}_+\hat{\sigma}_-\right), \quad (27)$$

which includes the relaxation with the rate Γ_1 and the pure dephasing with the rate Γ_ϕ. We also define $\Gamma_2 = \Gamma_1/2 + \Gamma_\phi$.

The master equation (27) allows us to calculate the two-time correlator by using the quantum regression theorem [25]. The result is [28]

$$S(\omega) = \frac{g_P^2}{4}\int_{-\infty}^{\infty} e^{i(\omega-\omega_0)t-\Gamma_2|t|}\left\langle e^{-i\zeta(\tau)}\right\rangle_\xi \mathrm{d}t, \quad (28)$$

where we have added averaging over different realisations of ξ, which becomes relevant under incoherent fluctuations. The dynamical phase $\zeta(t)$ (21), accumulated due to the fluctuations, is evidently an important quantity, since it determines the spectrum completely. We will emphasize this property in our discussions in the following sections. In the following, we will consider spectrum (28) in the cases of deterministic (coherent) and random (incoherent) modulations $\xi(t)$, together with related novel experiments.

3.2. Coherent modulation

Coherent modulations of the transition frequency can be further categorised in terms of the continuity of the time-dependent part of the Hamiltonian. Continuous modulations (as opposed to stepwise modulations) form an important class of modulations, especially because atomic or molecular systems are typically studied by perturbing the atomic energy levels with electromagnetic radiation via the dipole moment of atoms [23], leading to sinusoidal time-dependence in the semi-classical approximation.

Coherent modulation of the transition frequency occurs when $\xi(t+2\pi/\Omega) = \xi(t)$, i.e. when the modulation is correlated with itself at all times t. Such $\frac{2\pi}{\Omega}$-periodic modulations have attracted a lot of theoretical and experimental interest in the context of two-level systems [12, 14, 15, 29–36]. Here, we review the subject, show the sideband formation and demonstrate the longitudinal sideband control of qubit state populations. In addition, the periodic modulation serves as an introduction to the stochastic modulation of the transition frequency considered in section 3.4.

We assume that the static part $\bar{\xi} \equiv \int_0^{2\pi/\Omega}\xi(t)dt$ has been included into ω_0. Thus, also the dynamical phase becomes periodic, $\zeta(t+2\pi/\Omega) = \zeta(t)$, and the dynamical phase factor $A(t) = e^{i\zeta(t)}$ has the Fourier series representation

$$A(t) = \sum_{n=-\infty}^{\infty}\Delta_n e^{in\Omega t}, \quad (29)$$

where the Fourier coefficients Δ_n are obtained as

$$\Delta_n = \frac{\Omega}{2\pi}\int_0^{2\pi/\Omega} e^{-in\Omega t}e^{i\zeta(t)}. \quad (30)$$

In the interaction picture, Hamiltonian (24) can be written as

$$\hat{H}(t) = \frac{\hbar g_P}{2} \sum_{n=-\infty}^{\infty} \Delta_n \left(e^{i(\omega_0 + n\Omega + \omega)t} + e^{i(\omega_0 + n\Omega - \omega)t} \right) \hat{\sigma}_+ + \frac{\hbar g_P}{2} \sum_{n=-\infty}^{\infty} \Delta_n^* \left(e^{-i(\omega_0 + n\Omega + \omega)t} + e^{-i(\omega_0 + n\Omega - \omega)t} \right) \hat{\sigma}_-. \quad (31)$$

We thus see that the modulations in the transition energy are transformed into an effective transverse multi-photon drive of the qubit. We also notice that the effective coupling strength to a multi-photon mode m is $g_P|\Delta_m|$. In the Bloch sphere picture, this transformation corresponds to moving into a frame that rotates around the z-axis with the non-uniform and time-dependent angular velocity $\zeta(t)$.

Analytical calculation of spectrum for Hamiltonian (31) is difficult in the general case. Nevertheless, close to a multi-photon resonance, $\omega \approx \omega_0 + m\Omega$, when the strengths of the other driving fields are weak enough, $g_P|\Delta_n| < \Omega$ for $n \neq m$, one can make the rotating wave approximation (RWA) by neglecting all non-resonant driving fields. The resulting RWA-Hamiltonian can be written as

$$\hat{H}_{\mathrm{rwa}}(t) = \frac{\hbar g_P}{2} \left[\Delta_m e^{i(\omega_0 + m\Omega - \omega)t} \hat{\sigma}_+ + \Delta_m^* e^{-i(\omega_0 + m\Omega - \omega)t} \hat{\sigma}_- \right]. \quad (32)$$

As a consequence, one can calculate the spectrum for each mode m separately, and by adding the contributions from all modes, one obtains the so-called multi-photon sideband spectrum:

$$S(\omega) = \sum_{m=-\infty}^{\infty} \frac{g_P^2}{2} \frac{\Gamma_2 |\Delta_m|^2}{(\delta + m\Omega)^2 + \Gamma_2^2}, \quad (33)$$

where $\delta \equiv \omega_0 - \omega$ is the detuning between the static qubit and the probe. The sufficient criterion for such resolvable sidebands is that the spacing between the adjacent bands has to be larger than their linewidths, i.e. $\Omega > \Gamma_2$. We also notice that the sideband disappears whenever $\Delta_m = 0$. This bears similarity to the coherent destruction of tunnelling (CDT), discussed in references [30, 37] and observed in numerous experiments with an additional static coupling of stationary states. CDT is closely related to the phenomenon of "dynamic localization" [14]. The rotating wave approximation generally becomes insufficient as the probe amplitude g_P is increased. As a consequence, the resonance locations are shifted due to the enhanced contributions of the counter-rotating (Bloch-Siegert shift [38]) and other multi-mode (generalized Bloch-Siegert [39]) terms. However, in the case of direct probing of modulated transition energy, one can typically assume that the probe amplitude is weak and, thus, the RWA is valid. The corresponding shift of the resonance locations (so-called dynamic Stark effect) due to high intensity modulation occurs only when the stationary energy eigenstates experience static coupling, in addition to the time-dependent probe. We will study this in the following section.

In the case of conventional sinusoidal modulation, $\xi(t) = \xi \cos(\Omega t)$, the Fourier coefficients are

$$\Delta_m = \mathrm{J}_m(\xi/\Omega), \quad (34)$$

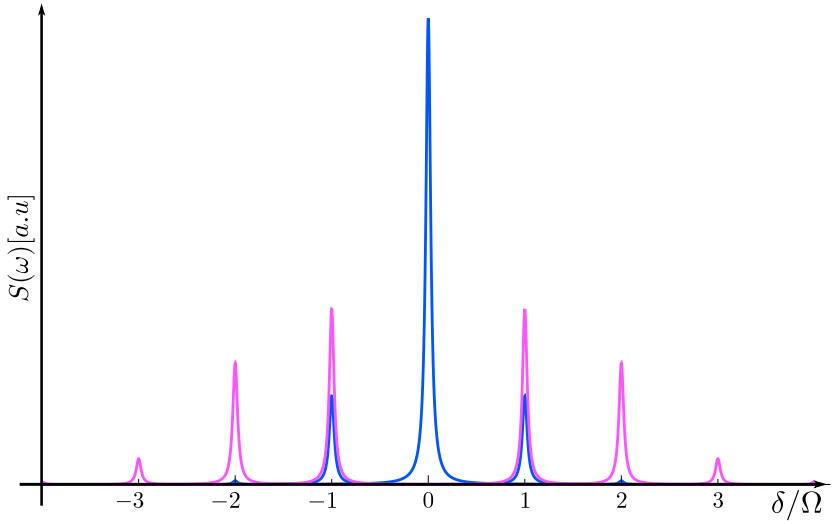

Figure 2. Spectrum of sinusoidally modulated transition as a function of the detuning δ. For low modulation amplitude $\xi/\Omega = 0.8$, five resonances ($m = -2, -1, 0, 1, 2$) are visible (blue). When the amplitude is increased to $\xi/\Omega = 2.4048$ one observes two additional peaks ($m = -3, 3$) and the disappearance of the $m = 0$ peak due to CDT (magenta). The plot is based on equations (33) and (34) and the width of the resonances is determined by $\Gamma_2/\Omega = 0.03$.

where J_m are the Bessel functions of the first-kind. This describes the absorbed power from the probe in terms of the transitions between levels whose transition energy is coherently modulated. We see that the modulation creates an infinite set of resonances, spaced by the modulation frequency Ω. The relative magnitudes of these multiphoton resonances are given by the corresponding Bessel functions J_n. In figure 2, we have plotted sinusoidal modulation spectrum (33) as a function of the detuning δ for two values of modulation amplitude ξ. Clearly, as the modulation amplitude is increased new multiphoton resonances become visible in the spectrum. Also, we observe the disappearance of the $m = 0$ peak for $\xi/\Omega = 2.4048$ which is the first zero of J_0.

The modulation of the transition frequency of a qubit does not need to be a simple sine or cosine as a function of time: any other shape can be used in principle [40]. So far there have been experiments with square pulses in transmons [20] and with bichromatic modulation in double quantum dots [41] and in a superconducting flux qubit [42]. In the latter case, the goal was to simulate universal conductance fluctuations in weakly-disordered mesoscopic systems. For the square pulses, i.e. periodic latching modulation, $\xi(t) = \xi\ \mathrm{sgn}\left[\cos(\Omega t)\right]$ and the sideband amplitudes can be written as [20]

$$\Delta_m = \frac{2}{\pi}\frac{\Omega\xi}{\Omega^2 m^2 - \xi^2}\sin\left(\frac{\pi m}{2} - \frac{\pi\xi}{2\Omega}\right). \tag{35}$$

We have compared the spectra resulting from the above two types of modulations in figure 3. One observes that the resonance heights are clearly dependent on the detailed form of the modulation. Especially, the CDT location $\xi/\Omega = 2.4048$ of the $m = 0$ resonance of the sinudoidal modulation spectrum is shifted to higher amplitudes

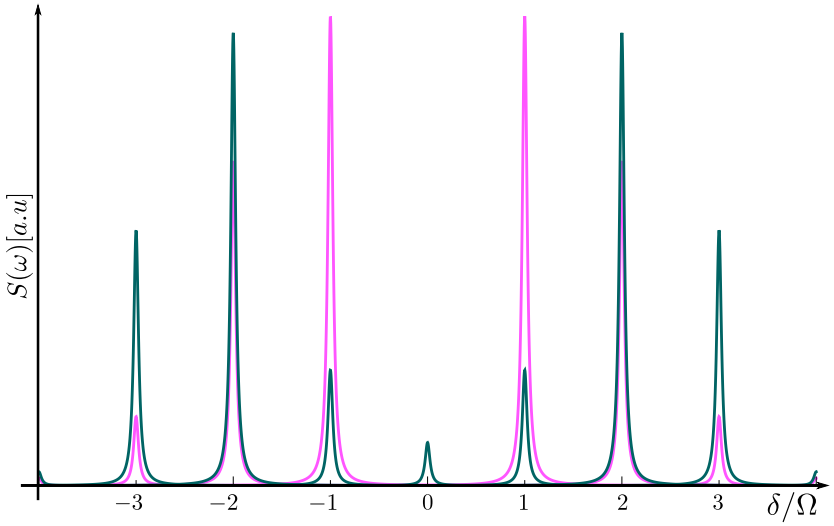

Figure 3. Comparison between the spectra for sinusoidally [magenta, equation (34)] and latching [green, equation (35)] modulated transition as a function of the detuning δ. The parameters are the same as those for the strong modulation spectrum in figure 2.

ξ due to the rescaling by $\pi/2$ in equation (35) [20]. This effect has been measured with a superconducting qubit whose transition energy was modulated with a square pulsed magnetic flux through its SQUID loop, created by an arbitrary current waveform generator for a bias coil.

Near each of the sidebands $\omega = \omega_0 + m\Omega$, $m = 0, \pm1, \pm2, \ldots$, the general Hamiltonian (31) can be transformed back into the Schrödinger picture:

$$\hat{H}_{\mathrm{rwa}} = \frac{\hbar}{2}\left[(\delta + m\Omega)\,\hat{\sigma}_z + g_P(\Delta_m\hat{\sigma}_+ + \Delta_m^\star\hat{\sigma}_-)\right]. \tag{36}$$

Thus, we see that the qubit energies are dressed by those of m modulation photons and a probe photon. The terms of equation (36), thus, describe the two nearly resonant longitudinally doubly dressed states and their coupling, respectively. Considering the dynamics in the Bloch sphere representation, Hamiltonian (36) generates precession around the vector $\Omega = (g_P\mathrm{Re}(\Delta_m), -g_P\mathrm{Im}(\Delta_m), \delta + m\Omega)$ with the Rabi frequency

$$g_{\mathrm{d}}^{(\mathrm{m})} = \sqrt{(\delta + m\Omega)^2 + g_P^2|\Delta_m|^2}. \tag{37}$$

In other words, by applying the transverse driving field at the frequency ω equal to the energy difference of the longitudinally dressed states $\omega_0 \pm m\Omega$, the coherent oscillations with the rate $g_{\mathrm{d}}^{(\mathrm{m})}$ are observed between the qubit eigenstates. This is a demonstration of the sideband control of the single qubit states using the frequency modulation, see also references [43, 44] for a qubit-oscillator state control realized using the frequency modulation.

3.2.1. Static coupling and Floquet approach In the more general case, the stationary energy eigenstates experience also a constant coupling with strength Δ, in addition

to the harmonic probe. This interaction can be modelled with the Hamiltonian [c.f. equation (8)]

$$\hat{H} = \frac{\hbar}{2}\left[\omega_0 + \xi(t)\right]\hat{\sigma}_z + \frac{\hbar\Delta}{2}\hat{\sigma}_x + \hbar g_P \cos(\omega t)\hat{\sigma}_x. \tag{38}$$

This kind of additional static coupling appears naturally in several types of experimental realisations, reaching from superconducting qubits to quantum dots and nuclear magnetic resonance (NMR). It is difficult to write the above Hamiltonian into the form of equation (8). Also, direct transformation into the interaction picture is complicated since the unprobed Hamiltonians at different times do not commute. However, one can apply the general procedure presented in Section 2 by noticing that the Hamiltonian without the probe,

$$\hat{H}_0(t) = \frac{\hbar}{2}\left[\omega_0 + \xi(t)\right]\hat{\sigma}_z + \frac{\hbar\Delta}{2}\hat{\sigma}_x, \tag{39}$$

is time-periodic with the period $2\pi/\Omega$. As a consequence, one can apply the Floquet method [14, 45–47].

Due to the periodicity, the time-dependent Schrödinger equation is solved by [48]

$$|\psi_\alpha(t)\rangle = |u_\alpha(t)\rangle e^{-i\varepsilon_\alpha t/\hbar}, \tag{40}$$

where $|u_\alpha(t)\rangle$ has the same periodicity as the Hamiltonian and, thus, can be written as a Fourier series. The quasienergies ε_α are the eigenvalues of the so-called Floquet Hamiltonian $\hat{H}_0^{\mathrm{F}} \equiv H_0(t) - i\hbar\partial_t$:

$$\hat{H}_0^{\mathrm{F}}|u_\alpha(t)\rangle = \varepsilon_\alpha|u_\alpha(t)\rangle. \tag{41}$$

The periodicity of $\hat{H}_0(t)$ is reflected in the fact that the state $|u_{\alpha,n}(t)\rangle \equiv \exp(in\Omega t)|u_\alpha(t)\rangle$ gives physically equivalent state to (40), but with shifted quasienergy $\varepsilon_{\alpha,n} \equiv \varepsilon_\alpha + \hbar n\Omega$. As a consequence, $\varepsilon_\alpha = \varepsilon_{\alpha,0}$ and $|u_\alpha(t)\rangle = |u_{\alpha,0}(t)\rangle$. By extending the stationary state basis with that of time-periodic functions, we obtain a composite space spanned by $\{|\sigma, n\rangle | \sigma = \downarrow\uparrow\ ;\ \langle t|n\rangle = e^{in\Omega t}, n \in \mathbb{Z}\}$. In this so-called Sambe space [49], the components of $\hat{H}_0^{\mathrm{F}}$ and $|u_{\alpha,n}(t)\rangle$ are time-independent and can be organized as a matrix $\hat{\mathcal{H}}_{\mathrm{F}}$ and a vector $|\alpha, n\rangle$. Thus, we see that the time-dependent Schrödinger equation is transformed into an eigenvalue equation of an infinite dimensional time-independent Hamiltonian with an infinitely repeating energy structure. For a two-level system, the repeating block consists of two energy eigenstates, which the repetition period of Ω. Due to the similarities with the one-dimensional Bloch's problem of solid state physics, these blocks are sometimes referred to as Brillouin zones. As the Floquet Hamiltonian $\hat{\mathcal{H}}_{\mathrm{F}}$ is diagonal and time-independent in the quasienergy basis $|\alpha, n\rangle$, we can calculate the probe absorption spectrum as in equation (18).

The calculation of the spectrum still requires the solution of the quasienergy eigenvalue equation (41). The solution is unavoidably numerical in the general case, and we limit the discussion here into the case where the coupling Δ is small and one can, therefore, treat it as a perturbation. We solve the eigenvalue equation in the absence of the coupling ($\Delta = 0$) and then calculate the first order corrections by using the

so-called generalized Van Vleck (GVV) perturbation theory. Formally, GVV has been discussed on a general level in references [50, 51], and in the context of the present case in reference [48, 52]. Also, reference [53] contains a discussion on the application of GVV into a multimode Floquet problem.

When $\Delta = 0$, the eigenstates of $\hat{H}_0^{\mathrm{F}}$ can be written as

$$|u^0_{\pm,n}(t)\rangle = |\uparrow\downarrow\rangle \exp\left[\mp i\zeta(t)/2 + in\Omega t\right], \tag{42}$$

whose corresponding quasienergies are $\varepsilon_{\pm,n} = \pm\omega_0/2 + n\Omega$. The superscript indicates the eigenstates of the unperturbed Hamiltonian. In the Sambe space, one can write the above quasienergy states as

$$|u^0_{\pm,n}\rangle = \sum_\ell \Delta^{(*)}_{\pm(n-\ell)}(\xi/2)\,|\uparrow\downarrow,\ell\rangle, \tag{43}$$

where ξ is the amplitude of the modulation. Next, we write the coupling term in this basis by noticing that the non-zero matrix elements of $\Delta\hat{\sigma}_x$ can be written as

$$\Omega_m \equiv \Delta\langle u^0_{-,m}|\hat{\sigma}_x|u^0_{+,0}\rangle = \Delta\sum_\ell \Delta_{m-\ell}(\xi/2)\Delta_\ell(\xi/2) = \Delta\Delta_m(\xi), \tag{44}$$

because $\Delta_\ell(\xi)$ are Fourier coefficients. This can be calculated once the Fourier coefficients (30) of the dynamical phase factor are known. For the special case of sinusoidal modulation, one obtains [48, 52]

$$\Omega_n = \Delta \mathrm{J}_n(\xi/\Omega). \tag{45}$$

As a consequence, Hamiltonian $\hat{\mathcal{H}}_{\mathrm{F}}$ can now be written in basis (43) as

$$\hat{\mathcal{H}}_{\mathrm{F}} = \sum_{\sigma=\pm,n} \varepsilon_{\sigma,n}|u^0_{\sigma,n}\rangle\langle u^0_{\sigma,n}| + \sum_{n,m}\left[\Omega_{n-m}|u^0_{-,n}\rangle\langle u^0_{+,m}| + \mathrm{h.c.}\right], \tag{46}$$

where h.c. stands for hermitian conjugate.

Correspondence with the RWA result (33) of the uncoupled case can be obtained by considering Floquet Hamiltonian (46) in the vicinity of the multi-photon resonance $\omega_0 \approx m\Omega$. Assuming that the coupling between the qubit states, characterized by Δ, can be assumed small, one can use GVV perturbation theory to find the eigenstates and the corresponding eigenenergies.

When $\omega_0 \approx m\Omega$, eigenstates $|u^0_{-,n+m}\rangle$ and $|u^0_{+,n}\rangle$ are nearly degenerate. In the weak coupling limit, one can neglect couplings to all other eigenstates. This is called the first order GVV perturbation theory which is equivalent to the rotating-wave approximation made in equation (32). Consequently, the Floquet Hamiltonian (46) reduces into a 2×2-matrix

$$\hat{\mathcal{H}}_{\mathrm{F}} \approx \frac{\hbar}{2}(\omega_0 - m\Omega)\hat{\sigma}_z^{\mathrm{F}} + \frac{\hbar}{2}\left[\Omega_m\hat{\sigma}_+^{\mathrm{F}} + \mathrm{h.c}\right], \tag{47}$$

where $\hat{\sigma}_z^{\mathrm{F}} \equiv |u^0_{+,k}\rangle\langle u^0_{+,k}| - |u^0_{-,k+m}\rangle\langle u^0_{-,k+m}|$ and $\hat{\sigma}_+^{\mathrm{F}} \equiv |u^0_{+,k}\rangle\langle u^0_{-,k+m}|$. Thus, eigenenergies, or the so-called quasienergies, in the RWA for the zeroth Brillouin zone are $\pm\frac{1}{2}\omega_{1,m} \equiv$

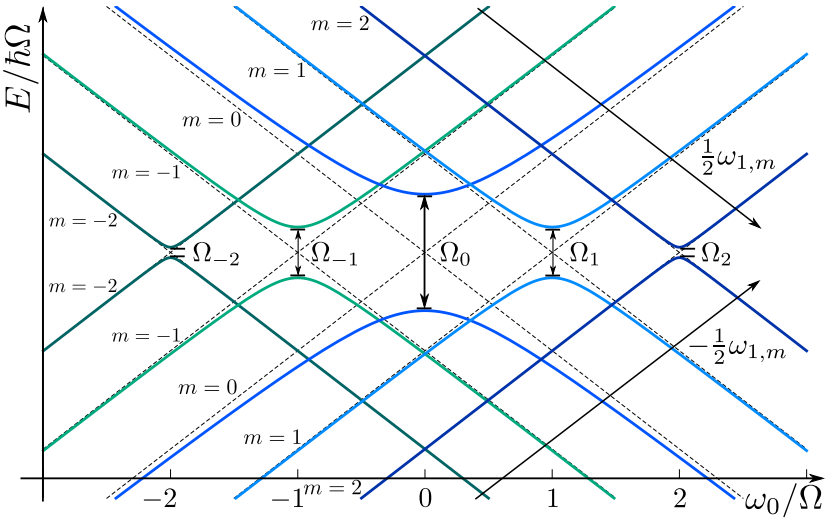

Figure 4. Quasienergies $\omega_{1,m}$ for $m = -2, \ldots, 2$ as a function of the bare transition frequency ω_0. We have used the parameter values: $\Delta/\Omega = 0.7$ and $\xi/\Omega = 0.8$.

$\pm\frac{1}{2}\sqrt{(\omega_0 - m\Omega)^2 + |\Omega_m|^2}$ [15, 33, 35, 48, 52]. The corresponding normalized eigenvectors are then

$$|u^1_{-,m}\rangle = \cos\frac{\theta}{2}|u^0_{-,k+m}\rangle - e^{-i\phi}\sin\frac{\theta}{2}|u^0_{+,k}\rangle \tag{48}$$

$$|u^1_{+,m}\rangle = \sin\frac{\theta}{2}|u^0_{-,k+m}\rangle + e^{-i\phi}\cos\frac{\theta}{2}|u^0_{+,k}\rangle, \tag{49}$$

respectively. In the above, we have defined $\tan\theta = |\Omega_m|/(\omega_0 - m\Omega)$ with $\theta \in [0, \pi]$, and $\phi \equiv \arg\,\Omega_m \in [0, 2\pi]$. In figure 4, we show a typical quasienergy structure by using sinusoidal modulation. We see that the longitudinal driving lifts the degeneracies at the multi-photon resonance locations resulting in characteristic avoided crossing structure. The minimum gaps are given by the Fourier coefficients $|\Omega_m|$.

In the Sambe space, the transformation into the interaction picture is straightforward in the sense that the Hamiltonian $\hat{H}^{\rm F}_0$ is time-independent. Therefore, the absorptive transition rate can be calculated by using equation (18). The probe Hamiltonian in the interaction picture has to be written as

$$\hat{V}(t) = e^{i\hat{H}^{\rm F}_0 t/\hbar} e^{i\omega t}\hat{V} e^{-i\hat{H}^{\rm F}_0 t/\hbar}. \tag{50}$$

Similar to the uncoupled case (33), we consider the case of resolved sidebands. In the vicinity of a multi-photon resonance $\omega_0 \approx m\Omega$, one can use the truncated RWA Hamiltonian (47). As a consequence, the probe Hamiltonian is written as

$$\hat{V}^{\rm F}_x(t) = \hbar g_P \cos(\omega t)|\Delta_m|\left[\frac{|\Omega_m|}{\omega_{1,m}}\hat{\sigma}^{\rm F}_z + \frac{\omega_0 - m\Omega}{\omega_{1,m}}\hat{\sigma}^{\rm F}_x\right]. \tag{51}$$

We thus see that the probe actually acquires a diagonal part when written in the eigenbasis of the RWA Floquet Hamiltonian. Additionally, we see that the off-diagonal part vanishes at resonance, which leads into the disappearance of the spectral line. If the coupling Δ is small, the region where the absorption peak is weak is, nevertheless,

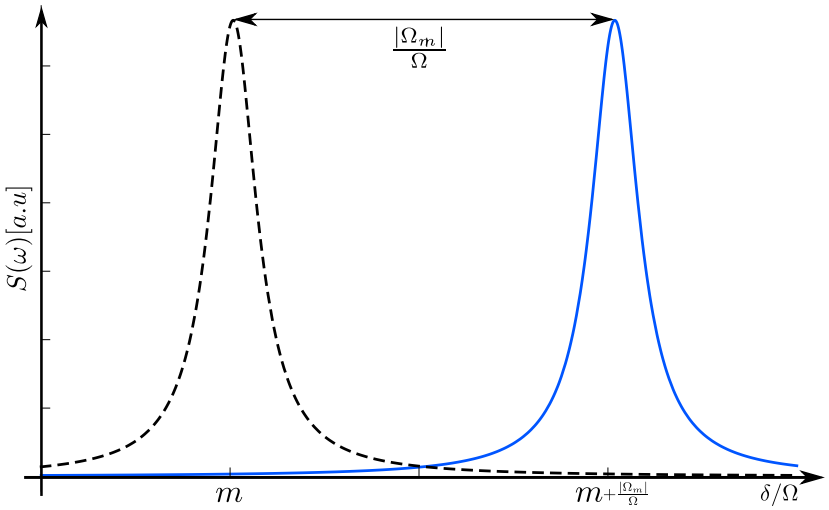

Figure 5. Quasienergy (longitudinal) probe spectrum for the $m = 1$ resonance of the sinusoidally modulated transition as a function of the detuning δ. The maximal shift occurs at $\xi/\Omega = 1.8412$, which is the first maximum of the Bessel function J_1 (blue curve). This is compared with the uncoupled case which can be retrieved by large amplitude modulation (black dashed curve).

narrow. On the other hand, by coupling the probe to $\hat{\sigma}_z$ one obtains by, again, writing the probe in the RWA basis [39, 54]:

$$\hat{V}_z^{\mathrm{F}}(t) = \hbar g_P \cos(\omega t) \left[\frac{\omega_0 - m\Omega}{\omega_{1,m}} \hat{\sigma}_z^{\mathrm{F}} - \frac{|\Omega_m|}{\omega_{1,m}} \hat{\sigma}_x^{\mathrm{F}} \right], \tag{52}$$

where we have used Parseval's identity which states that $\sum_k |\Delta_k|^2 = 1$. With both types of probe coupling, the longitudinal terms do not induce transitions, and can be neglected in the weak probe limit. Longitudinal probing (52) has been used in measurements of modulated superconduting qubits with static coupling [39].

The absorption spectrum in the resolved-sideband limit can now be written as

$$S(\omega) = \sum_{m=-\infty}^{\infty} \frac{g_P^2}{2} \frac{\Gamma_2 |\langle u_{+,m}^1 | \hat{V}^{\mathrm{F}} | u_{-,m}^1 \rangle|^2}{(\omega_{1,m} - \omega)^2 + \Gamma_2^2}, \tag{53}$$

where $\hat{V}^{\mathrm{F}} = V^{\mathrm{F}} \hat{\sigma}_x$ and $V^{\mathrm{F}} = |\Delta_m| \frac{\omega_0 - m\Omega}{\omega_{1,m}}$ or $V^{\mathrm{F}} = \frac{|\Omega_m|}{\omega_{1,m}}$ for transverse and longitudinal probes, respectively. We see immediately that for the transverse probe (51) in the limit of $\Delta \to 0$ we recover the spectrum (33). Notice that instead of bare atomic energies, spectrum (53) gives information on the quasienergy structure of a strongly modulated system with an off-diagonal static coupling. As an example, we consider here the case of longitudinal probing of a bare qubit which is in m^{th} multi-photon resonance, i.e. $\omega_0 = m\Omega$. We see that the probe absorption peak is shifted from $\delta = 0$ to $\delta = |\Omega_m(\xi/\Omega)|$. One can recover the uncoupled multi-photon resonance locations only asymptotically when $\xi/\Omega \to \infty$. This is depicted in figure 5 for sinusoidal modulation of the coupled transition. In the more general case of non-resonant bare qubit frequency ($\omega_0 \neq m\Omega$),

shift of the resonance is given by $\omega = \sqrt{(\omega_0 - m\Omega)^2 + |\Omega_m|^2}$.

In the above, we have approximated that the relaxation rates between the quasienergy states are characterised by those of the non-modulated system. Corrections to the resolved sideband approximation and to the relaxation rates can be obtained by applying the so-called Floquet-Born-Markov formalism which combines the Floquet formalism and detailed coupling to the environment [14, 48, 55–61]. Notice also that in the RWA, and by neglecting the diagonal probe in equation (51), we obtain in the frame rotating at ω:

$$H_0^{\mathrm{F}} = \frac{\hbar}{2}\left[\omega_{1,m} - \omega\right]\hat{\sigma}_z - \frac{\hbar g_P}{2} V^{\mathrm{F}} \hat{\sigma}_x, \tag{54}$$

which reduces into equation (36) when $\Delta = 0$ for a transverse probe.

Sideband resolved multiphoton resonances similar to (53) have been observed in terms of Ramsey interference fringes in Rydberg atoms [11, 62], in quantum dots as resolved sideband emission due to surface acoustic waves [31], and in numerous experiments on superconducting qubits [20, 33, 35, 63] with microwave modulation. Also, other experiments [34, 64, 65] can interpreted in terms of non-resolvable Floquet theory, if the dissipation is taken into account with a proper care. The characteristic of these experiments is that the heights of the multi-photon resonances are modulated by the corresponding Fourier coefficients Δ_m of dynamical modulation phase factor $e^{i\zeta(t)}$, which are dependent on the modulation amplitude ξ. These multi-photon resonances and the accompanying modulations can also be interpreted as resulting from quantum interference, see Sec. 3.3.

3.2.2. Dynamic Stark effect and basis dependence of RWA It should be emphasized that the above RWA result is strongly basis dependent [66]. The general problem of finding an optimal basis for RWA has not been addressed, up to our best knowledge. Corrections to the RWA result can be obtained by including the second order corrections in the GVV calculation. As a consequence, the m-photon resonance is shifted by

$$\delta_m = \frac{1}{2}\sum_{\ell \neq m} \frac{|\Omega_\ell|^2}{\omega_0 - \ell\Omega}, \tag{55}$$

resulting in the quasienergy $\omega_2 \equiv \sqrt{(\omega_0 + \delta_m - m\Omega)^2 + \Omega^2}$. Notice that this is more general than the original Bloch-Siegert shift [38] that includes only the counter-rotating correction $\ell = -m$. In general, the deviation between the true modulated transition energy and the RWA result ω_1 is called the generalized Bloch-Siegert shift [39]. The deviation between the uncoupled multi-photon resonance $\omega_0 = m\Omega$ and the true modulated resonance is called dynamic Stark shift. The conventional Bloch-Siegert shift has been observed in strongly modulated Rydberg atoms [67]. The generalized Bloch-Siegert correction was needed in the studies of radiative shifts of magnetic resonances [68] and of superconducting qubits with highly nonlinearly coupled sinusoidal modulation [39]. Also, the Bloch-Siegert effect has been observed at quantum level in circuit-QED [69]. In figure 6, we plot the second order correction to the quasienergies. In addition to the

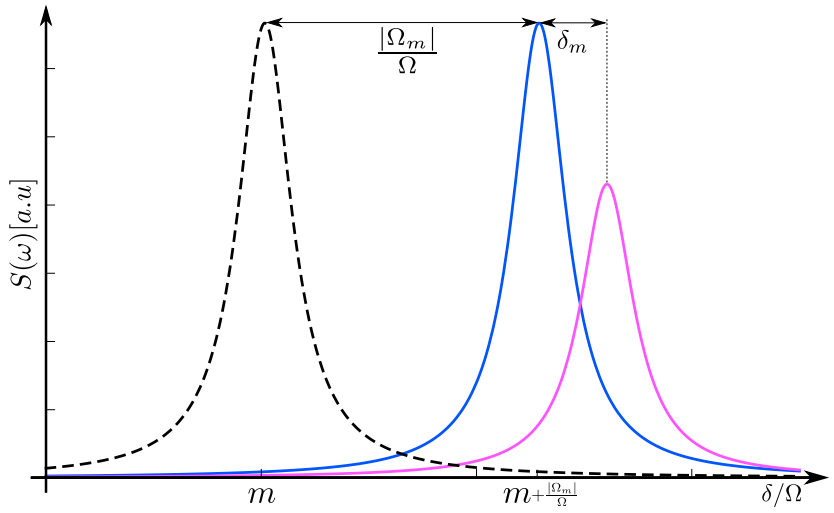

Figure 6. Second order generalized Bloch-Siegert shift. Quasienergy resonance is shifted by δ_m due to the second order couplings to non-resonant states.

location of the resonance, we observe that the magnitude of the resonance is changed due to the non-resonant corrections.

3.2.3. Steady state population Additional insight to the spectrum can be gained by studying the steady state population of the qubit. Also, in some experiments [33], the steady state population is directly measured instead of the probe absorption spectrum. The results in the absence of static coupling can be recovered by setting $\Delta = 0$, and by considering transversely coupled probe.

When the coupling to the probe is weak but non-negligible, the sideband control has to be revealed by studying the steady state population of the qubit (20). If the excitation drive $\hbar g_P \cos(\omega t)\hat{\sigma}_x$ is in resonance with a longitudinal sideband transition, then the steady state population would deviate from the ground state. To find the steady state population, the master equation (27) for Hamiltonian (36) can be solved analytically around every resolvable resonance [27]. By summing the contributions of all independent resonances one results with

$$P_e = \frac{g_P^2}{2} \sum_{m=-\infty}^{\infty} \frac{\frac{\Gamma_2}{\Gamma_1} |\langle u^1_{+,m}|\hat{V}^{\mathrm{F}}|u^1_{-,m}\rangle|^2}{\Gamma_2^2 + (\omega_{1,m} - \omega)^2 + \frac{g_P^2 \Gamma_2}{\Gamma_1} |\Delta_m|^2} \tag{56}$$

for the the steady state occupation probability for the qubit excited state $|u^1_{+,m}\rangle$ [20,28,33]. Thus, as a consequence of multiphoton absorption from the probe, the excited state occupation of the excited state increases. We have obtained another intuitive result that the absorptive transition rate (33) is obtained from the steady state population as $S(\omega) = \Gamma_1 P_e$, which is a restatement of energy conservation. Also, when the coupling is off ($\Delta = 0$) and the probe frequency zero ($\omega = 0$), one obtains the familiar results of the Bloch equation for a qubit with off-diagonal static coupling g_P on each resolvable

sideband. By including the probe explicitly to the master equation, we also observe that the widths of the sidebands are broadened, compared with the decoherence rate Γ_2, due to the power broadening of the strong transverse driving with the effective amplitude $g_P\Delta_m$ [27], which produces linewidth $\lesssim \sqrt{\Gamma_2^2 + g_P^2|\Delta_m|^2\Gamma_2/\Gamma_1}$. Also, when $\Delta_m = 0$ the contribution to the excited state population due to the corresponding multiphoton resonance disappears, which is conventionally referred to as coherent destruction of tunnelling (CDT).

We presented here a discussion that includes the probe, but similar results can be obtained for the excited state population $|u^0_{+,m}\rangle$ in the absence of probe by setting $g_P = \Delta$ and $\omega = 0$. In the following, we give an alternative interpretation to the origin of the increased excited state population in terms of Landau-Zener-Stückelberg (LZS) interference [1, 3, 4].

3.3. Discretized periodic time-evolution

Here we consider the generic LZS-Hamiltonian

$$H_{\rm LZS}(t) = \frac{\hbar}{2}\left[\omega_0 + \xi(t)\right]\hat{\sigma}_z + \frac{\hbar\Delta}{2}\hat{\sigma}_x. \tag{57}$$

This Hamiltonian is exactly the unprobed part of (38), and can also be obtained from the probed and modulated uncoupled Hamiltonian (20) by making a transformation into a frame rotating with ω and by denoting $g_P = \Delta$. In such case, one talks about photon-assisted LZ-processes between modulation dressed states [28].

We are interested in the time-evolution operator $\hat{U}(0,t)$ which describes the dynamical change of the state vector: $|\psi(0)\rangle \to |\psi(t)\rangle$. Often, one can separate the free adiabatic time-evolution from the non-adiabatic transition processes. As a consequence, the time-evolution operator of a transition process occurring instantaneously at $t_1 \in [0, t_2]$ can be discretized formally as

$$\hat{U}_(0,t_2) \equiv \hat{U}_{\varphi_2}\hat{U}_T\hat{U}_{\varphi_1}, \tag{58}$$

where $\hat{U}_T$ is the unitary evolution operator for the transition, and can be quite generally written in the eigenbasis $\{|\psi_-(t)\rangle, |\psi_+(t)\rangle\}$ of the instantaneous Hamiltonian, i.e. in the adiabatic eigenbasis, into the form [12, 15, 20]

$$\hat{U}_T = \begin{pmatrix} \sqrt{1-p}e^{-i\tilde{\phi}_S} & \sqrt{p} \\ -\sqrt{p} & \sqrt{1-p}e^{i\tilde{\phi}_S} \end{pmatrix}, \tag{59}$$

where $\sqrt{p} \equiv \langle\psi_+(t_2)|\psi(t_2)\rangle$ is the transition probability amplitude for the transition $|\psi(0)\rangle \to |\psi_+(t_2)\rangle$. Similarly, $\sqrt{1-p} \equiv \langle\psi_m(t_2)|\psi(t_2)\rangle$. We have also taken into account the possibility of non-adiabatic phase shift $\tilde{\phi}_S$ during the transition. In a Landau-Zener tunnelling process, this phase shift is determined by the Stokes phase [70–72] $\phi_S = \tilde{\phi}_S + \pi/2$, and defined as the difference between the dynamic phases collected by

the diabatic and adiabatic states during the transition process (see the following section). The adiabatic time-evolution operator is defined as

$$\hat{U}_\varphi \equiv e^{-i\varphi\hat{\sigma}_z} = \begin{pmatrix} e^{-i\varphi} & 0 \\ 0 & e^{i\varphi} \end{pmatrix}, \tag{60}$$

and $\varphi_i = \frac{1}{2}\int_{t_{i-1}}^{t_i} \omega(t)dt$ with $t_0 = 0$. In the above, we have assumed that the transition occurs instantaneously at $t = t_1$. We have also denoted the adiabatic transition energy with

$$\omega(t) = \sqrt{(\omega_0 + \xi(t))^2 + \Delta^2}. \tag{61}$$

We are interested here in periodic modulation of the transition energy. For a single-period evolution, the time-evolution operator is simply a product of two single-transition operators [12]:

$$\hat{U}_{\mathrm{St}} = \hat{U}_{\varphi_4}\hat{U}_T\hat{U}_{\varphi_3}\hat{U}_{\varphi_2}\hat{U}_T\hat{U}_{\varphi_1} = \begin{pmatrix} \alpha & \gamma \\ -\gamma^* & \alpha^* \end{pmatrix} \tag{62}$$

$$\alpha = (1-p)e^{-i\zeta_+} - pe^{-i\zeta_-} \tag{63}$$

$$\gamma = 2\sqrt{p(1-p)}\sin\left[\Phi + \phi_S\right] e^{i(\phi_4 - \phi_1)} \tag{64}$$

$$\zeta_+ = \phi_1 + \Phi + \phi_4 + 2\phi_S - \pi \tag{65}$$

$$\zeta_- = \phi_1 + \phi_4 - \Phi, \tag{66}$$

where $\tilde{\phi}_S = \phi_S - \pi/2$, $T = t_4 - t_0$ is the period and $\Phi \equiv \phi_2 + \phi_3$ is the adiabatic phase collected in between the transitions. As a consequence, the excited state population after a single period can be written as

$$P_{\mathrm{St}} = |\langle\psi_+(t_4)|\psi(t_4)\rangle|^2 = |\langle\psi_+(t_1)|\hat{U}_{\mathrm{St}}|\psi_-(t_1)\rangle|^2 \tag{67}$$

$$= 4p(1-p)\cos\left[\Phi + \phi_S\right], \tag{68}$$

since $t_4 \sim t_1$ due to the periodicity. We thus see that the population oscillates as a function of the phase $\Phi + \phi_S$. These are called Stückelberg oscillations [4] of the transition probability. The oscillations can be interpreted physically as quantum interference between the two paths the system can evolve. The constructive interference occurs when $\Phi + \phi_S = n \cdot 2\pi$, with $n \in \mathbb{Z}$. Stückelberg oscillations have been observed in inelastic scattering cross-sections of atoms [6] and in microwave excitations of Rydberg atoms [11, 62]. The analogous interference phenomenon appearing in Mach-Zehnder interferometers has been seen in references [73, 74].

In the case of multiple successive driving periods, one can observe interference also between the periods. The situation is analogous to a multi-pass Mach-Zehnder interferometer [33]. The discretized time-evolution operator over N periods can be calculated by diagonalizing the single-period unitary time-evolution taking the N^{th} power. By averaging over many periods, we then obtain the modulated Stückelberg, i.e. steady state, population of the excited state [12, 75]:

$$P_+ = \frac{P_{\mathrm{St}}}{\sin^2\eta}, \tag{69}$$

where

$$\sin^2\eta = P_{\rm St} + \left[(1-p)\sin\zeta_+ - p\sin\zeta_-\right]^2 . \tag{70}$$

We thus see that constructive interference occurs when $P_{\rm St}$ has a maximum and $\sin^2\eta$ has a minimum. The resulting resonance conditions can be written as

$$\zeta_+ - \zeta_- = k\times 2\pi \tag{71}$$

$$\zeta_+ \quad\quad = \ell\times\pi \quad \text{(constructive interference)} \tag{72}$$

$$\zeta_- \quad\quad = m\times\pi, \tag{73}$$

respectively. The destructive interference occurs at zeroes of $P_{\rm St}$:

$$\zeta_+ - \zeta_- = (2k+1)\times\pi \quad \text{(destructive interference)}. \tag{74}$$

In the above, all constants k,ℓ,m are integers.

One can gain insight on the locations of the multiphoton resonances observed in (56) by considering the locations of constructive interference. When $p\ll 1$, the constructive interference is determined by ζ_+. Due to the small probability amplitude for transition, the system follows the adiabatic state. Thus, the phase ζ_+ is often referred to as the adiabatic phase. When $p\sim 1$ the constructive interference location is determined by the dynamical phase ζ_-, which is therefore called the diabatic phase. By assuming that the coupling Δ is small, we obtain

$$\zeta_- = \frac{\pi}{\Omega}\omega_0, \tag{75}$$

which implies the familiar multiphoton resonance condition $\omega_0 = m\Omega$. This is natural since by neglecting Δ the adiabatic eigenstates are actually the same as the stationary basis states. The above discussion also clarify the concept of the dynamic Stark shift, which in the case of finite Δ can be seen to arise from the fact that the transitions due to the probe are not between the stationary uncoupled states $|u^0_{\pm,m}\rangle$ but, instead, between the (adiabatic) eigenstates of the coupled Hamiltonian. Further progress requires additional knowledge on the transition amplitude $\sqrt{p}$.

3.3.1. Landau-Zener transition probability Value of the probability amplitude $\sqrt{p}$ depends on the explicit form of the modulation $\xi(t)$. Quite often in the case of continuous modulation, the modulation amplitude is so large that the diabatic states become degenerate at some time $t=t_0$ of the period, i.e. $\omega_0+\xi(t_0)=0$. Typically, the degeneracy is reached twice during the period. In the vicinity of the degeneracy, the Hamiltonian of the system can be approximated as

$$\hat{H}(t) = \frac{\hbar\omega_0}{2}\hat{\sigma}_z + \frac{\hbar\Delta}{2}\hat{\sigma}_x + \frac{\hbar v_{\rm LZ}t}{2}\hat{\sigma}_z, \tag{76}$$

where $v_{\rm LZ} = \hbar d\xi(t_0)/dt$ is the rate of change of the transition energy at the degeneracy point, and without any loss of generality we can assume that $\Delta>0$. This is a prototype example of the so-called Landau-Zener (LZ) Hamiltonian [1,3–5]: It describes an avoided

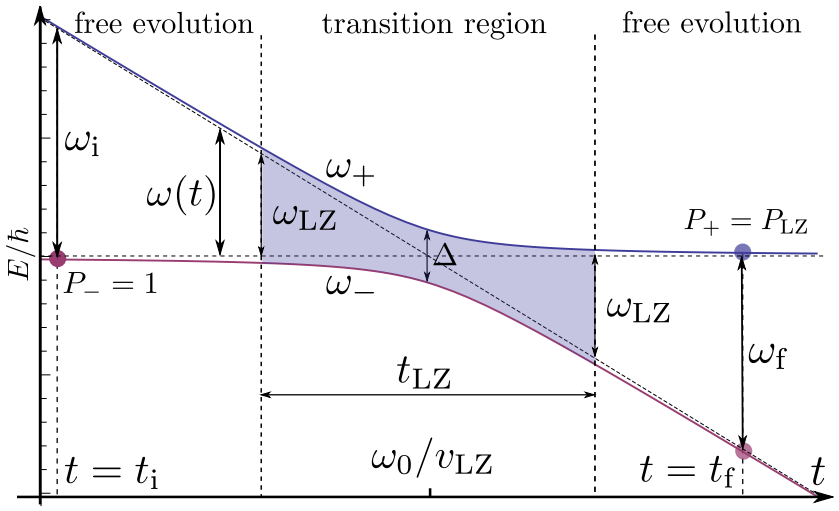

Figure 7. Schematic of an LZ process at an avoided crossing. Notice that for the plot we set the zero of energy at $-\omega(t)$.

crossing of two adiabatic energy states $|\pm\rangle$, whose eigenfrequencies can be written into the form

$$\omega_\pm(t) = \pm\frac{1}{2}\sqrt{\omega^2(t) + \Delta^2}, \tag{77}$$

where $\omega(t) = \omega_0 + v_{\rm LZ}t$. In equation (4), the computational diabatic basis is defined as $\{|\downarrow\rangle, |\uparrow\rangle\}$. The crossing of the diabatic states occurs with the rate $v_{\rm LZ}$.

The LZ-scheme is depicted in figure 7. The basic problem is to study a system that is initially in state $|-\rangle$ at $\omega_{\rm i} \equiv \omega(t_{\rm i})$, travels across the avoided crossing, and finishes in state $|+\rangle$ at $\omega_{\rm f} \equiv \omega(t_{\rm f})$. When $t_{\rm i} = -\infty$, one can find an analytic solution of the transition probability $p_{\rm LZ} \equiv p_{-\to+}(t_{\rm f} = \infty)$ between the adiabatic states. The solution to this so-called Landau-Zener problem is [1, 3–5]

$$p_{\rm LZ} = \exp\left[-2\pi\gamma\right], \tag{78}$$

where $\gamma \equiv \Delta^2/(4|v_{\rm LZ}|)$. This is the celebrated Landau-Zener formula. The adiabaticity criterion can be written into the form $\Delta^2/|v_{\rm LZ}| \gg 1$. Clearly, in the adiabatic limit $p_{\rm LZ} \approx 0$. At the opposite limit, i.e. when $\Delta^2/|v_{\rm LZ}| \ll 1$, the system follows its diabatic eigenstate and $p_{\rm LZ} \approx 1$.

In addition to the LZ-probability, one can find the whole quantum mechanical state at $t_{\rm f} = +\infty$ for an arbitrary initial state, expressed analytically in terms of Weber functions. However, the derivation is rather involved and we encourage the reader to refer to references [12, 76] for a proof with modern notation. Here, we give the resulting unitary transition matrix

$$\hat{U}_{\rm LZ} = \sqrt{1 - p_{\rm LZ}}\exp(-i\tilde{\phi}_S\hat{\sigma}_z) + i\sqrt{p_{\rm LZ}}\hat{\sigma}_y \tag{79}$$

in the adiabatic basis, where $\tilde{\phi}_S = \phi_S - \pi/2$ and

$$\phi_S \equiv \frac{\pi}{4} + \arg\left[\Gamma(1 - i\gamma)\right] + \gamma(\ln\gamma - 1) \tag{80}$$

is the so-called Stokes phase which accounts for the dynamical phase collected during the non-adiabatic time-evolution [71]. We emphasize that by describing the tunneling process with transformation (79) one implicitly assumes that the transition is located exactly at the avoided crossing. In addition, the system undergoes a free adiabatic phase evolution, characterized by the operator

$$\hat{U}_{\varphi} = \exp(-i\varphi\hat{\sigma}_z). \tag{81}$$

Consequently, the time-evolution of the general LZ process, starting from $t_\mathrm{i} = (\omega_0 - \omega_\mathrm{i})/v_\mathrm{LZ}$, and ending at $t_\mathrm{f} = (\omega_0 - \omega_\mathrm{f})/v_\mathrm{LZ}$, can be discretized by the unitary time evolution operator

$$\hat{U} = \hat{U}_{\varphi_\mathrm{f}}\hat{U}_\mathrm{LZ}\hat{U}_{\varphi_\mathrm{i}}. \tag{82}$$

In the above, $\varphi_\mathrm{i} = \int_{t_\mathrm{i}}^{t_0}[\omega_+(t) - \omega_-(t)]dt$ and $\varphi_\mathrm{f} = \int_{t_0}^{t_\mathrm{f}}[\omega_+(t) - \omega_-(t)]dt$. This is an asymptotic result and holds exactly only when $|t_\mathrm{i}|, t_\mathrm{f} \to \infty$. Similar transfer matrix method has been reported by Child in reference [70]. Also, the Weber equation and the Stokes phase appear naturally in the studies of scattering from an inverted parabolic potential [77]. Notice that the above transition matrix (82) is exactly of the same form as in equation (59).

3.3.2. Validity of the LZ-formula A vast number of avoided crossings of adiabatic energy states occuring in nature can be modelled with good accuracy in terms of the time-evolution operator given in equation (82). However in reality, the LZ-transition is not instantaneous, but has a finite duration t_LZ [17–19] that scales as

$$t_\mathrm{LZ} \sim \frac{2}{\Delta}\sqrt{\gamma}\max(1, \sqrt{\gamma}). \tag{83}$$

This is depicted in figure 7 as the shaded region. Consequently, the LZ transition is not located strictly at the avoided crossing but, on the contrary, the so-called transition region $\omega_\mathrm{LZ} \equiv |v_\mathrm{LZ}|t_\mathrm{LZ}/2$ has a finite width:

$$\omega_\mathrm{LZ} \sim \frac{\Delta}{4\sqrt{\gamma}}\max(1, \sqrt{\gamma}). \tag{84}$$

Thus, equation (82) is applicable only when $|\omega_{\mathrm{i,f}}| \geq \omega_\mathrm{LZ}$. Thus, in the adiabatic limit, the LZ formula can be applied whenever $|\omega_{\mathrm{i,f}}| \geq \Delta/4$. In the opposite limit, the situation is more involved. Even though $t_\mathrm{LZ} \to 0$ when $|v_\mathrm{LZ}| \to \infty$, the width of the transition region diverges as $\omega_\mathrm{LZ} \sim \sqrt{|v_\mathrm{LZ}|}$. In certain experimentally realisable cases [20], this means that the LZ transition matrix (79) cannot be used and one has to come up with another way of describing the non-adiabatic time-evolution.

3.3.3. Sudden approximation Whenever $\omega_\mathrm{i} \to \omega_\mathrm{f}$ can be taken to be instantaneous ($|v_\mathrm{LZ}| \to \infty$), so that the state of the system does have time to adjust itself to the change [78], one can replace equation (79) with

$$\hat{U}_{\mathrm{i}\to\mathrm{f}} = \sqrt{1 - p_\mathrm{s}} + i\sqrt{p_\mathrm{s}}\hat{\sigma}_y, \tag{85}$$

where $\sqrt{p_s} \equiv \langle +_f | -_i \rangle$ and $\sqrt{1-p_s} \equiv \langle -_f | -_i \rangle$, and p_s is real because $\hat{H}$ is symmetric. This so-called *sudden approximation* holds whenever [20, 78]

$$\left(\frac{\omega_i - \omega_f}{2}\right)^4 \frac{1}{v_{LZ}^2} \frac{\Delta^2}{\Delta^2 + \omega_i^2} \ll 1. \tag{86}$$

We emphasize that adiabaticity condition (4) and sudden approximation transition matrix (85) are valid irrespective of whether the system travels across an avoided crossing or not. On the contrary, the LZ approach relies on the fact that such a crossing lies on the temporal trajectory of the system. The sudden approximation and the LZ formula agree only when the system travels instantaneously across an avoided crossing and $|t_i|, t_f \to \infty$. For finite t_i and t_f, one has to rely on the sudden approximation results.

3.3.4. Multi-level Landau-Zener In their original papers, Landau, Zener and others [1, 5] implicitly assumed that apart from the two adiabatic energy states considered, the other states do not undergo an avoided crossing. A generalization to this is the so-called general multi-level LZ Hamiltonian

$$\hat{H} = \hat{\Delta} + \hat{v}t, \tag{87}$$

where $\hat{\Delta}$ and $\hat{v}$ are Hermitian $n \times n$ matrices. Brundobler and Elser [79] conjectured that sequential LZ approximation gives an exact result in some multi-level crossing cases. Shytov [80] showed that the above conjecture holds for the existent exact solutions for Hamiltonian (87).

3.3.5. Dynamic and geometric phases via control of detuning In general, a shift Δ in the transition frequency of a qubit results in the accumulation of a phase Δt under the time evolution. One immediate application of this observation is in the realization of phase gates for quantum computing. Another application is quantum simulation: by changing randomly the detuning, one can emulate weak localization, with the detuning playing the role of the phase accumulated by an electron scattered as it moves in a disordered medium [81]. Similar ideas can be used to simulate time-reversal symmetry and universal fluctuations, in this case by driving the system across the Landau-Zener transition using a bichromatic modulation [82, 83].

Even with a fixed but nonzero detuning it is possible to probe fundamental effects such as Berry's phase accumulation for closed adiabatic trajectories in the Hamiltonian parameter space [84]. Here the analogy between a spin-1/2 in a magnetic field of variable direction and the qubit driven by a microwave field with externally-tunable detuning and amplitude is employed. Indeed, for a qubit with Larmor frequency ω_0 driven by a field with frequency ω_d, phase φ, and Rabi coupling strength ξ_d, we have in general

$$H = \frac{\hbar\omega_0}{2}\hat{\sigma}_z + \hbar\xi_d \cos(\omega_d t + \phi)\hat{\sigma}_x. \tag{88}$$

In a rotating frame at the drive frequency, defined by the unitary $\hat{U}(t) = \exp(i\omega_d t\hat{\sigma}_z/2)$ we transform the Hamiltonian to $\hat{H} \to \hat{U}\hat{H}\hat{U}^{-1} - i\hbar\hat{U}(d\hat{U}^{-1}/dt)$ and neglect the fast

rotating terms. This yields

$$\hat{H} = \frac{\hbar}{2}\left[\delta_d\hat{\sigma}_z + \xi_d\cos(\phi)\hat{\sigma}_x + \xi_d\sin(\phi)\hat{\sigma}_y\right], \tag{89}$$

where the detuning is $\delta_d = \omega_0 - \omega_d$. This is a Hamiltonian of the type $\hat{H} = -(\hbar/2)\vec{R}\vec{\sigma}$, representing a spin-1/2 in a magnetic field. By keeping the detuning fixed and changing the phase φ from 0 to 2π, the vector $\vec{R}$ describes a cone. The Berry phase accumulated is then equal to the solid angle encompassed by this cone,

$$\gamma_{\mathrm{B}} = 2\pi\left(1 - \frac{\delta_d}{\sqrt{\xi_d^2 + \delta_d^2}}\right). \tag{90}$$

This phase can be measured in a Ramsey interference setup, with a first $\pi/2$ pulse preparing a superposition of $|0\rangle$ and $|1\rangle$, followed by the adiabatic manipulation of the qubit Hamiltonian, and finally a $\pi/2$ pulse is used to read the accumulated phase. In practice, it is convenient to use a spin-echo sequence, which not only reduces the noise caused by the dephasing but also cancels exactly the nonadiabatic dynamical phase.

3.4. Incoherent modulation

It is well known that off-diagonal external fluctuations in a quantum system can induce transitions between energy eigenstates, and thus lead to dissipation. This is known in the literature as the fluctuation-dissipation theorem [85]. In addition, also the transition frequency can experience incoherent and typically low-frequency fluctuations, which do not lead into resonant energy exchange between the system and its environment but still cause losses in the quantum coherence due to the random and unequal phase evolution of the eigenstates. We will refer to this as dephasing or classical noise and emphasize a distinction to decoherence, which is seen as a consequence of environmental entanglement [86]. Review for quantum noise has been given in reference [24].

As the deterministic modulations would serve as a possible generator for quantum gates and quantum simulations [87], the random modulations can, in principle, be used as an analog simulator of atomic dephasing effects caused by different environments [88]. For example, the dephasing due to quantum entanglement with environment has been simulated with classical fluctuations of parameters in ion traps qubits with engineered reservoirs [89, 90], and with superconducting qubits [28] with experimentally controllable noise in the magnetic flux bias. Understanding of the nature and origins of dephasing is essential in all fields of experimental quantum physics, and becomes crucial in the development of quantum computational devices [91–93].

In the conventional theory of classical dephasing noise, the essentially weak and linear quantum mechanical coupling to an external bath of fluctuators is approximated as a classical incoherent modulation of the energy levels of the studied system. In atomic ensembles and condensed-matter systems, such incoherent transition frequency modulations can occur due to variations of the electronic state populations, chemical potential, molecular conformation, effective magnetic fields, lattice vibrations, micro-electric fields producing ac-Stark shifts *etc.* [26, 94–98]. The spectrum for an atom (or

an atomic ensemble) whose transition frequency changes randomly is known since the early days of NMR physics [26, 94] with the name motional averaging or narrowing due to atom movement where the uncertainty of transition frequency was typically caused by temporal variations of the local magnetic field for rotating or moving atoms, or exchange narrowing due to exchange interactions of electronic magnetic moments. In all these situations, one has a large number of particles and the experimentalist can only indirectly attempt to change the properties of the external fluctuation processes, generally by modifying temperature or pressure.

Different methods to suppress dephasing have been developed since the invention of the spin echo technique [99], which uses designed pulse sequences to eliminate the variations in the local external magnetic environment. Similar procedure has been developed for a generic quantum mechanical two-level system, i.e. a qubit, where the dephasing effects arising from coupling to a thermal bath of harmonic oscillators is suppressed by repeated time-reversal operations on the coupled system and bath. This is referred to as quantum bang-bang control [100]. Quantum bang-bang is a special case of dynamical decoupling [101], where the irreversible open system evolutions are manipulated with external controllable interactions. In addition, the dephasing can be suppressed by actively monitoring and conditionally correcting the quantum state quantum error-correction codes [102, 103]. Also, suppression of qubit dephasing by superconducting qubit motion has been observed [104].

3.4.1. Generating function The modulated spectrum (28) is again determined by the phase factor

$$A(t) = \left\langle e^{i\int_0^t \xi(\tau)d\tau} \right\rangle = \left\langle e^{i\int_0^t \xi(\tau)d\tau} \right\rangle_\xi = \int e^{i\int_0^t \xi(\tau)d\tau} P[\xi(t)]d\xi, \tag{91}$$

where the first expectation value is calculated over the whole ensemble. In addition to averages over ensemble of particles, one can study individual transitions and averages over different realisations of incoherent modulations, denoted as $\langle\cdot\rangle_\xi$ in the second equality. The third equality gives the means to calculate the average in terms of the probability distribution $P[\xi(t)]$ of different realisations of $\xi(t)$. The connection to the dephasing of a two-level system can be obtained by considering the decay of the off-diagonal density matrix element $\hat{\rho}_{01} = \rho_{01}|0\rangle\langle 1|$:

$$\rho_{01}(t) \equiv \langle\hat{\rho}_{01}(t)\rangle_\xi = \rho_{01}(0)e^{-i\omega_0 t}A^*(t), \tag{92}$$

where $\hat{\rho}(t)$ is the representation of the density operator in the interaction picture. Later, we will show that with certain assumptions for the noise process, $A(t)$ can be written into the typical form of a dephasing element: $A(t) \sim e^{-|t|\Gamma_\phi}$, where the Γ_ϕ is the effective dephasing rate.

Equation (91) describes classical noise as phase diffusion due to the random fluctuations. It is the characteristic functional of the stochastic process $\xi(t)$ and, thus,

also its moment and cumulant generating function [105–107]:

$$A(t) = \sum_{n=0}^{\infty} \frac{i^n}{n!} \int \cdots \int \langle \xi(t_1) \cdots \xi(t_n) \rangle_\xi dt_1 \cdots dt_n \tag{93}$$

$$= \exp\left[\sum_{n=1}^{\infty} \frac{i^n}{n!} \int \cdots \int \langle \xi(t_1) \cdots \xi(t_n) \rangle_\xi^c dt_1 \cdots dt_n \right], \tag{94}$$

where $\langle \xi(t_1) \cdots \xi(t_n) \rangle_\xi$ and $\langle \xi(t_1) \cdots \xi(t_n) \rangle_\xi^c$ are the n^{th} moment and cumulant of the random process $\xi(t)$, respectively. Without any loss of generality we can assume that the average modulation over different realisations of flucutations vanishes, i.e. $\langle \xi(t) \rangle_\xi = 0$. We will also simplify our discussion by assuming that the noise processes are stationary:

$$\langle \xi(t_1 + \tau) \cdots \xi(t_n + \tau) \rangle = \langle \xi(t_1) \cdots \xi(t_n) \rangle, \tag{95}$$

i.e. they are not affected by a shift in time. The above condition should hold for all n, τ and $t_1, \ldots, t_n$. The detailed modelling of the environment can be done in a couple of ways. Near the thermodynamic equilibrium, many different types of fluctuations can be treated as Gaussian. Such Gaussian models of the fluctuations can be treated universally with a linear coupling to a bath of harmonic oscillators [108], which in the case of a single transition is the so-called spin-boson model [13, 109]. However, not all noise sources are Gaussian. Typical counter-examples arise when either the bath [110] or the coupling to the bath [92] is nonlinear. Inherently non-Gaussian random telegraph noise (RTN) of the transition energy is created when the environment goes through random and discrete frequency fluctuations [26, 94]. Nevertheless, the central limit theorem states that when there are several RTN fluctuators the collective statistical behaviour should recover Gaussian form. Gaussian and random-telegraph noises belong to a small set of stochastic processes that are experimentally relevant and also allow analytic solutions. Generally, one has to rely on numerical solutions of the stochastic master equation for the system [58, 111].

3.4.2. Gaussian modulation The characteristic of a Gaussian random process is that the cumulants above $n = 2$ are zero. When $\langle \xi(t) \rangle_\xi = 0$, we have that $\langle \xi(t_1)\xi(t_2) \rangle_\xi^c = \langle \xi(t_1)\xi(t_2) \rangle$ [105], and the random process is characterized solely by the second order moment. As a consequence, the probe spectrum of the incoherently modulated transition is completely determined once the noise power spectral density

$$S_\xi(\omega) = \int_{-\infty}^{\infty} \langle \xi(t)\xi(0) \rangle e^{i\omega t} dt \tag{96}$$

is known. Spectral density encapsulates the physical properties of the environment that are responsible for the incoherent modulations [86]. Thus, in order to find the experimentally relevant form for the power spectral density of the classical dephasing noise, one has to have a detailed microscopic model for the processes that create the fluctuations. Prototype examples include the spin-boson model [13], spin-fluctuator model [112–114], and quasiparticle tunnelling [115].

The dynamical phase factor can be written in terms of the spectral density as

$$A(t) = \exp\left[-\frac{1}{2}\int_0^t\int_0^t \langle\xi(t_1)\xi(t_2)dt_1dt_2\right] \tag{97}$$

$$= \exp\left[-\frac{1}{2}\int_{-\infty}^{\infty}\frac{d\omega}{2\pi}S_\xi(\omega)\frac{\sin^2(\omega t/2)}{(\omega/2)^2}\right], \tag{98}$$

where in the second equality we have substituted the inverse Fourier transform of (96), and conducted the time-integrals. This is a standard result in the theory of decoherence.

Consider then times much larger than the coherence time t_c of the autocorrelation function, i.e. $t \gg t_c$. As a consequence, the function $\sin^2(\omega t/2)/(\omega t/2)^2$ is strongly peaked at $\omega \approx 0$, thus we see that its behaviour is of window-type. Accordingly, the off-diagonal element of the density operator can be written into the form

$$\rho_{01}(t) = \rho_{01}(0)e^{-i\omega_0 t - |t|\Gamma_\phi}, \tag{99}$$

where we have defined the decoherence rate in terms of the zero frequency fluctuations as

$$\Gamma_\phi = \frac{1}{2}S_\xi(\omega = 0), \tag{100}$$

provided that the spectral density is defined at $\omega = 0$. This loss of quantum coherence occurs due to the pure dephasing of the energy levels. In addition, another contribution to the decoherence rate Γ_2 comes from the transverse fluctuations [91].

On the other hand, let us consider $1/f$-noise, with spectral density $S(\omega) \sim 1/\omega$, which is the experimentally relevant dephasing noise in the case of solid-state qubits [116–118]. By restricting the discussion into time scales $t < \omega^{-1}$ where $S(\omega)$ is negligible, we can make a short-time expansion for the window-function and obtain

$$\rho_{01}(t) = \rho_{01}(0)e^{-i\omega_0 t - (t\Gamma_\phi^{1/f})^2}, \tag{101}$$

where

$$\Gamma_\phi^{1/f} = \left[\int_{-\infty}^{\infty}\frac{d\omega}{4\pi}S_\xi(\omega)\right]^{\frac{1}{2}}. \tag{102}$$

Such nonlinear exponential decay is characteristic of $1/f$-noise [93]. However, it is not at all certain that real experimental $1/f$-noise is Gaussian [119].

3.4.3. Increasing the dephasing time of qubits by motional narrowing Consider now what happens when instead of a single qubit we have a system of N physical qubits, positioned at different locations. The Hamiltonian of such a system, in the absence of driving or any other interactions, reads

$$\hat{H} = \frac{\hbar}{2}\sum_{j=1}^{N}(\omega_0^{(j)} + \xi_j)\hat{\sigma}_z^{(j)}(t), \tag{103}$$

where j is the qubit index and $\omega_0^{(j)}$ is the bare frequency.

Now, one can relay a logical qubit between the physical qubits j by using SWAP gates, with the logical qubit spending an equal time t/N at each physical qubit. The

swapping operation is assumed to be faster than the single-qubit dephasing time and has unit fidelity. In this case, a state $\alpha_j|0\rangle_j + \beta_j|1\rangle_j$ imprinted on the j'th qubit is moved to qubit k, which was initially in the state $\alpha_k|0\rangle_k + \beta_k|1\rangle_k$,

$$(\alpha_j|0\rangle_j + \beta_j|1\rangle_j) \otimes (\alpha_k|0\rangle_k + \beta_k|1\rangle_k) \stackrel{SWAP}{\longrightarrow} \tag{104}$$

$$(\alpha_j|0\rangle_k + \beta_j|1\rangle_k) \otimes (\alpha_k|0\rangle_j + \beta_k|1\rangle_j) \tag{105}$$

Let us assume now that there is no correlation between the noises at different qubits, in other words $\langle \xi_j(0)\xi_k(t)\rangle = 0$ if $k \neq j$, while the noise of each qubit has a power spectral density $S_\xi^{(j)}(\omega)$. This allows us to factorize the averages,

$$\rho_{01}(t) = \Pi_{j=0}^N \langle e^{-i\int_0^t dt' \xi^{(j)}(t')} \rangle_{\xi^{(j)}}, \tag{106}$$

and further

$$\rho_{01}(t) = \rho_{01}(0) e^{-\frac{1}{\pi}\int d\omega \frac{\sin^2 \frac{\omega t}{2N}}{\omega^2} \sum_{j=1}^N S_\xi^{(j)}(\omega)}. \tag{107}$$

We can already see that the decay of the off-diagonal matrix element contains a quite nontrivial dependence on N. To see this more clearly, consider the low-frequency 1/f noise, which is the experimentally-relevant dephasing noise in the case of superconducting qubits. The function $\sin^2(\omega t/2N)/\omega^2 = (t/2N)^2 \mathrm{sinc}^2(\omega t/2N)$ appearing in equation (107) is of window type, with width given by the first-order zeroes $\pm 2\pi N/t$. Thus, if the noise $S(\omega) \sim 1/\omega$ is negligible at $\omega = \pm 2\pi N/t$, we can expand the window function around small ω, obtaining

$$\rho_{01}(t) = \rho_{01}(0) e^{-t^2/\tau_{\mathrm{deph}}^2}, \tag{108}$$

with

$$\tau_{\mathrm{deph}} = \sqrt{2N/\sigma}, \tag{109}$$

where $\sigma = (2\pi)^{-1} \int d\omega S_\xi^{(j)}(\omega)$ is the low-frequency noise power of each physical qubit. In other words the dephasing time when N physical qubits are is increased by a factor of $\sqrt{N}$ compared to the single-qubit dephasing. This phenomenon is qualitatively similar to the motional narrowing effect described in more detail in the following section. Let us summarize the mechanism here: for low-frequency noise the dephasing depends quadratically on time, therefore each physical qubit contributes to the dephasing by an amount proportional to $(t/N)^2$. The total dephasing coefficient in the exponent is the sum of all N contributions from each physical qubit, and as result the scaling of the exponent is as $-t^2/N$.

This prediction has been recently tested experimentally by measuring Ramsey interference fringes for a logical qubit moved between $N = 2$ and $N = 3$ physical qubits (phase qubits and X-mons). Ramsey experiments can indeed provide a direct measurement of τ_{deph}. In Ramsey experiments, a $\pi/2$ pulse is applied to the qubit to the $|0\rangle \to |1\rangle$ transition putting these two states in an equal superposition, then the qubit is left to evolve freely during a time t, and finally another $\pi/2$ pulse is applied to read the phase difference accumulated between the two states during the time interval t. In this

case the envelope of the oscillation in the population measured in the experiments is of the form

$$e^{-\frac{1}{2}\Gamma_1 t - \frac{t^2}{\tau_{\rm deph}^2}}, \tag{110}$$

where Γ_1 is the single-qubit relaxation rate. The relaxation rate can be measured in a separate experiment, for example by exciting the qubit with a π pulse and measuring the exponential decay of the population in the state $|1\rangle$. The Gaussian decay rate with time constant $t_{\rm deph}$ can therefore be extracted from the experiment.

3.4.4. Random telegraph noise and motional effects When the incoherent modulation is non-Gaussian, the contributions from higher order correlation functions become relevant. Typical example arises in real and artificial atomic systems with environments whose fluctuations result in random jumping between two different values of the transition energy, leading into characteristic phenomena of motional averaging and narrowing [26,94] of spectral lines as a function of the jumping amplitude. Such processes occur naturally in atomic ensembles and condensed-matter systems which experience variations in the electronic state populations, chemical potential, molecular conformation, effective magnetic fields, lattice vibrations, microelectric fields producing ac-Stark shifts and so on [26, 94–98]. Also, discrete and random modulations of the transition frequency arise when one studies $1/f$-noise caused by random two-level fluctuators in superconducting qubits [120]. Closely related phenomena include the Dyakonov-Perel effect [121], the Dicke line narrowing of Doppler spectra [122], and the quantum Zeno effect [123].

The incoherent modulation of the transition energy between two discrete values can be modelled as a random-telegraph noise (RTN) created by a symmetric two-valued Poisson fluctuation process. The statistical properties of the RTN are, thus, described by the factorization rule [124]

$$\langle \xi(t_1)\xi(t_2)\cdots\xi(t_n)\rangle_\xi = \langle \xi(t_1)\xi_(t_2)\rangle_\xi \langle \xi(t_3)\cdots\xi(t_n)\rangle_\xi. \tag{111}$$

Thus, the RTN is inherently non-Gaussian. Nevertheless, a symmetric ($\langle\xi(t)\rangle_\xi = 0$) RTN is completely defined by the second order moment (autocorrelation function)

$$\langle \xi(t)\xi(0)\rangle_\xi = \xi^2 e^{-2\Omega|t|}, \tag{112}$$

where ξ is the fluctuation amplitude and Ω is the average fluctuation frequency. A Gaussian process with similar autocorrelation function is called Ornstein-Uhlenbeck process, and used to characterize Brownian motion [125].

A possible generalization for the symmetric random telegraph noise would be that one allows different correlations $\langle \xi(t_{n+1})\xi(t_n)\rangle$ between the sequential values of a given realisation of the noise, which could modelled, for example, so that the values of the process $\xi(t)$ would be sampled from a stationary distribution $P(\xi)\,{\rm d}\xi$ instead of choosing $\pm\xi$ one after another. Another generalization would be that the dwelling (waiting) time $t = t_{n+1} - t_n$ would be distributed otherwise than exponentially. Experimentally, one can attempt to control the noise processes and correlations by invoking the methods used in a superconducting qubit measurement [28] where the RTN of the transition energy was

simulated by creating random magnetic flux pulses with an arbitrary waveform generator. In such case, the generalizations need only reprogramming of the waveform generator, and it could enable, e.g., simulation of motional effects for e.g. continuous heavy-tailed stationary distributions [126]. Nevertheless, we consider here the pure random telegraph noise.

Without going deeper in the qubit dynamics, two intuitive asymptotic limits can be found by a simple argumentation. First, in the fast jumping limit, the energy fluctuations $\Delta E = \hbar\xi$ occur so frequently, with average spacing $\Delta t = \Omega^{-1}$, that the ability to resolve them is limited by the profound energy-time uncertainty relation [23]: $\Delta E \Delta t = \hbar\xi/\Omega \gtrsim \hbar$. Then, external driving or measuring pulse observes that the transition frequency is dynamically averaged to ω_0, although the system is at any time in either one of the states $\omega_0 \pm \xi$ and spends no time in between. This is referred to as motional averaging. In contrast to that, when the mean time $\Delta t = \Omega^{-1}$ between the jumping events is long enough so that $\xi/\Omega \gg 1$, then one can consider the system as a statistical average over two systems with transition frequencies $\omega_0 \pm \xi$. This is denoted as the slow jumping limit. In this limit, one can simply ignore the dynamics of the $\xi(t)$-process as measurement or control pulses needed to resolve the energy difference $\Delta E = \hbar\xi$ are shorter than Ω^{-1}. In the cross-over region, neither the statistical nor dynamical averaging works and one has to take into account the frequency fluctuations explicitly.

Again, the accumulated phase factor $A(t) = e^{i\zeta(t)}$ is evidently an important quantity. Sample paths of $\zeta(t) = \int_0^t \xi(\tau)d\tau$ are shown in figure 8. In the slow jumping limit (blue, $\Omega \ll \xi$), the slopes are well resolvable between the jumping events. In contrast to that, in the fast jumping limit (green, $\Omega \gg \xi$), the trajectory becomes diffusive and the slopes are indistinguishable. In this limit, the spectral broadening, i.e., the uncertainty of the frequency becomes proportional to the diffusion coefficient ξ^2/Ω of the process [127]. For a physical insight, one can draw an analogy between the $\xi(t)$-process and a randomly sign-changing velocity of a 1D particle, which implies that the accumulated phase $u(t)$ is analogous to the position of the 1D particle. Deriving further, the transition from the slow jumping to the fast jumping limit is analogous to the transition from the ballistic to the diffusive evolution under an increasing rate of elastic collisions, i.e., the rate of sign changes in the 1D velocity [126].

For the RTN process $\xi(t)$, equation (28) gives (see references [26, 28, 94, 124])

$$S(\omega) = \frac{g_P^2}{2} \frac{2\chi\xi^2 + \Gamma_2\left[(\Gamma_2 + 2\Omega)^2 + \delta^2 + \xi^2\right]}{\left[\xi^2 - \delta^2 + \Gamma_2(\Gamma_2 + 2\Omega)\right]^2 + 4(\Gamma_2 + \chi)^2\delta^2}, \tag{113}$$

where $\delta = \omega_0 - \omega$. The full spectrum reduces to the intuitive forms at the asymptotic limits

$$S(\omega) = \frac{g_P^2}{4} \frac{\Gamma_2 + \Omega}{\left[\delta \pm \xi)\right]^2 + (\Gamma_2 + \Omega)^2}, \ \Omega \ll \xi, \tag{114}$$

$$S(\omega) = \frac{g_P^2}{2} \frac{\Gamma_2 + \xi^2/2\Omega}{\delta^2 + (\Gamma_2 + \xi^2/2\Omega)^2}, \ \Omega \gg \xi, \tag{115}$$

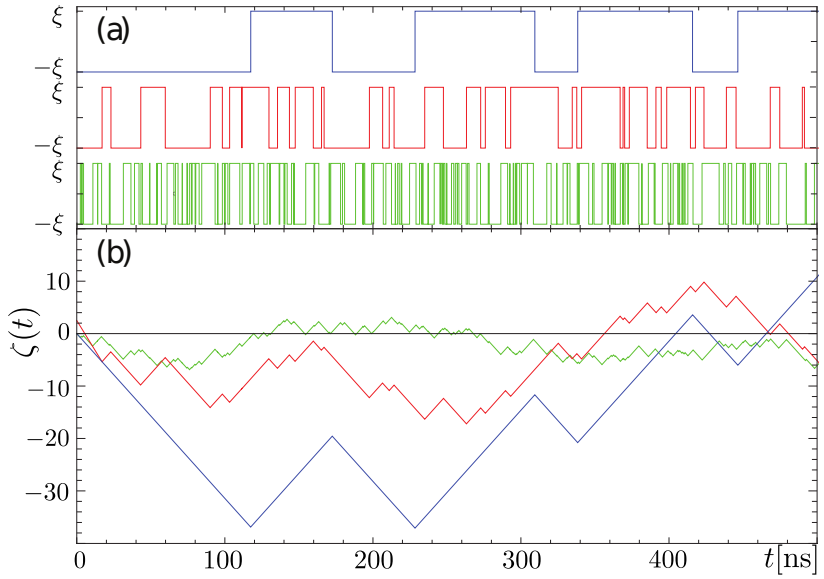

Figure 8. (a) Sample trajectories of $\xi(t)$ at jumping frequencies $\Omega = 10$ MHz (blue), 100 MHz (red), and 400 MHz (green) measured in arbitrary frequency (time) units and shifted vertically for clarity. (b) The corresponding trajectories of the accumulated phase $\zeta(t) = \int_0^t \xi(\tau)\,\mathrm{d}\tau$ with $\xi/2\pi = 5$ in the same arbitrary units.

which confirms the intuitive argumentation of the slow and fast jumping limits. In the slow jumping limit, the qubit absorbs at $\omega = \omega_0 \pm \xi$ and the decoherence rate is increased by Ω, in agreement with the mean lifetime $1/\Omega$ of the energy levels $\omega_0 \pm \xi$ (exchange broadening [94]). At the fast jumping limit, the qubit absorbs at the average frequency $\omega = \omega_0$ with the excess $\xi^2/2\Omega$ of the decoherence rate. In the fast jumping limit, we see that the decoherence rate is inversely proportional to the fluctuation frequency. This is referred to as motional narrowing [26, 94].

The effects of power broadening due to, e.g., the probe signal can be taken into account by calculating the excited state population in the steady state with stochastic master equation [28, 128]. This can be done analytically by employing the final value theorem, and the result can be written as

$$P_e = \frac{g_P^2\Omega[2\xi^2\Omega + \Gamma_2(\Omega_p^2 + 4\Omega^2)}{D} \tag{116}$$

where g_P is the probe amplitude, $\Omega_p \equiv \sqrt{\delta^2 + g_P^2}$, and

$$\begin{aligned} D = {} & 4\Gamma_1\xi^2\Omega\delta|\delta| + 2\Gamma_1\xi^4\Omega + \xi^2[g_P^2\Gamma_1\Gamma_2 + 4\Omega^2(g_P^2 + 2\Gamma_1\Gamma_2)] \\ & + 2\Omega(\Omega_p^2 + 4\Omega^2)\left[g_P^2\Gamma_2 + \Gamma_1[\Gamma_2^2 + \delta^2]\right]. \end{aligned} \tag{117}$$

4. Harmonic oscillator

The harmonic oscillator is the most commonly used model in physics, both in its classical and quantum versions. The generic Hamiltonian of a harmonic oscillator

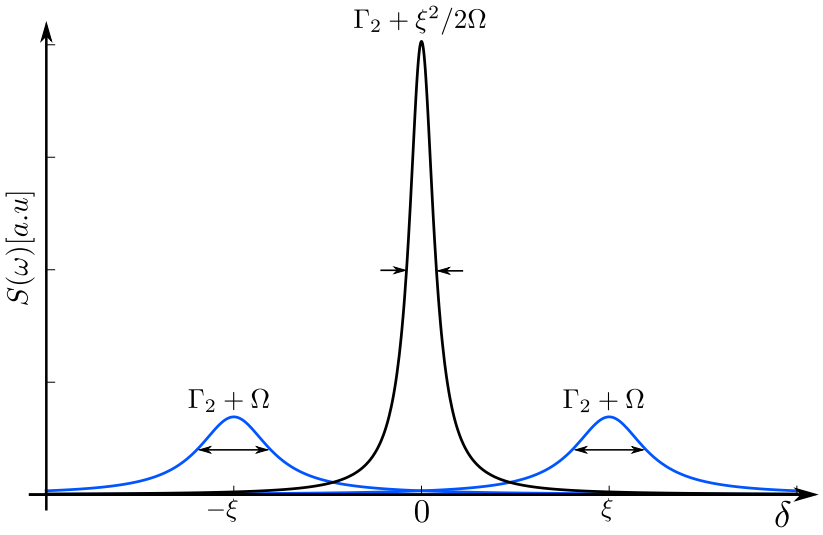

Figure 9. Schematic of the motional effects. In the slow jumping limit ($\Omega \ll \xi$, the qubit absorbs energy at the frequencies $\omega = \omega_0 \pm \xi$ (blue). The linewidth is given by $\Gamma_2 + \Omega$. When the jumping frequency is increased to $\Omega \gg \xi$, the two resonance peaks experience motional averaging and merge into a single peak at $\omega = \omega_0$. Also, the width of the peak experiences motional narrowing, and is given by $\Gamma_2 + \xi^2/2\Omega$.

is $H = \frac{1}{2m}p^2 + \frac{1}{2}kx^2$. Here we have used the canonical variables x and p, which can correspond to a particle's coordinate and momentum, and the parameters k and m, which can correspond to the spring constant and the mass of the particle. The eigenfrequency of the oscillator is $\omega_0 = \sqrt{k/m}$. After quantization, the Hamiltonian can be written $\hat{H} = \hbar\omega_0(\hat{a}^\dagger\hat{a} + \frac{1}{2})$, where $\hat{a}^\dagger$ and $\hat{a}$ are creation and annihilation operators. The energy spectrum consists of equally spaced levels $E_n = \hbar\omega_0(n + \frac{1}{2})$ with $n = 0, 1, \ldots$.

Besides the two-state system, the harmonic oscillator is another basic model for studying frequency modulation. The frequency can be modulated by changing nonpropotionally either m or k resulting in a different eigenfrequency $\omega_1 = \omega_0(1 - \frac{\Delta m}{2m} + \frac{\Delta k}{2k})$ to the first order in the displacements Δm and Δk. Measuring the changes in an oscillator can be used as an ultra-sensitive probe to various physical phenomena. These type of approaches have demonstrated remarkable single-atom [129], single-molecule [130–132], single-spin [133] and sub 100 nm imaging [134] resolutions. We concentrate here on reviewing some quantum phenomena of frequency modulations of an oscillator, that is, squeezing and dephasing.

4.1. Squeezing by sudden frequency modulations

Let us consider a harmonic oscillator with a Hamiltonian

$$\hat{H}_0 = \hbar\omega_0\Big(\hat{a}_0^\dagger\hat{a}_0 + \frac{1}{2}\Big), \tag{118}$$

and assume that the frequency of the oscillator changes suddenly $\omega_0 \to \omega_1$ resulting in a new Hamiltonian

$$\hat{H}_1 = \hbar\omega_1\Big(\hat{a}_1^\dagger\hat{a}_1 + \frac{1}{2}\Big). \tag{119}$$

With the term 'sudden' we mean a change occurring in the time scale much smaller than any natural timescale of the system, such as the oscillation periods $2\pi/\omega_i$. In a sudden change, there is no time evolution during the transition, that is, the quantum state stays completely untouched, only the Hamiltonian changes $\hat{H}_0 \to \hat{H}_1$ [21, 78]. For example, the ground state of the Hamiltonian before the transition can be a non-trivial excited state of the Hamiltonian after the transition.

Let us study the transition $\hat{H}_0 \to \hat{H}_1$ and assume, for simplicity, that the frequency change occurs due to change in the spring constant. Notice that in equations (118)-(119) the creation $\hat{a}$ and destruction $\hat{a}^\dagger$ operators are not identical before and after the change since they depend explicitly on the eigenfrequency of the oscillator,

$$\hat{a}_i = \sqrt{\frac{m\omega_i}{2\hbar}}\left(\hat{x} + \mathrm{i}\frac{\hat{p}}{m\omega_i}\right), \tag{120}$$

written with the help of the position $\hat{x}$ and momentum $\hat{p}$ operators. Since the quantum state stays unchanged also physical observables such as position $\langle\hat{x}\rangle$ and momentum $\langle\hat{p}\rangle$ cannot change either during the transition. This gives a justification to solve the relation between old and new bosonic creation and destruction operators in equation (120) using the unchanged position and momentum operators:

$$\hat{a}_1 = \frac{\omega_1+\omega_0}{2\sqrt{\omega_0\omega_1}}\hat{a}_0 + \frac{\omega_1-\omega_0}{2\sqrt{\omega_0\omega_1}}\hat{a}_0^\dagger = \cosh r\,\hat{a}_0 - \sinh r\,\hat{a}_0^\dagger. \tag{121}$$

This Bogoliubov transformation is in fact a squeezing transformation $\hat{a}_1 = \hat{S}(r)\hat{a}_0\hat{S}^\dagger(r)$ with the squeezing unitary $\hat{S}(r) = \exp(\frac{r}{2}\hat{a}_0^2 - \frac{r^*}{2}(\hat{a}_0^\dagger)^2)$ and the squeezing parameter $r = \ln\sqrt{\omega_0/\omega_1}$. After a sudden change of the frequency, the quantum state of the oscillator becomes squeezed [135–137]. Squeezed states are of great interest for high-precision measurements since for them the uncertainties of the two quadratures are unequal. Assuming $\omega_0 > \omega_1$, the uncertainty of the other quadrature is squeezed by the factor of $\exp(-r) = \sqrt{\omega_1/\omega_0}$ and the other increased by the factor of $\exp(r) = \sqrt{\omega_0/\omega_1}$ and the product still satisfies the Heisenberg uncertainty principle, see more in reference [25].

It is quite likely that in the practical point of view that the amount of squeezing production that can be achieved a single frequency change is limited. To overcome this limitation, it is natural to ask whether it would be possible to generate squeezing by repeating a cycle where the sudden change $\omega_0 \to \omega_1$ is followed by a slow, adiabatic change $\omega_1 \to \omega_0$. Notice that one cannot make another sudden change back since it would invert the squeezing achieved during the first part of the cycle. Let us denote the overall time-dependence of modulated frequency as $\omega(t)$. Then we can use a time-dependent version of the squeezing transformation (121) $\hat{S}(t) = \hat{S}(r(t))$ to express the effective time-dependent Hamiltonian in a fixed basis [138] $\hat{H}'(t) = \hat{S}(t)\hat{H}\hat{S}^\dagger(t) - \mathrm{i}\hbar[\partial_t\hat{S}(t)]\hat{S}^\dagger(t)$:

$$\hat{H}'(t) = \hbar\omega(t)\Big(\hat{a}_0^\dagger\hat{a}_0 + \frac{1}{2}\Big) + \frac{\mathrm{i}\hbar}{4}\frac{\mathrm{d}\ln\omega(t)}{\mathrm{d}t}\left[\hat{a}_0^2 - (\hat{a}_0^\dagger)^2\right]. \tag{122}$$

This form clearly shows that rapid changes in $\omega(t)$ will generate squeezing through the latter term in the Hamiltonian. Notice that the squeezing by Hamiltonian (122) occurs along a fixed direction of the X-quadrature in the phase space. When considering incremental squeezing it is important to notice the squeezed state rotates in the phase space by the linear part of Hamiltonian (122) such that the period of the frequency modulation cycle needs to be timed so that sudden change of the frequency incrementally increases the squeezing always along the same direction. Squeezing production via this route was originally studied and proposed in references [139, 140] in a general setting. Recently, new theoretical interest has arisen in this problem [138, 141] motivated by superconducting circuit technology where the superconducting oscillator parameters are rapidly and accurately tunable.

Indeed, a transmission line is described as an ensemble of harmonic modes associated to each wave vector. If the line contains tunable elements such as SQUID loops, then it is possible to change rapidly the frequency of these modes. In the Lagrangian of the transmission line, this means changing the inductance per unit length, while the capacitance per unit length remains constant. If this change is realized over a distance comparable to the wavelength of the mode, one can regard this as a change in the speed of propagation or in the index of refraction. If the change is local, over a distance much shorter than the wavelength, then it can be assimilated to a change in a boundary condition of the field. Using this observation, one can create parametric perturbations and observe effects that are analogous to those expected in vastly different systems: from vacuum instability due to strong electric fields (Schwinger effect) to the Hawking radiation emitted at the event horizon of black holes [142]. An example of such an effect that has been observed is the dynamic Casimir effect [143, 144]. The (static) Casimir effect is the attraction between two plates of metal that realize boundary conditions for the electromagnetic field due to different vacuum energies of the field between and outside the plates. One wonders what happens if the plates move: in this case, real photons are generated from vacuum fluctuations. To realize this experimentally, one could use either a single modulated SQUID at the end of the line [143] or many SQUIDs that form a leaky cavity [144]: in both cases, this creates an effective tunable boundary condition for the incoming vacuum-state field. The observed photons are two-mode squeezed, as one expects from theoretical considerations similar to those leading to equation (122).

A related development is the recent surge of interest in using similar devices as parametric amplifiers [145]. In this case, the input field is not the vacuum but a real signal that we wish to amplify. In nanoelectronics, these amplifiers have important advantages over semiconductor-based HEMT amplifiers: the added noise referred to the input is near the limit permitted by quantum physics and equals 1/2 for large gain, thus enabling a consistent increase in the signal-to-noise ratio in sensitive measurements. Currently they are indispensable in the research on superconducting qubits. Several designs based on modulated SQUIDs in ring configuration [146, 147] or arrays of SQUIDs were proven successful [148, 149], and wideband traveling-wave versions based on the phase matching of the four-wave mixing by using resonant inclusions were developed

recently [150].

4.2. Dephasing by stochastic frequency changes

Let us now turn attention to stochastic variation of the frequency of the oscillator, $\omega(t) = \omega_0 + \xi(t)$. Here, $\xi(t)$ denotes the displacement of the frequency from the mean value ω_0. Furthermore, $\xi(t)$ is assumed to be a stochastic process whose time-evolution is characterized by probabilistic laws. In the perspective of Hamiltonian (122), every time there is a change in the stochastic displacement $\xi(t)$ one observes also squeezing production. But because the squeezing is in random directions with variable magnitudes it averages out. Hence, it is safe to neglect the squeezing part and consider the intuitive time-dependent Hamiltonian,

$$\hat{H}(t) = \hbar[\omega_0 + \xi(t)]\Big(\hat{a}^\dagger\hat{a} + \frac{1}{2}\Big). \tag{123}$$

The literature of random changes in the frequency of a harmonic oscillator has a long history since it is easy to imagine various uncontrolled physical process, which can be modeled by as stochastic modulations of the oscillator frequency. Just to mention a few, stochastic frequency fluctuations can be caused by changes in the interacting environment [94, 151], fluctuations of spurious two-level systems [152], attachment and diffusion of molecules or atoms [129, 132, 153, 154], or uncontrolled transitions in an coupled ancillary qubit [155, 156].

Consider a quantum superposition of two Fock states $|\psi\rangle = (|n\rangle + |n+1\rangle)/\sqrt{2}$ that evolves under the fluctuating Hamiltonian (123). By ignoring the phase evolution by the mean ω_0, we get that the time-evolved state is $\hat{\rho}(t) = |\psi(t)\rangle\langle\psi(t)|$

$$\begin{aligned}\hat{\rho}(t) = \frac{1}{2}\Big(&|n\rangle\langle n| + \mathrm{e}^{\mathrm{i}\int_0^t \xi(\tau)\,\mathrm{d}\tau}|n+1\rangle\langle n| \\ &+ \mathrm{e}^{-\mathrm{i}\int_0^t \xi(\tau)\,\mathrm{d}\tau}|n\rangle\langle n+1| + |n+1\rangle\langle n+1|\Big),\end{aligned} \tag{124}$$

where we clearly observe that the dynamical phase factor $A(t) = \exp(\mathrm{i}\int_0^t \xi(\tau)\,\mathrm{d}\tau)$ has an important role. As we have no knowledge on the specific realization of the stochastic process the best we can do is to average $A(t)$ over all possible realizations resulting in

$$\begin{aligned}\hat{\rho}(t) = \frac{1}{2}\Big(&|n\rangle\langle n| + \langle \mathrm{e}^{\mathrm{i}\int_0^t \xi(\tau)\,\mathrm{d}\tau}\rangle_\xi |n+1\rangle\langle n| \\ &+ \langle \mathrm{e}^{-\mathrm{i}\int_0^t \xi(\tau)\,\mathrm{d}\tau}\rangle_\xi |n\rangle\langle n+1| + |n+1\rangle\langle n+1|\Big),\end{aligned} \tag{125}$$

which shows that the averaging (denoted by $\langle\cdot\rangle_\xi$) leads to dephasing since $\hat{\rho}$ is a mixed state when $|\langle\exp(\mathrm{i}\int_0^t \xi(\tau)\,\mathrm{d}\tau)\rangle_\xi| < 1$. The above discussion can be generalized to

$$\hat{\rho}(t) = \sum_{nm} c_{nm}\langle \mathrm{e}^{(n-m)\mathrm{i}\int_0^t \xi(\tau)\,\mathrm{d}\tau}\rangle_\xi |n\rangle\langle m|, \tag{126}$$

showing that phase coherence decays faster for pairs with larger energy difference.

Let us consider a simple example demonstrating loss of phase coherence and the role of temporal fluctuations in $\xi(t)$. Assume that $\xi(t)$ has no temporal fluctuations or the fluctuations are so slow that in a relevant time scale of the experiment they can be

neglected. Then we need to know only a static distribution of ξ that is now assumed to be Gaussian distribution centered at zero and with variance δ^2. The static distribution characterizes the frequency variation of an oscillator between different experimental runs or the statistical static variation in an ensemble of oscillators. The resulting phase factor is $\langle e^{i\int_0^t \xi(\tau)\,d\tau}\rangle_\xi = \int_{-\infty}^{\infty} P(\xi)e^{i\xi t}\,d\xi = \exp(-\delta^2 t^2/2)$ which implies that in the limit $t \to \infty$ the state (125) approaches a fully mixed state because of lost of phase coherence by ensemble averaging. What if we now assume that $\xi(t)$ is a genuine stochastic process with temporal fluctuations, but at every time instance it has frequency distribution that is a Gaussian distribution centered at zero and with variance δ^2. In section 3.4, we saw that for the Gaussian modulations of a two-level system, the fluctuation lead to motional narrowing, that is, the phase factor decaying slower, $\exp(-t\Gamma_\phi)$, in the presence of fluctuations. Sagi *et al.* in reference [126] show that this is generally true regardless of the type of the temporal fluctuations if the marginal frequency distribution is Gaussian. They also show that for heavy-tailed frequency distributions temporal fluctuations are expected to result in motional broadening which is that the phase factor decays faster than in the static case.

5. Coupled systems

Frequency modulations in coupled system is a vast topic and we will not be able to give an exhaustive review on its developments here. We will concentrate on two prototype examples, the Jaynes-Cummings and radiation pressure Hamiltonians, and consider non-interacting and interacting many-body systems consisting of identical particles in the following section. The examples are chosen both of their broad applicability to multitude of different physical realisations, and also because of their timely character in the modern literature.

5.1. Modulated Jaynes-Cummings Hamiltonian

The Jaynes-Cummings (JC) model [25] is the backbone for the study of the intertwining of matter and light. It has found its application in a myriad of different physical systems, ranging from quantum optics and quantum electrodynamics (QED) to ion traps, vibronic transitions in molecules and solid-state quantum information science. In its simplicity, the JC model couples a two-level atom (transition frequency ω_0) with a quantized radiation (electromagnetic) field mode (ω_c). The coupling is characterised by the coupling strength g, and it allows the coherent exchange of an energy quantum between the atom and the radiation field. Quantum effects are expected to be seen in the strong coupling limit, where $g > \kappa$, with κ being the cavity dissipation. In addition, the coupling of the two-level atom with the environment is modelled with the coupling constant γ. The typically weak interaction can be strengthened by confining the atom and the field inside an optical or microwave cavity, which decreases the mode volume and, thus, increases the coupling [157]. Also, by coupling superconducting artificial atoms to microwave cavities

formed by co-planar waveguide resonators, one achieves a broad control over all of the parameters of the JC problem [158]. This circuit version of the more conventional cavity QED has been dubbed in the literature as circuit QED.

The Jaynes-Cummings Hamiltonian is given by

$$\hat{H} = \hbar\omega_c \hat{a}^\dagger \hat{a} + \frac{\hbar\omega_0}{2}\hat{\sigma}_z + \hbar g(\hat{a}^\dagger \hat{\sigma}_- + \hat{a}\hat{\sigma}_+), \tag{127}$$

where we have neglected the energy related to the zero-point fluctuations of the cavity. The above Hamiltonian is obtained from the more general Rabi Hamiltonian by making a RWA where the $\hat{a}^\dagger\hat{\sigma}_+$, $\hat{a}\hat{\sigma}_-$ dependent terms that do not conserve the excitation number have been neglected. These terms are negligible with naturally occurring coupling rates ($\kappa \ll \omega_c$) in the NMR, the cavity QED or in the major experiments of the circuit QED. With an innovative sample design, the ultrastrong coupling can be reached in a circuit QED setups [69, 159]. In addition to the engineering, the ultrastrong coupling can be achieved with a quantum simulation [160] in a JC system with two properly chosen external fields.

When the cavity is driven strongly, the JC Hamiltonian reduces to the transversely driven qubit Hamiltonian, which leads into Rabi oscillations of the excited state population of the atom [161]. As a consequence, the emission spectrum of the atom displays the so-called Mollow triplet [162]. In this review, we concentrate on the situation where the coupling between the cavity and the atom is at the quantum level, but either of the qubit and cavity frequencies is modulated. We build our discussion on the two previous sections, which dealt each of the modulated subsystems separately.

5.1.1. Spectrum of the Jaynes-Cummings Hamiltonian The eigenproblem for the non-modulated JC Hamiltonian is readily solved by analytic means. As a result, one obtains the characteristic ladder of energies given by

$$E_{\pm,n} = n\hbar\omega_c \pm \frac{\hbar}{2}\sqrt{\delta_c^2 + 4ng^2}, \tag{128}$$

where $\delta_c \equiv \omega_0 - \omega_c$ is the detuning between the qubit and cavity frequencies, and n is a positive integer. The states appear as pairs $|\pm, n\rangle$, but the ground state $|\downarrow, 0\rangle$ is a single state with energy $E_0 = -\hbar\omega_0/2$. The doublets are created by the interaction g, which is most clearly seen in resonance ($\delta_c = 0$) as the removal of the degeneracy between the states $|\uparrow, n\rangle$ and $|\downarrow, n+1\rangle$. The resulting energy levels are depicted in figure 10.

Spectrum (18) for the non-modulated JC Hamiltonian is readily solved. As a consequence, the bare qubit transition is split and observed in the spectrum as two Lorentzians at $\omega = \omega_{\pm,1} \equiv (E_{\pm,1} - E_0)/\hbar$, separated by the vacuum Rabi frequency $2g$. The necessary condition to resolve the doublet is that the so-called strong coupling regime, $g > \kappa$ (κ is the cavity dissipation), is achieved. This phenomenon of vacuum Rabi mode splitting [163, 164] was first observed with ensembles of atoms in optical cavities [165–167], and later in semiconductor heterostructures [168–170] and with an ensemble of Rydberg atoms in a superconducting high-Q microwave cavity [171]. Finally, also the single atom interplay with the cavity field was observed at quantum level with Rydberg atoms [172].

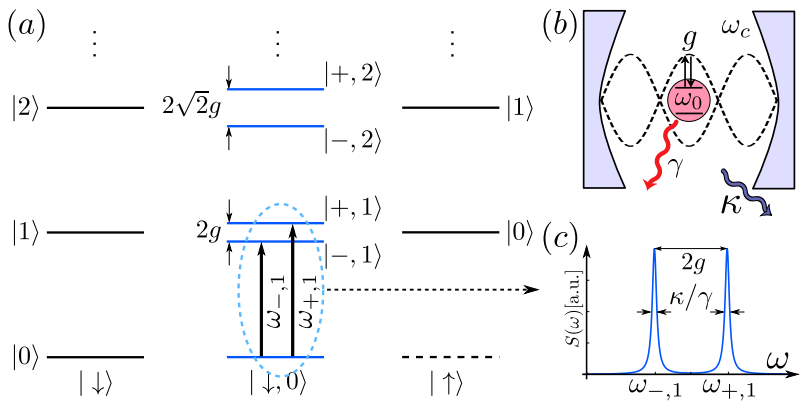

Figure 10. (a) Energy level diagram of the JC Hamiltonian. We show with black the uncoupled basis states for the qubit (left to right) and for the cavity (down to up). The JC energies are shown in blue. The vertical dots emphasize the continuation of the energy levels with increasing n. (b) Sketch of the JC interaction between the two-level atom and the cavity field. (c) Probe spectrum displaying the vacuum Rabi mode splitting in the strong coupling regime. The widths of the peaks are determined by κ or γ, depending on to which degree of freedom the probe couples.

Recently, vacuum Rabi oscillations and the level splitting were observed in a circuit QED system [173, 174], and has since then demonstrated in various systems by either spectroscopic means and/or in the time domain. Vacuum Rabi mode splitting is, at least in some sense, analogous to the normal mode splitting of two coupled classical oscillators. Thus it has been pointed out [175], that in order to show the quantum character of the interaction one should demonstrate the $\sqrt{n}$ scaling of the doublet splittings. This was achieved with circuit QED [176] and in a quantum-dot/microcavity system [177].

5.1.2. Modulation of the atom frequency One of the most intriguing applications of quantum two-level systems is the envisioned universal quantum simulator, or quantum computer [178]. In a nutshell, the information in a quantum computer is stored and processed in logical bits formed by quantum two-level systems, i.e. qubits. Accordingly, the working principles of such a device have to be described in terms of quantum laws and, thus, the resulting behaviour relates on the concepts of interference and entanglement. It has been shown that if such a machine were ever to be built, it could speed-up certain computational tasks considerably [179–181]. Recent progresses with different experimental approaches [182] have made the realisation of this dream plausible.

Working quantum computer requires means to transform information between qubits. One of the most promising realisations for this is the cavity-QED setup [87, 183], where the cavity acts as a storage and a mediator of information between qubits. The unitary time-evolution operator related to such an elementary two or many qubit process is called a quantum gate. In the cavity QED scheme, multiqubit gates can be constructed by coupling the qubits to a joint cavity where multiqubit interactions can be produced

by real or virtual excitations between the qubits, created by sequences of rapid control pulses [44]. It was discussed in the context of trapped ion qubits that also sideband transitions could be used for such purposes [87]. Conventionally, such sidebands are created by transverse driving on either the qubit [184, 185] or the cavity [183, 186, 187]. However, sidebands created in such way unavoidably rely on two-photon processes which are proportional in g^2 and, thus, result in slow two-qubit gates.

Recently, it was proposed that the sidebands created by the longitudinal coherent modulation $\xi(t)\hat{\sigma}_z/2$ (see also section 3.2) with $\xi(t) = \xi\cos(\Omega t)$ are of first-order in g and, therefore, can be used to create faster two-qubit gates [43]. In reference [43], one can find a detailed discussion on dynamics related in a red sideband process, consider the error coming from the interaction with a spectator qubit, and show how a controlled-NOT gate can be created in presence of a second excited state. They also give a suggestion for physical implementation with transmon [188] qubits. Experimental demonstration of sideband transitions in a transmon system can be found in reference [44].

Typically, the interactions between the environment and the qubit-cavity system are treated separately when the coupling is weak, i.e. $g < \kappa, \gamma$ [189]. In the context of quantum information processing, and physics in general, one wishes to have as strong coupling as possible. When the coupling is ultra-strong, $g > \omega_c, \omega_0$, the RWA applied in the derivation of the JC Hamiltonian becomes insufficient. As a consequence, one should use the Rabi Hamiltonian in the calculation of the eigenstates and the corresponding energies of the qubit-cavity system. Especially, the inclusion of the terms that do not conserve the excitation number cause the Rabi ground state to deviate from the JC ground state. Thus, the dissipation model relaxing the system towards the JC ground state at zero temperature unavoidably brings the system out of its Rabi ground state. Reference [190] develops a Lindbladian master equation for the approximately diagonalized Rabi Hamiltonian and uses it to solve the issues arising from the application of the JC master equation for the Rabi Hamiltonian. As a result of this, the peaks in the vacuum Rabi splitting spectrum depicted in figure 11 become asymmetric, i.e. have different widths and heights due to the different dissipation rates for the two transitions.

5.1.3. Modulation of the cavity frequency Modulations of the cavity frequency can possibly also be used to create entanglement between two qubits coupled to the same cavity [191]. On a more fundamental level, the frequency modulation of the cavity can be created, e.g., by allowing one of its mirrors to vibrate. We assume here again that the modulation created by the vibrations is sinusoidal: $\xi(t) = \xi\cos(\Omega t + \theta)$, where θ is the phase of the modulation which turns out to have an effect on the peak heights in the spectrum. When the modulation can be assumed slow, we can apply the adiabatic approximation (see section 2) and as a result the modulated cavity Hamiltonian can be written as $\omega(t)\hat{a}^\dagger\hat{a}$. Cavity QED setup with the modulated cavity was studied in the JC approximation in references [192–194], and also in a Kerr-like medium in reference [195]. By calculating the two-time correlation spectrum for the qubit, one can show [192] that the vacuum Rabi splitting can further be split into two doublets caused by the frequency

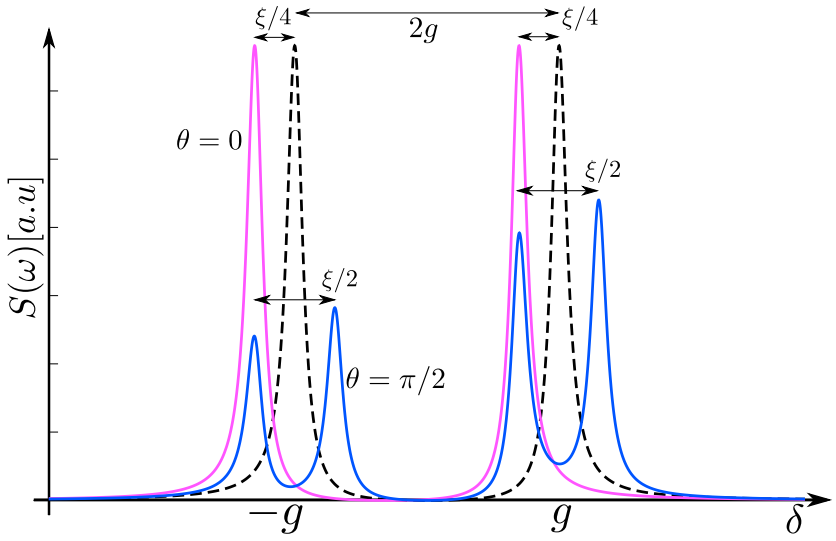

Figure 11. Probe spectrum displaying the splitted vacuum Rabi peaks. When $\theta = 0$ the vacuum Rabi peaks experience only a BS-type shift (magenta) with respect to the non-modulated peaks (dashed, c.f. figure 10(c)). When $\theta = \pi/2$ the vacuum Rabi peaks are split because the JC eigenstates $|\pm, 1\rangle$ are dressed by the modulation. The widths of the peaks are determined by the bare qubit relaxation rate Γ_1.

modulation of the cavity. The resulting spectrum can be written into the form [192]

$$S(\omega) = N\Big|\frac{\alpha}{\Gamma_1 + i(\delta + g - \xi/4)} + \frac{\beta}{\Gamma_1 + i(\delta + g + \xi/4)} \tag{129}$$

$$+ \frac{\alpha^*}{\Gamma_1 + i(\delta - g - \xi/4)} + \frac{\beta^*}{\Gamma_1 + i(\delta - g + \xi/4)}\Big|^2, \tag{130}$$

where $\delta = \omega_0 - \omega$, N is a normalization constant and

$$\alpha = 1 - e^{-i\theta}, \quad \beta = 1 + e^{-i\theta}. \tag{131}$$

In figure 11, we plot the vacuum Rabi doublets with the values $\theta = 0, \pi/2$ for the modulation phase. When $\theta = 0$ the vacuum Rabi oscillations are shifted in frequency by $\xi/4$ due to the BS-type correction (see also section 3.2. In the case of $\theta = \pi/2$, the modulation dresses the JC-eigenstates $|\pm, 1\rangle$, resulting in four quasienergy states and corresponding four different spectral peaks. In addition, the two Rabi doublets are asymmetric due to the interference between the between the doubly dressed states. [192]

Quantum fluctuations in the cavity occupation n lead into photon shot noise [196–198]. As a consequence, the qubit linewidth is broadened and, thus, represents the cavity backaction on the qubit. In references [196–198], the transmon setup with photon shot noise was considered in the dispersive strong coupling regime where $\kappa < g \ll |\omega_0 - \omega_c|$. Due to the shot noise $\delta n(t)$, the qubit gains a relative phase

$$\phi(t) = \frac{2g}{\omega_0 - \omega_c} \int_0^t d\tau \delta n(\tau). \tag{132}$$

By assuming that the noise process is Gaussian, with photon correlation function (white photon noise)

$$\langle \delta n(t)\delta n(0)\rangle = \bar{n}e^{-\kappa|t|/2}, \tag{133}$$

one obtains Lorentzian qubit resonance which is broadened as $\Gamma_2 \to \Gamma_2 + 2\theta_0^2\bar{n}\kappa$, where $\theta_0 = 2g^2/(\kappa(\omega_0 - \omega_c)$ [196, 197]. In the above, we assume that the mean number of the cavity quanta $\bar{n}$ is small. On the other hand, in the large-$\bar{n}$ limit one observes a spectrum which is a convolution of a Lorentzian and Gaussian lineshapes, instead of a pure exponential decay. As a consequence, the resonance width scales as $\sqrt{\bar{n}}$ [197].

5.1.4. The simulated ultrastrong coupling by frequency modulation In addition to the engineering, the ultrastrong coupling in a JC system can be achieved with a quantum simulation [160] by using two properly chosen driving fields. In reference [160], the driving fields were both transverse, but a similar effect can also be accomplished by using longitudinal coupling for one of the fields (see supplement of reference [28]). The starting point is the doubly modulated strongly coupled JC Hamiltonian:

$$\hat{H} = \hbar\omega_c\hat{a}^\dagger\hat{a} + \frac{\hbar}{2}\left[\omega_0 + \xi\cos(\Omega t)\right]\hat{\sigma}_z \tag{134}$$

$$+ \hbar g(\hat{a}^\dagger\hat{\sigma}_- + \hat{a}\hat{\sigma}_+) + \hbar G\cos(\Omega_G t)\hat{\sigma}_x. \tag{135}$$

The above Hamiltonian can be written into the form

$$\hat{H} = \hbar\tilde{\omega}_c\hat{a}^\dagger\hat{a} + \frac{\hbar\tilde{\omega}_0}{2}\hat{\sigma}_z + \hbar\tilde{g}(\hat{a}^\dagger + \hat{a})\hat{\sigma}_x, \tag{136}$$

by choosing $\Omega = g$ and by making two RWAs in properly chosen rotating frames [28]. In the above Hamiltonian, we have defined $\tilde{\omega}_c \equiv \omega_c - \omega$, $\tilde{\omega}_0 \equiv \xi/2$, and $\tilde{g} \equiv g/2$. One sees that the Hamiltonian is of Rabi Hamiltonian form. Especially, the qubit and cavity frequencies can be controlled with the longitudinal modulation amplitude and transverse drive frequency, respectively. Especially, the ratio $\tilde{g}/\tilde{\omega}_c \gtrsim 0.1$ with experimentally realisable parameters [28] and, thus, the above scheme has a prospect of being used as an analog simulator of cavity QED with ultra-strong coupling. Reference [28] discusses the above idea in circuit QED environment, which allows for fast tuning of the effective qubit and cavity frequencies.

5.2. Modulated radiation pressure Hamiltonian

Optomechanics studies the interplay between light and mechanical motion. A characteristic model can be created by connecting one of the cavity mirrors to a spring, as depicted in figure 12. One of most intriguing current goals in the optomechanics research is achieving the strong coupling regime where the interplay between the radiation field and mechanical motion would occur at single-quantum level. This would ultimately allow cooling of the oscillator to the quantum mechanical ground state, and the first realisation of truly quantum *mechanical* motion. Different physical realisations and the whole topic is reviewed in reference [199].

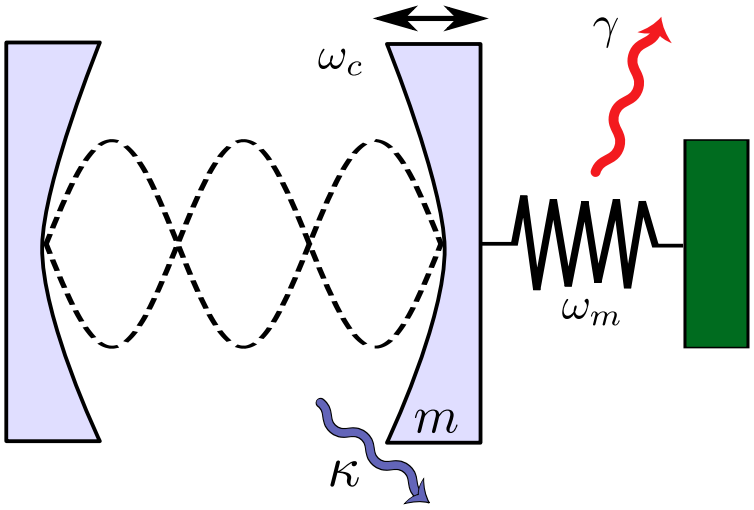

Figure 12. Schematic of the optomechanical setup.

The prototype Hamiltonian of the optomechanical system can be written as

$$\hat{H} = \hbar\omega_c \hat{a}^\dagger \hat{a} + \hbar\omega_m \hat{b}^\dagger \hat{b} + \hbar g \hat{a}^\dagger \hat{a}(\hat{b}^\dagger + \hat{b}), \tag{137}$$

where $\hat{a}$ and $\hat{b}$ are the annihilation operators for the cavity and mechanical oscillators, respectively. The so-called radiation pressure term g describes the momentum transfer from cavity photons to the mechanical motion. Coherent modulation of the mechanical frequency in the optomechanical setup has been studied in reference [200]. They have shown that the quantum effects such as squeezing, entanglement, and discord are all enhanced in the steady state when the modulation frequency $\Omega = 2\omega_m$. This is interpreted as parametric phase locking between the modulation force and mechanical motion. Also, the effects of mechanical frequency modulations on cooling of the mechanical motion have been studied in reference [201]. In addition to mechanical modulations, they allowed also the mechanical dissipation $\gamma(t)$ to be dependent on time. They found that additional cooling resonances appear when strong periodic mechanical frequency modulations are applied in the resolved sideband limit [201]. In addition, when the modulations are weaker or the cavity linewidths are larger, these resonances overlap and can be influenced by adjusting the pulse shape.

The cavity frequency modulations have been studied in the setup where two cavities are coupled via photon hopping and mechanical oscillation in the so-called "membrane-in-the-middle" configuration [202]. When the cavity frequencies are coherently modulated, there exists a set of conditions such that a single photon can displace the mechanical membrane even in the weak coupling regime where $g \ll \omega_m$.

6. Many-body systems

6.1. Motional averaging with hot atomic gases

A spectacular application of motional averaging is the realization of a surprisingly simple interface between photons and an ensemble of atoms [203], allowing write/read operations on the collective atomic quantum state. In general, the advantage of using an ensemble is that the interaction between a single photon and a collective mode such as the Dicke state scales as $g\sqrt{N}$, where g is the interaction strength between a single photon and a single atom and N is the number of atoms. For systems such as atoms or spins (*e.g.* NV centers in diamond), this increases the interaction and thus decreases the write/read time to values below the coherence time [204]. The experiment by Borregaard et al [203] uses thermal (room-temperature) atomic vapors in microcells with spin-protecting alkene coating. This contrasts with the usual realization of collective-effects quantum memories in atomic ensembles, which requires typically low temperatures, long coherence times, and localized atoms. Here the idea is that the atoms would cross randomly the laser beam, thus erasing the information about with which atom the photon has interacted.

The atoms have a Λ-level structure, with excited state $|e\rangle$, ground state $|0\rangle$, and a metastable state $|1\rangle$. Initially, the system starts in with all the atoms pumped in the state $|0\rangle$; the so-called write process consists of adding a single excitation, that is, the creation of a collective state with one excitation, distributed between all the atoms. This state is known as symmetric Dicke state, or W state. W states are also relevant for the foundations of quantum physics, and it can be shown that they are incompatible with hidden-variable theories [205]. To create this state, one drives the $|0\rangle \to |e\rangle$ transition with a weak laser pulse. The interaction part of the Hamiltonian of the system reads

$$\hat{H} = \hbar \sum_{j=1}^{N} \left[\delta_d \hat{\sigma}_{ee}^{(j)} - \left(\frac{\xi_j(t)}{2} \hat{\sigma}_{e0}^{(j)} + g_j(t) \hat{a}_{\text{cell}} \hat{\sigma}_{e1}^{(j)} + \text{h.c.} \right) \right], \tag{138}$$

where $\delta_d = \omega_{e0} - \omega_d$ is the detuning, ω_d is the frequency of the driving laser, ξ_j is the coupling to the laser field, and g_j is the coupling to the cavity $\hat{a}_{\text{cell}}$, and $\hat{\sigma}_{mn}^{(j)} = |m\rangle_j\langle n|$ are the creation/annihilation operators associated to the transition $m \leftrightarrow n$ for the atom j. Then, the emission of a single photon due to the $|e\rangle \to |1\rangle$ decay heralds the creation of the symmetric Dicke state

$$\frac{1}{\sqrt{N}} \left(|100..0\rangle + |0100..0\rangle + |001..0\rangle + ... |000..1\rangle \right) \tag{139}$$

The essential phenomenon employed to create the superposition is the absence of which-atom information: we cannot know, even in principle, that the detected photon has resulted from the decay of a specific atom in the ensemble. In the readout process, the protocol is run backwards: the $|1\rangle \to |e\rangle$ transition is driven by a classical pulse and the photon resulting from the decay $|e\rangle \to |0\rangle$ is recovered.

Next, one studies the Langevin equations corresponding to Hamiltonian (138) with decay rates γ and κ_1 for the atoms and respectively the cavity. These equations can be solved in the approximation that the interaction between the atoms and the field is a

small perturbation. Under these conditions the Langevin equations can be integrated, and assuming that $\hat{\sigma}_{10}(t)$ is a slow variable one gets [203]

$$\hat{a}_{\text{cell}}(t) = -\frac{1}{2}\sum_{j=1}^{N}\Theta_j(t)\hat{\sigma}_{10}^{(j)}, \tag{140}$$

where

$$\Theta_j(t) = \int_0^t dt' \int_0^{t'} dt'' e^{-\frac{\kappa_1}{2}(t-t')} e^{-(\frac{\gamma}{2}+i\delta_d)(t'-t'')} g_j^*(t')\xi_j(t'') \tag{141}$$

From equation (140) one clearly sees that the detection of a photon in the cell would project the state of the atoms onto a symmetric Dicke state, provided that $\Theta_j(t)$ is not dependent on the atom j. This atom-independence is realized through the averaging of the motion of the atoms as they move into and out of the laser beam due to thermal motion: for each atom, this happens many times during the duration of the laser pulse due to the collision and trajectory reversal at the walls of the cavity. These collision preserve the phase information.

If the photons are detected only within a very narrow bandwidth, the operator a in time-domain will have a broad distribution. This increases the effect of motional averaging, since it includes more events of passing into the beam in equation (141), resulting in the same value of $\Theta_j(t)$ for all the atoms. Since increasing the finesse of the cell cavity is not easy to realize, another solution [203] is to use a filter cavity with decay rate κ_2 placed after the cell cavity. The photons are eventually detected at the output of this cavity. Treating this as a two-cavity cascaded system, the input-output theory gives for the output field [203]

$$\hat{a} = -\frac{\kappa_2\sqrt{\kappa_1}}{4}\sum_{j=1}^{N}\theta_j(t)\hat{\sigma}_{10}^{(j)}, \tag{142}$$

where

$$\theta_j(t) = \int_0^t dt' e^{-\frac{\kappa_2}{2}(t-t')}\Theta_j(t'). \tag{143}$$

The method is rather general, and can be employed in any many-body system where there exist fluctuations in the coupling.

6.2. Three-level systems

When a three-level system with states $|0\rangle, |1\rangle, |2\rangle$ is subjected to irradiation by two fields of amplitude ξ_{01} and ξ_{12} that are nearly resonant with the first two transitions $|0\rangle \to |1\rangle$ and $|1\rangle \to |2\rangle$, the Hamiltonian reads

$$\begin{aligned}\hat{H} = &\sum_{i=0}^{2}\hbar\omega_i\hat{\sigma}_{i,i} + \frac{\hbar\xi_{01}}{2}\cos(\omega_{01}^{(\xi)}t)\sum_{i=0}^{1}(\hat{\sigma}_{i,i+1} + \text{h.c.}) \\ &+ \frac{\hbar\xi_{12}}{2}\cos(\omega_{12}^{(\xi)}t)\sum_{i=0}^{1}(\hat{\sigma}_{i,i+1} + \text{h.c.}),\end{aligned} \tag{144}$$

where $\hat{\sigma}_{i,j} = |i\rangle\langle j|$ and $\omega_{01}^{(\xi)}, \omega_{12}^{(\xi)}$ are the drive frequencies.

Let us now perform the transformation $\hat{H} \to \hat{U}\hat{H}\hat{U}^\dagger + i\hbar(d\hat{U}/dt)\hat{U}^\dagger$ with

$$\hat{U}(t) = \hat{\sigma}_{0,0} + e^{i\omega_{01}^{(\xi)}t}\hat{\sigma}_{1,1} + e^{i\left(\omega_{01}^{(\xi)}+\omega_{12}^{(\xi)}\right)t}\hat{\sigma}_{2,2} \tag{145}$$

and neglect the fast-rotating terms, which brings us to a multiple-rotating frame with effective three-level Hamiltonian

$$H(t) = \frac{\hbar}{2}\begin{pmatrix} 0 & \xi_{01} & 0 \\ \xi_{01} & 2\delta_{01} & \xi_{12} \\ 0 & \xi_{12} & 2(\delta_{01}+\delta_{12}) \end{pmatrix}. \tag{146}$$

Here the detunings are

$$\delta_{j,j+1} = \omega_{j+1} - \omega_j - \omega_{j,j+1}^{(\xi)}. \tag{147}$$

Hamiltonian (146) is the basis of several experiments realized with superconducting qubits at fixed detuning. Notably, using ξ_{12} as a relatively strong coupling field, the transition $|0\rangle \to |1\rangle$ becomes dark, which can be probed by doing spectroscopy with ξ_{12}. The initial $|0\rangle \to |1\rangle$ spectral line splits into two lines, a process known in atomic physics as the Autler-Townes splitting [206–208]. This phenomenon has been observed also in time-domain, with ξ_{12} turned on and off [209]. A related effect due to the coherent simultaneous drive with two fields is the destructive interference on the first excited state, which results in electromagnetically-induced transparency [210, 211]. Finally, by adiabatically turning on and off the Rabi frequencies ξ_{12} and ξ_{01} in the so-called counterintuitive order (first ξ_{12}, then ξ_{01}) it is possible to transfer the population from the state $|0\rangle$ to the state $|2\rangle$ without populating at all the intermediate state $|1\rangle$. This technique is known in atomic physics as STIRAP (stimulated adiabatic Raman passage) [212].

6.3. Topological transitions

In 1988 Duncan Haldane introduced a model that showed for the first time that an external magnetic field is not a necessary condition for the phenomenology of the quantum Hall effect (quantized Hall conductivity σ_{xy} and the appearance of topologically protected edge states) to occur in a system. To create topological nontrivial states, the key concept is that of Berry curvature [22]. This idea has been very fertile, generating in recent years the field of topological insulators. By engineering time-dependent lattice potentials and detunings, the Berry curvature can be realized in a controlled way and measured not only in natural materials but also in artificial systems such as superconducting qubits and degenerate ultracold gases.

Haldane's model [213] consists of a honeycomb lattice, similar to graphene, but with a second-neighbour hopping that includes a phase φ_{H} that changes alternatively from one link to another. The latter can be realized by a staggered local magnetic field around the edges of the hexagons, resulting in zero average magnetic flux over the cell. In addition, a difference in the chemical potentials of the two sublattices is assumed, which produces a mass term m_0.

By expanding the lattice Hamiltonian around the nonequivalent corners $\boldsymbol{K}$ and $\boldsymbol{K}'$ of the first Brillouin zone, and keeping only the small-momentum contributions $\boldsymbol{k}_\pm$ measured with respect to these points (upper sign for $\boldsymbol{K}$, lower sign for $\boldsymbol{K}'$, all vectors in x-y plane), the Haldane Hamiltonian becomes

$$\hat{H}_\pm = \hbar v_{\mathrm{F}} \left(k_\pm^x \hat{\sigma}_x \pm k_\pm^y \hat{\sigma}_y \right) + (m_0 \mp m_t)\hat{\sigma}_z \tag{148}$$

The astute reader familiar with the physics of graphene will immediately recognize the part linear in $k_\pm^x$ and $k_\pm^y$ as the Hamiltonian for Dirac fermions with Fermi velocity v_{F}, namely $\hbar v_{\mathrm{F}} \boldsymbol{k}_+ \cdot \hat{\boldsymbol{\sigma}}$ for the Dirac cone at $\boldsymbol{K}$ and $\hbar v_{\mathrm{F}} \boldsymbol{k}_- \cdot \hat{\boldsymbol{\sigma}}^*$ for the Dirac cone at $\boldsymbol{K}'$. In addition to this, the Haldane Hamiltonian contains also a mass term $(m_0 \mp m_t)\sigma_z$: as mentioned above, the mass m_0 arises from the sublattice inversion symmetry breaking, while m_t is a mass term resulting from the second-order hopping terms with amplitude t_2 and variable phase ϕ, $m_t = 3\sqrt{3} t_2 \sin \varphi_{\mathrm{H}}$. For this model, Haldane predicted that there should exist two phases: a trivial insulating phase if $m_0 > |m_t|$ and a topologically non-trivial phase for $m_0 < |m_t|$.

Consider now the case of a qubit with Larmor frequency ω_0 driven by a microwave fields with frequency ω_d and Rabi coupling ξ_d. In a rotating frame of the driving field, the Hamiltonian is

$$\hat{H} = \frac{\hbar}{2} \left(\delta_d \hat{\sigma}_z + \xi_d \hat{\sigma}_x \cos\phi + \xi_d \hat{\sigma}_y \sin\phi \right), \tag{149}$$

where the detuning is $\delta_d = \omega_0 - \omega_d$ and ϕ is the phase of the driving field. Already at this point one could see that there is a resemblance to the k-space Haldane Hamiltonian (148). To make this correspondence more precise, let us introduce a parametrization of δ and ξ_d in terms of an angle χ, defined by $\delta_d = \delta_0 + \delta_r \cos\chi$ and $\xi_d = \xi_r \sin\chi$. Let us take δ_0 and δ_r to be positive for the simplicity of the argument. Then the drives in the x and y directions in equation (149) can be written as $\xi_x = \xi_r \sin\chi \cos\phi$ and $\xi_y = \xi_r \sin\chi \sin\phi$. This leads to a parameter surface in the form of an ellipsoid,

$$\frac{(\delta_d - \delta_0)^2}{\delta_r^2} + \frac{\xi_x^2 + \xi_y^2}{\xi_r^2} = 1. \tag{150}$$

Now, the possibility of controlling the detuning δ_d in these systems enables the adiabatic exploration of this ellipsoidal manifold, see figure 13. The experiment starts with $\chi(t=0) = 0$, where $\xi_d = 0$, $\delta_d = \delta_0 + \delta_r$, and the qubit is in the eigenstate $|0\rangle$ corresponding to the Bloch vector pointing to the North Pole of the Bloch sphere. Then χ is increased linearly in time until it reaches the value π, where again $\xi_d = 0$ but in this case $\delta_d = \delta_0 - \delta_r$. We can see that at this end point in the parameter space (χ, ϕ) the orientation of the Bloch vector depends on whether $\delta_0 > \delta_r$ or $\delta_0 < \delta_r$. In the first case the Bloch vector points to the North, while in the second to the South. Thus, if now we follow adiabatically the Bloch vector from $\chi = 0$ to $\chi = \pi$, in the first case it will only slightly move around the North Pole, while in the second case it will move from the North to the South, wrapping the entire Bloch sphere. The first case corresponds to a topological trivial phase, while the second to a topological nontrivial phase, see figure 13.

This difference has a precise mathematical characterization by the so-called first Chern number [214],

$$Ch_1 = \frac{1}{2\pi}\int_{\mathcal{S}} F_{\mu\nu} dS_{\mu\nu} \tag{151}$$

where $\mathcal{S}$ is a closed manifold, $dS_{\mu\nu}$ is an area element of the surface, and $F_{\mu\nu}$ is the Berry curvature. The first Chern number is the quantization number of the transversal conductance in the integral quantum Hall effect, where we have $\sigma_{xy} = (e^2/h)Ch_1$, and is also called TKNN invariant [215, 216] in this context. The Berry curvature is the analog of a magnetic field, being defined as

$$F_{\mu\nu} = \partial_\mu A_\nu - \partial_\nu A_\mu, \tag{152}$$

where the Berry connection, defined as

$$F_{\mu\nu} = i\langle\psi|\partial_\mu|\psi\rangle \tag{153}$$

is the analog of the magnetic vector potential. The origin $\delta_d = 0$, $\xi_x = \xi_y = 0$ of the coordinate system in the parameter space, where the eigenvectors become degenerate with eigenvalue zero, is the analog of a magnetic monopole. The phase transition occurs when this point passes though the surface of the ellipsoid. Note that the existence of a topological transition does not depend on having the specific ellipsoid shape of the parameter surface: the important thing is that we have a closed surface and the degeneracy point (the monopole) passes into or outside this surface.

To demonstrate a topological transition one should measure the Berry curvature and calculate the Chern invariant as the system crosses the phase transition. This has been demonstrated in two experiments with superconducting qubits [217, 218]. Differently from the work on geometric phases, as we show below, the measurement techniques in these works is not an interferometric scheme. Rather, it is based on finding the response of the system under small deviations from adiabaticity.

Indeed, it can be shown that the Berry curvature can be found directly from the following expansion [219]

$$\langle\partial_\phi \hat{H}\rangle = \langle\partial_\phi \hat{H}\rangle_0 + v_\chi F_{\chi\phi} + \mathcal{O}(v^2), \tag{154}$$

where $v_\chi = d\chi/dt$ is constant in the experiment (χ is varied linearly in time), and corrections of second order or higher in v_χ are neglected. The quantity $-\langle\partial_\phi \hat{H}\rangle$ has the meaning of a force, analogous to the Lorenz force in a magnetic field. Because of the symmetry of the parameter manifold (the ellipsoid) with respect to the angle ϕ, it is enough to consider $\phi = 0$ when calculating the Berry curvature,

$$F_{\chi\phi} = \frac{\langle\partial_\phi \hat{H}\rangle|_{\phi=0}}{v_\chi} = \frac{\xi_r \sin\chi}{2v_\chi}\langle\hat{\sigma}_y\rangle. \tag{155}$$

The quantity $\langle\hat{\sigma}_y\rangle$ is obtained by performing quantum tomography at each time, that is, at each point in the parameter space [218]. From the values of the Berry curvature the Chern number can be calculated by integration, using the symmetry with respect to ϕ,

$$Ch_1 = \frac{1}{2\pi}\int_0^\pi d\chi \int_0^{2\pi} d\phi F_{\chi\phi} = \int_0^\pi F_{\chi\phi} d\theta. \tag{156}$$

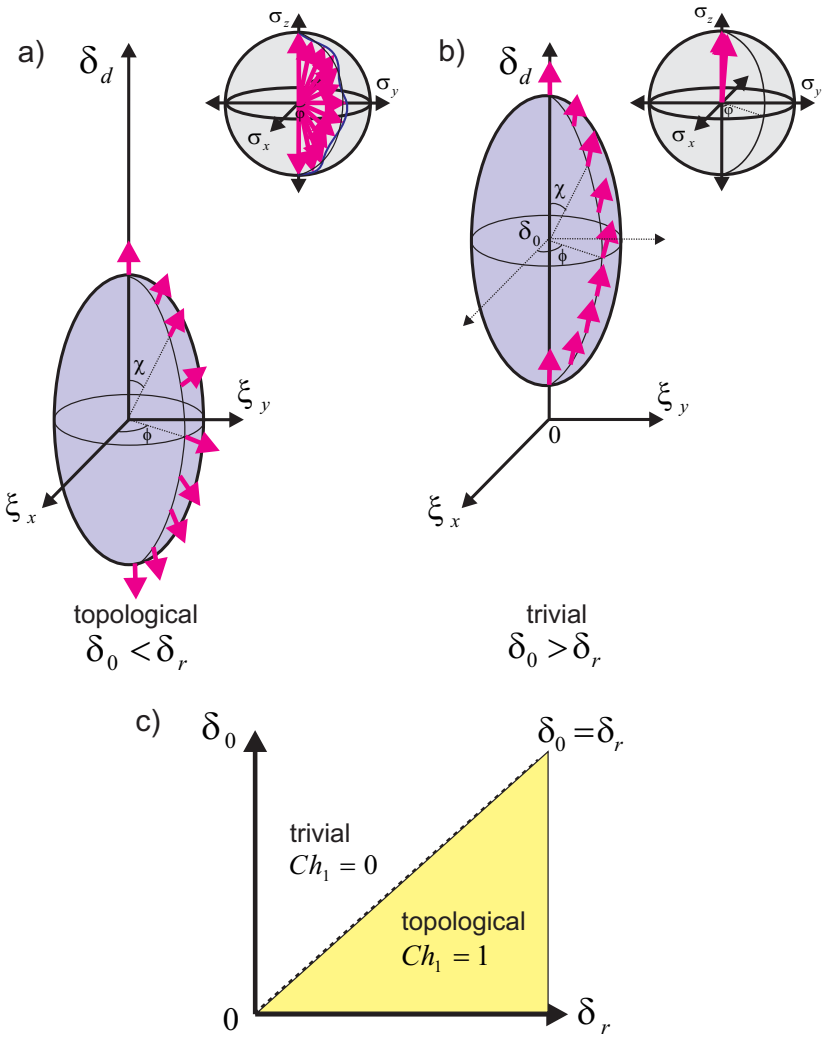

Figure 13. (color online) Bloch sphere representation corresponding to the quasi-adiabatic dynamics of a two-level system, with $|0\rangle$ as the starting state, for two cases: a) $\delta_0 = 0$ and b) $\delta_0 > \delta_r$. In the diagrams below, the Bloch vector is represented as an arrow for each point on the surface of the ellipsoid in the coordinates ξ_x, ξ_y, and ξ_z. For a perfect adiabatic transport, the angle φ from the σ_x axis on the Bloch sphere should equal ϕ (both are zero in the experiments in references [217, 218]). Nonadiabaticity produces shifts in the Bloch vectors away from the plane $\varphi = 0$, and this leads to a measurable response function which, in the first order in the speed $v_\chi = d\chi/dt$, is precisely the Berry curvature. In a) the vector wraps the sphere, and this phase is topologically nontrivial with the first Chern number $Ch_1 = 1$. In b) the phase is topologically trivial, $Ch_1 = 0$. c) Phase diagram showing the expected transition between the two phases at $\delta_0 = \delta_r$, obtained experimentally in references [217, 218] by measuring the Berry curvature and using equation (156).

Next, the parameter manifold (θ, ϕ) is explored and the Chern number is obtained for several values of the ratio δ_0/δ_r. It is found that, if $\delta_0 < \delta_r$, the Chern number is close to 1 within two percentages. This is the hallmark of the topological phase. For $\delta_0 > \delta_r$ the Chern number becomes zero, and the system is in a trivial phase.

A step forward toward employing these ideas has been done using two coupled qubits [217], with an $x - x$ interaction Hamiltonian $\hat{H}_{\rm int} = (\hbar g/2)(\hat{\sigma}_x^1\hat{\sigma}_x^2 + \hat{\sigma}_y^1\hat{\sigma}_y^2)$. In this experiment, a nonzero detuning δ_0 was applied only to the first qubit: thus, when the qubits were unconnected ($g = 0$) the second qubit remained all the time in the topological phase with Chern number 1, while the first qubit was driven across the transition, changing its Chern number from 0 to 1. Thus, the total Chern number of the system varied between 1 and 2. Surprisingly, when the interaction g was turned on, a new phase appeared, characterized by zero Chern number.

6.4. Cold atomic gases

In the previous sections we have studied systems with discrete energy levels. Such cases are well known in few-particle systems but occur also in systems having macroscopic number of particles. In particular, we have discussed superconducting qubits, where the macroscopic wave function has discrete states when sufficiently constrained spatially. Similar macroscopic wave functions occur also in Bose condensed dilute gases. Placing a cold gas to an optical lattice allows to limit to discrete macroscopic states. Below we consider some example cases of driving cold gases in optical lattices.

Let us consider an ultracold gas of bosonic atoms. By using standing waves of laser light, it is possible to form a periodic potential $V \propto \cos(2\pi x/d)$ for the atoms, an optical lattice. The period of the lattice is $d = \lambda/2$, where λ is the wave length of the light. The low energy states of a particle in the lattice form energy bands. If the temperature of the gas is small compared to the first band gap and the interactions between the atoms sufficiently weak, we need to consider only the lowest band. In the simplest case (small tunneling between the lattice sites), the system can be described by a tight-binding Hamiltonian, where the tunneling is directly only to the neighboring lattice sites. Such a system can be described by the Bose-Hubbard model [220, 221]

$$\hat{H}_0 = -J\sum_\ell(\hat{b}_\ell^\dagger\hat{b}_{\ell+1} + \hat{b}_{\ell+1}^\dagger\hat{b}_\ell) + \frac{U}{2}\sum_\ell \hat{n}_\ell(\hat{n}_\ell - 1). \tag{157}$$

Here $\hat{b}_\ell$ and $\hat{b}_\ell^\dagger$ are the annihilation and creation operators for the lattice site ℓ, $J > 0$ is the hopping matrix element, $\hat{n}_\ell = \hat{b}_\ell^\dagger\hat{b}_\ell$ is the number operator at site ℓ, and U parametrizes the on-site interaction. Model (157) is written here for a simple one-dimensional lattice and for particles without internal degrees of freedom, but can be generalized to more general cases. In the following we concentrate on the superfluid part of the phase diagram of $\hat{H}_0$ (157), where the tunneling dominates the interaction. In the absence of other effects, the atoms Bose condense in the lowest Bloch state corresponding to crystal momentum $k = 0$ in the first Brillouin zone $|k| < \pi/d$.

Suppose the optical lattice potential is made to oscillate, $V(x) = V_0(x - X_0(t))$ with a time dependent coordinate $X_0(t)$. Experimentally this can be achieved by changing periodically the phase shift of the counter propagating laser beams. By appropriate transformations this can be seen as a gauge field affecting the momentum $p \to p - m\dot{X}_0(t)$, where m is the atomic mass. It can further be transformed to add to the Bose-Hubbard Hamiltonian (157) the term

$$\hat{H}_1 = -F(t)d\sum_\ell \ell\hat{n}_\ell. \tag{158}$$

Here $F(t) = -m\ddot{X}_0(t)$ is a time dependent force that shifts the energies of the levels localized at different lattice sites. This form resembles the Hamiltonian studied above (39): the sites ℓ correspond to different states whose energies are modulated in time. The potential can be used to induce different effects.

Let us consider sinusoidal driving, $F(t) = F_0 \sin(\omega t)$. As discussed above in equation (45), it modifies the effective tunneling,

$$J \to J_{\text{eff}} = J\mathrm{J}_0(F_0 d/\hbar\omega). \tag{159}$$

Here J_n is the Bessel function of order n. The modulation also causes coupling to the excited modes of the Bose gas [222]. Choosing the parameters appropriately ($\hbar\omega$ large compared to band width but small compared to band gap), these couplings can be neglected, and thus the only effect that remains is the scaling of the tunneling (159). This effect has been studied experimentally in reference [223]. The value of J_{eff} was determined by letting the gas to expand along the lattice direction and then recording the spatial distribution. The observations accurately agree with the Bessel function modulation, including the first zeros of J_0. The zeros mean vanishing of tunneling, and according to the Bose-Hubbard model (157) there should be transition from a superfluid state to Mott insulator phase. The vanishing of tunneling by modulation in a lattice has been termed "dynamic localization". It has long been studied theoretically and experimentally in different systems [14], for example, in semiconductor superlattices.

A more or less similar phenomenon to dynamical localization occurs in a double-well potential [14] and is discussed in section 3.2. This has been realized using single atoms in an optical lattice consisting of double-wells separated by higher barriers [224]. Note that this experiment uses single atoms rather than a condensate. The atoms enter perpendicular to the lattice direction x and their momentum distribution in the x direction is monitored after they have traversed a finite distance parallel to the minima of the potential (y direction). Under sinusoidal modulation, suppression of tunneling is observed at Bessel zeros (159). If one uses a saw-tooth pulse instead of sinusoidal form, the tunneling is not suppressed [224]. This arises from breaking of the symmetry $F(t + T/2) = -F(t)$, where T is the period of the modulation [14].

What happens when the sign of the tunneling element changes in crossing a Bessel zero (159)? In a two-state system this means a change of the coupling phase by π. In a lattice, this leads to the inversion of the Bloch band, the lowest energy Bloch level becomes the maximum energy level and vice versa. The effect of this on Bose

condensation has been studied experimentally in reference [225]. They find indeed that the momentum distribution of the condensate is peaked at the Brillouin zone boundaries $k = \pm\pi/d$.

A recent trend in cold gases has been to generate artificial gauge fields [226]. This means generating complex-valued $J = |J|e^{i\phi}$, where ϕ is called the Peierls phase. Such a phase appears naturally for a charged particle in magnetic field. As the standard cold atomic gases are uncharged, one has to think other ways to generate the Peierls phase. One of the methods is by shaking the lattice. A sinusoidal shaking of the lattice changes the hopping matrix element, but keeps it real valued (159). Complex values are possible for a more complicated time dependence. For example, the modulation period T consists of a period of sine in time T_1 and is constant for time $T_2 = T - T_1$. The complex valued hopping matrix element makes the Bose condensation to a state of finite crystal momentum corresponding to lowest average energy, as demonstrated by measurements in reference [227]. An interesting outlook is to generate a net phase shift going around a plaquette of a 2D lattice, similar as occurs for charged particles in magnetic field. The shaking does not do this for a square lattice, but in more complicated lattices it is possible to generate an effective staggered magnetic field [228, 229]. In particular, reference [229] realizes the Haldane model (section 6.3) with fermionic atoms in a shaken lattice.

In order to simulate a uniform (not staggered) magnetic field, the following procedure can be used [230, 231]. First one has two orthogonal standing laser beams in directions x and y to generate a 2D lattice potential. In x direction one applies a constant gradient, for example by gravity or by magnetic dipole force. This blocks the tunneling in the x direction when the energy separation Δ between neighboring sites in the x direction exceeds J. Two additional laser fields (wave vectors $\boldsymbol{k}_1$ and $\boldsymbol{k}_2$) are used to shake the lattice. Selecting their frequency difference $\omega = \Delta/\hbar$ restores the tunneling in the x direction as a photo assisted process,

$$J_{\mathrm{eff}}^{(x)} = J\langle e^{i(F_0 d/\hbar\omega)\sin(\omega t+\phi_0)-i\Delta t/\hbar}\rangle = J\mathrm{J}_1(F_0 d/\hbar\omega)e^{i\phi_0}. \tag{160}$$

Here the location dependent phase of the additional lasers $\phi_0(\boldsymbol{r}) = (\boldsymbol{k}_1 - \boldsymbol{k}_2)\cdot\boldsymbol{r}$ is imprinted on the tunneling in the x direction and allows to generate a nonzero phase shift in tunneling around a plaquette. This makes it possible to study the interplay of magnetic field and crystal lattice using cold gases in optical lattice, which would require enormous magnetic fields in ordinary crystals.

7. Conclusions

In this review we discussed the topic of frequency modulation in several different quantum mechanical systems. We tried to keep our theoretical examples simple enough, so that the presentation of the conveyed physics would be clear. We have mostly presented results that have been subjected to an experimental test or demonstration, and as such their relevance is validated by laboratory practice. There are certainly other

concepts, theoretical developments, and proposals that no doubt will find a connection to experiment in the forthcoming years.

The modulation of the frequency of a quantum system produces a variable quantum phase difference, and we emphasized its connection with the measured spectrum, both for coherent and incoherent modulations. Many of the experiments discussed are from the field of superconducting systems, where spectacular advances in reducing the decoherence and in developing the quantum control have been achieved recently, but the concepts have general applicability.

We started our analysis with an extensive discussion of the case of two-level systems, and showed that the coherent modulations lead to the formation of multi-photon sidebands, to the observations of coherent destruction of tunnelling, dynamic Stark effect and LZS-interference. When the modulations are incoherent, we reviewed the connection with classical theory of dephasing. We showed that the conventional exponential phase damping can be obtained with Gaussian noise process and a short correlation time. Also, the phenomena of motional narrowing and motional averaging arise naturally when the phase experiences random telegraph noise or other kind of temporal fluctuations. Next, we discussed the paradigmatic case of the harmonic oscillator under frequency modulation, and showed that this can lead to phenomena such as squeezing and dephasing.

As an example of coupled few-level systems, we analyzed the Jaynes-Cummings and the optomechanical Hamiltonians. The variation of the qubit frequency in a Jaynes-Cummings system can be harnessed to create fast two-qubit gates for quantum information processing. On the other hand, modulations of the cavity frequency cause additional splitting of the vacuum Rabi doublet. In optomechanical systems, the modulations of the mechanical frequency show enhancement of several quantum effects, such as entanglement between the mechanical and radiation degrees of freedom, squeezing, cooling, and quantum discord. Modulations in the cavity frequency are promising for the creation of strong coupling effects in the weak coupling regime.

Finally, we considered the effect of frequency modulation in a variety of many-body systems, from atomic gases to simulators of topological phase transitions in coupled qubits. We showed how the phenomenon of motional averaging and narrowing led to the realization of quantum memories in hot atomic gases. With superconducting qubits, by manipulating adiabatically the drive strength and the detuning it was possible to emulate the Haldane model, which displays topological transitions. The same was achieved in ultracold gases, via a rather complex modulation of the trapping potential. In more simpler situations, when the lattice modulation is sinusoidal, the result is that the tunneling is modified in the same way as the coupling for the qubit case: it becomes multiplied by a Bessel function. This leads to the phenomenon of dynamical localization and the subsequent transition from the superfluid to Mott insulator state.

Given the progress in the recent years, we can confidently predict that we will see more and more experiments where the modulation of frequency is used in clever ways. For almost any task in quantum information processing, this remains an invaluable tool.

The topic of artificial gauge fields created by various forms of modulation will no doubt sustain the interest of the condensed-matter community. With better and better control of the experimental systems, we will probably see more and more of what we can call "Floquet materials" - quantum system where the band structure is built by time-domain modulation rather than spatial periodicity.

Acknowledgments

M.P.S. acknowledges funding from the Finnish Academy of Science and Letters (Vilho, Yrjö and Kalle Väisälä Foundation), the National Graduate School of Materials Physics, Army Research Office W911NF-14-1-0011 and NSF DMR-1301798. E.V.T. acknowledges funding from the Academy of Finland and Tauno Tönning foundation. G.S.P. acknowledges support from the Academy of Finland (project 263457 and Center of Excellence in Low Temperature Quantum Phenomena and Devices - project 250280), and FQXi.

References

[1] L. Landau. Zur theorie der energieubertragung. ii. Physikalische Zeitschrift der Sowjetunion, 2:26–51, 1932.

[2] Lev Landau. Zur theorie der energieübertragung bei stössen, i. Phys. Z. Sowjetunion, 1:88, 1932.

[3] C. Zener. Non-adiabatic crossing of energy levels. Proceedings of the Royal Society of London A: Mathematical, Physical and Engineering Sciences, 137(833):696–702, 1932.

[4] E. C. G. Stückelberg. Theorie der unelastischen stösse zwischen atomen. Helv. Phys. Acta, 5:369–422, 1932.

[5] E. Majorana. Atomi orientati in campo magnetico variabile. Il Nuovo Cimento, 9(2):43–50, 1932.

[6] Evgenii E Nikitin and M Ya Ovchinnikova. Interference phenomena in atomic scattering. Soviet Physics Uspekhi, 14(4):394, 1972.

[7] I. I. Rabi, S. Millman, P. Kusch, and J. R. Zacharias. The molecular beam resonance method for measuring nuclear magnetic moments. the magnetic moments of $_3Li^6$, $_3Li^7$ and $_9F^{19}$. Phys. Rev., 55:526–535, Mar 1939.

[8] I. I. Rabi. Space quantization in a gyrating magnetic field. Phys. Rev., 51:652–654, Apr 1937.

[9] F. Bloch and I. I. Rabi. Atoms in variable magnetic fields. Rev. Mod. Phys., 17:237–244, Apr 1945.

[10] F. Bloch. Nuclear induction. Phys. Rev., 70:460–474, Oct 1946.

[11] M. C. Baruch and T. F. Gallagher. Ramsey interference fringes in single pulse microwave multiphoton transitions. Phys. Rev. Lett., 68:3515–3518, Jun 1992.

[12] S.N. Shevchenko, S. Ashhab, and Franco Nori. Landauzenerstckelberg interferometry. Physics Reports, 492(1):1 – 30, 2010.

[13] A. J. Leggett, S. Chakravarty, A. T. Dorsey, Matthew P. A. Fisher, Anupam Garg, and W. Zwerger. Dynamics of the dissipative two-state system. Rev. Mod. Phys., 59:1–85, Jan 1987.

[14] Milena Grifoni and Peter Hänggi. Driven quantum tunneling. Physics Reports, 304(56):229 – 354, 1998.

[15] S. Ashhab, J. R. Johansson, A. M. Zagoskin, and Franco Nori. Two-level systems driven by large-amplitude fields. Phys. Rev. A, 75:063414, Jun 2007.

[16] Jingwei Zhou, Pu Huang, Qi Zhang, Zixiang Wang, Tian Tan, Xiangkun Xu, Fazhan Shi, Xing Rong, S. Ashhab, and Jiangfeng Du. Observation of time-domain rabi oscillations in the landau-zener regime with a single electronic spin. Phys. Rev. Lett., 112:010503, Jan 2014.

[17] K. Mullen, E. Ben-Jacob, Y. Gefen, and Z. Schuss. Time of zener tunneling. Phys. Rev. Lett., 62:2543–2546, May 1989.

[18] N. V. Vitanov and B. M. Garraway. Landau-zener model: Effects of finite coupling duration. Phys. Rev. A, 53:4288–4304, Jun 1996.

[19] B. M. Garraway and N. V. Vitanov. Population dynamics and phase effects in periodic level crossings. Phys. Rev. A, 55:4418–4432, Jun 1997.

[20] M. P. Silveri, K. S. Kumar, J. Tuorila, J. Li, A. Vepsäläinen, E. V. Thuneberg, and G. S. Paraoanu. Stückelberg interference in a superconducting qubit under periodic latching modulation. New J. Phys., 17:043058, 2015.

[21] L. I. Schiff. Quantum Mechanics. McGraw-Hill, Inc., 3rd edition, 1955.

[22] M. V. Berry. Quantal phase factors accompanying adiabatic changes. Proceedings of the Royal Society of London A: Mathematical, Physical and Engineering Sciences, 392(1802):45–57, 1984.

[23] J. J. Sakurai. Modern Quantum Mechanics. Addison-Wesley, Massachusetts, 1994.

[24] A. A. Clerk, M. H. Devoret, S. M. Girvin, Florian Marquardt, and R. J. Schoelkopf. Introduction to quantum noise, measurement, and amplification. Rev. Mod. Phys., 82:1155–1208, Apr 2010.

[25] D. F. Walls and G. J. Milburn. Quantum Optics. Springer, 2008.

[26] A. Abragam. Principles of Nuclear Magnetism. Oxford University Press, 1986.

[27] L. Allen and J. H. Eberly. Optical resonance and two-level atoms. Addison-Wesley, Massachusetts, 1987.

[28] J. Li, M. P. Silveri, K. S. Kumar, J.-M. Pirkkalainen, A. Vepsäläinen, W. C. Chien, J. Tuorila, M. A. Sillanpää, P. J. Hakonen, E. V. Thuneberg, and G. S. Paraoanu. Motional averaging in a superconducting qubit. Nat. Commun., 4:1420, 2013.

[29] Michael W. Noel, W. M. Griffith, and T. F. Gallagher. Frequency-modulated excitation of a two-level atom. Phys. Rev. A, 58:2265–2273, Sep 1998.

[30] F. Grossmann, T. Dittrich, P. Jung, and P. Hänggi. Coherent destruction of tunneling. Phys. Rev. Lett., 67:516–519, Jul 1991.

[31] M. Metcalfe, S. M. Carr, A. Muller, G. S. Solomon, and J. Lawall. Resolved sideband emission of InAs/GaAs quantum dots strained by surface acoustic waves. Phys. Rev. Lett., 105:037401, Jul 2010.

[32] Lilian Childress and Jean McIntyre. Multifrequency spin resonance in diamond. Phys. Rev. A, 82:033839, Sep 2010.

[33] William D. Oliver, Yang Yu, Janice C. Lee, Karl K. Berggren, Leonid S. Levitov, and Terry P. Orlando. Mach-zehnder interferometry in a strongly driven superconducting qubit. Science, 310(5754):1653–1657, 2005.

[34] Mika Sillanpää, Teijo Lehtinen, Antti Paila, Yuriy Makhlin, and Pertti Hakonen. Continuous-time monitoring of landau-zener interference in a cooper-pair box. Phys. Rev. Lett., 96:187002, May 2006.

[35] C. M. Wilson, T. Duty, F. Persson, M. Sandberg, G. Johansson, and P. Delsing. Coherence times of dressed states of a superconducting qubit under extreme driving. Phys. Rev. Lett., 98:257003, Jun 2007.

[36] A.P. Saiko, G.G. Fedoruk, and S.A. Markevich. Effective field and the bloch-siegert shift at bichromatic excitation of multiphoton epr. JETP Letters, 84(3):130–135, 2006.

[37] Yosuke Kayanuma. Role of phase coherence in the transition dynamics of a periodically driven two-level system. Phys. Rev. A, 50:843–845, Jul 1994.

[38] F. Bloch and A. Siegert. Magnetic resonance for nonrotating fields. Phys. Rev., 57:522–527, Mar 1940.

[39] Jani Tuorila, Matti Silveri, Mika Sillanpää, Erkki Thuneberg, Yuriy Makhlin, and Pertti Hakonen. Stark effect and generalized bloch-siegert shift in a strongly driven two-level system. Phys. Rev. Lett., 105:257003, Dec 2010.

[40] Ralf Blattmann, Peter Hänggi, and Sigmund Kohler. Qubit interference at avoided crossings: The role of driving shape and bath coupling. Phys. Rev. A, 91:042109, Apr 2015.

[41] F. Forster, M. Mhlbacher, R. Blattmann, D. Schuh, W. Wegscheider, S. Ludwig, and Kohler S. Landau-zener interference at bichromatic driving.

[42] Simon Gustavsson, Jonas Bylander, and William D. Oliver. Time-reversal symmetry and universal conductance fluctuations in a driven two-level system. Phys. Rev. Lett., 110:016603, Jan 2013.

[43] Félix Beaudoin, Marcus P. da Silva, Zachary Dutton, and Alexandre Blais. First-order sidebands in circuit qed using qubit frequency modulation. Phys. Rev. A, 86:022305, Aug 2012.

[44] J. D. Strand, Matthew Ware, Félix Beaudoin, T. A. Ohki, B. R. Johnson, Alexandre Blais, and B. L. T. Plourde. First-order sideband transitions with flux-driven asymmetric transmon qubits. Phys. Rev. B, 87:220505, Jun 2013.

[45] Jon H. Shirley. Solution of the schrödinger equation with a hamiltonian periodic in time. Phys. Rev., 138:B979–B987, May 1965.

[46] Ya. B. Zeldovich. The quasienergy of a quantum-mechanical system subjected to a periodic action. Sov. Phys. JETP, 24:1006, 1967.

[47] Shih-I Chu and Dmitry A. Telnov. Beyond the floquet theorem: generalized floquet formalisms and quasienergy methods for atomic and molecular multiphoton processes in intense laser fields. Physics Reports, 390(12):1 – 131, 2004.

[48] Johannes Hausinger and Milena Grifoni. Dissipative two-level system under strong ac driving: A combination of floquet and van vleck perturbation theory. Phys. Rev. A, 81:022117, Feb 2010.

[49] Hideo Sambe. Steady states and quasienergies of a quantum-mechanical system in an oscillating field. Phys. Rev. A, 7:2203–2213, Jun 1973.

[50] Phillip R. Certain and Joseph O. Hirschfelder. New partitioning perturbation theory. i. general formalism. The Journal of Chemical Physics, 52(12):5977–5987, 1970.

[51] P. K. Aravind and J. O. Hirschfelder. Two-state systems in semiclassical and quantized fields. The Journal of Physical Chemistry, 88(21):4788–4801, 1984.

[52] Sang-Kil Son, Siyuan Han, and Shih-I Chu. Floquet formulation for the investigation of multiphoton quantum interference in a superconducting qubit driven by a strong ac field. Phys. Rev. A, 79:032301, Mar 2009.

[53] Tak-San Ho and Shih-I Chu. Semiclassical many-mode floquet theory. iv. coherent population trapping and su(3) dynamical evolution of dissipative three-level systems in intense bichromatic fields. Phys. Rev. A, 32:377–395, Jul 1985.

[54] Matti Silveri, Jani Tuorila, Mika Kemppainen, and Erkki Thuneberg. Probe spectroscopy of quasienergy states. Phys. Rev. B, 87:134505, Apr 2013.

[55] R. Blümel, R. Graham, L. Sirko, U. Smilansky, H. Walther, and K. Yamada. Microwave excitation of rydberg atoms in the presence of noise. Phys. Rev. Lett., 62:341–344, Jan 1989.

[56] R. Blümel, A. Buchleitner, R. Graham, L. Sirko, U. Smilansky, and H. Walther. Dynamical localization in the microwave interaction of rydberg atoms: The influence of noise. Phys. Rev. A, 44:4521–4540, Oct 1991.

[57] C. M. Wilson, G. Johansson, T. Duty, F. Persson, M. Sandberg, and P. Delsing. Dressed relaxation and dephasing in a strongly driven two-level system. Phys. Rev. B, 81:024520, Jan 2010.

[58] H.-P. Breuer and F. Petruccione. The Theory of Open Quantum Systems. Oxford University Press, 2006.

[59] M. C. Goorden, M. Thorwart, and M. Grifoni. Entanglement spectroscopy of a driven solid-state qubit and its detector. Phys. Rev. Lett., 93:267005, Dec 2004.

[60] Daniel W. Hone, Roland Ketzmerick, and Walter Kohn. Statistical mechanics of floquet systems: The pervasive problem of near degeneracies. Phys. Rev. E, 79:051129, May 2009.

[61] S. Gasparinetti, P. Solinas, S. Pugnetti, R. Fazio, and J. P. Pekola. Environment-governed dynamics in driven quantum systems. Phys. Rev. Lett., 110:150403, Apr 2013.

[62] S. Yoakum, L. Sirko, and P. M. Koch. Stueckelberg oscillations in the multiphoton excitation of helium rydberg atoms: Observation with a pulse of coherent field and suppression by additive noise. Phys. Rev. Lett., 69:1919–1922, Sep 1992.

[63] David Gunnarsson, Jani Tuorila, Antti Paila, Jayanta Sarkar, Erkki Thuneberg, Yuriy Makhlin, and

Pertti Hakonen. Vibronic spectroscopy of an artificial molecule. Phys. Rev. Lett., 101:256806, Dec 2008.

[64] A. Izmalkov, S. H. W. van der Ploeg, S. N. Shevchenko, M. Grajcar, E. Il'ichev, U. Hübner, A. N. Omelyanchouk, and H.-G. Meyer. Consistency of ground state and spectroscopic measurements on flux qubits. Phys. Rev. Lett., 101:017003, Jul 2008.

[65] S. N. Shevchenko, S. H. W. van der Ploeg, M. Grajcar, E. Il'ichev, A. N. Omelyanchouk, and H.-G. Meyer. Resonant excitations of single and two-qubit systems coupled to a tank circuit. Phys. Rev. B, 78:174527, Nov 2008.

[66] Matti Silveri, Jani Tuorila, Mika Sillanpää, Erkki Thuneberg, Yuriy Makhlin, and Pertti Hakonen. Basis dependence of approximative energy levels in a strongly driven two-level system. Journal of Physics: Conference Series, 400(4):042054, 2012.

[67] D. Fregenal, E. Horsdal-Pedersen, L. B. Madsen, M. Førre, J. P. Hansen, and V. N. Ostrovsky. Multiphoton intrashell resonances in rydberg atoms: Bloch-siegert shifts and widths. Phys. Rev. A, 69:031401, Mar 2004.

[68] C Cohen-Tannoudji, J Dupont-Roc, and C Fabre. An experimental check of higher order terms in the radiative shift of a coherence resonance. Journal of Physics B: Atomic and Molecular Physics, 6(8):L218, 1973.

[69] P. Forn-Díaz, J. Lisenfeld, D. Marcos, J. J. García-Ripoll, E. Solano, C. J. P. M. Harmans, and J. E. Mooij. Observation of the bloch-siegert shift in a qubit-oscillator system in the ultrastrong coupling regime. Phys. Rev. Lett., 105:237001, Nov 2010.

[70] M. S. Child. Curve-crossing and the WKB approximation. Molecular Physics, 20:171–184, 1971.

[71] Y. Kayanuma. Stokes phase and geometrical phase in a driven two-level system. Phys. Rev. A, 55:R2495–R2498, Apr 1997.

[72] M. Wubs, K. Saito, S. Kohler, Y. Kayanuma, and P. Hänggi. Landau-zener transitions in qubits controlled by electromagnetic fields. New J. Phys., 7:218, 2005.

[73] Y. Ji, Y. Chung, D. Sprinzak, M. Heiblum, D. Mahalu, and H. Shtrikman. An electronic mach-zehnder interferometer. Nature, 422:415, 2003.

[74] L. Pezzé, A. Smerzi, G. Khoury, J. F. Hodelin, and D. Bouwmeester. Phase detection at the quantum limit with multiphoton mach-zehnder interferometry. Phys. Rev. Lett., 99:223602, Nov 2007.

[75] Jani Tuorila, Matti Silveri, Mika Sillanpää, Erkki Thuneberg, Yuriy Makhlin, and Pertti Hakonen. Charge qubit driven via the josephson nonlinearity. Superconductor Science and Technology, 26(12):124001, 2013.

[76] J. Tuorila. Spectroscopy of Artificial Atoms and Molecules. PhD thesis, University of Oulu, 2010.

[77] J. N. L. Connor. On the analytical description of resonance tunnelling reactions. Molecular Physics, 15:37–46, 1968.

[78] A. Messiah. Quantum Mechanics. John Wiley&Sons,, New York, 1961.

[79] S. Brundobler and V. Elser. S-matrix for generalized landau-zener problem. J. Phys. A, 26:1211, 1993.

[80] A. V. Shytov. Landau-zener transitions in a multilevel system: An exact result. Phys. Rev. A, 70:052708, Nov 2004.

[81] Yu Chen, P. Roushan, D. Sank, C. Neill, Erik Lucero, Matteo Mariantoni, R. Barends, B. Chiaro, J. Kelly, A. Megrant, J. Y. Mutus, P. J. J. O'Malley, A. Vainsencher, J. Wenner, T. C. White, Yi Yin, A. N. Cleland, and John M. Martinis. Emulating weak localization using a solid-state quantum circuit. Nat. Commun., 5, 2014.

[82] Jonas Bylander, Mark S. Rudner, Andrey V. Shytov, Sergio O. Valenzuela, David M. Berns, Karl K. Berggren, Leonid S. Levitov, and William D. Oliver. Pulse imaging and nonadiabatic control of solid-state artificial atoms. Phys. Rev. B, 80:220506, Dec 2009.

[83] Simon Gustavsson, Jonas Bylander, and William D. Oliver. Time-reversal symmetry and universal conductance fluctuations in a driven two-level system. Phys. Rev. Lett., 110:016603, Jan 2013.

[84] P. J. Leek, J. M. Fink, A. Blais, R. Bianchetti, M. Gppl, J. M. Gambetta, D. I. Schuster, L. Frunzio,

R. J. Schoelkopf, and A. Wallraff. Observation of berry's phase in a solid-state qubit. Science, 318(5858):1889–1892, 2007.

[85] Herbert B. Callen and Theodore A. Welton. Irreversibility and generalized noise. Phys. Rev., 83:34–40, Jul 1951.

[86] M. Schlossauer. The quantum-to-classical transition and decoherence. arXiv:1404.2635v1, 2014.

[87] J. I. Cirac and P. Zoller. Quantum computations with cold trapped ions. Phys. Rev. Lett., 74:4091–4094, May 1995.

[88] O.-P. Saira, V. Bergholm, T. Ojanen, and M. Möttönen. Equivalent qubit dynamics under classical and quantum noise. Phys. Rev. A, 75:012308, Jan 2007.

[89] S. Schneider and G. J. Milburn. Decoherence in ion traps due to laser intensity and phase fluctuations. Phys. Rev. A, 57:3748–3752, May 1998.

[90] C. J. Myatt, B. E. King, Q. A. Turchette, C. A. Sackett, D. Kielpinski, W. M. Itano, C. Monroe, and D. J. Wineland. Decoherence of quantum superpositions through coupling to engineered reservoirs. Nature, 403:269, 2000.

[91] Yuriy Makhlin, Gerd Schön, and Alexander Shnirman. Quantum-state engineering with josephson-junction devices. Rev. Mod. Phys., 73:357–400, May 2001.

[92] Yuriy Makhlin and Alexander Shnirman. Dephasing of solid-state qubits at optimal points. Phys. Rev. Lett., 92:178301, Apr 2004.

[93] G. Ithier, E. Collin, P. Joyez, P. J. Meeson, D. Vion, D. Esteve, F. Chiarello, A. Shnirman, Y. Makhlin, J. Schriefl, and G. Schön. Decoherence in a superconducting quantum bit circuit. Phys. Rev. B, 72:134519, Oct 2005.

[94] P. W. Anderson. A mathematical model for the narrowing of spectral lines by exchange or motion. Journal of the Physical Society of Japan, 9(3):316–339, 1954.

[95] L. Jiang, M. V. Gurudev Dutt, E. Togan, L. Childress, P. Cappellaro, J. M. Taylor, and M. D. Lukin. Coherence of an optically illuminated single nuclear spin qubit. Phys. Rev. Lett., 100:073001, Feb 2008.

[96] T. Kohmoto, Y. Fukuda, M. Kunitomo, K. Ishikawa, M. Tanigawa, K. Ebina, and M. Kaburagi. Hole burning in well-defined noise fields: Motional narrowing. Phys. Rev. B, 49:15352–15355, Jun 1994.

[97] A. Berthelot, I. Favero, G. Cassabois, C. Voisin, C. Delalande, Ph. Roussignol, R. Ferreira, and J. M. Gerard. Unconventional motional narrowing in the optical spectrum of a semiconductor quantum dot. Nat. Phys., 2:759–764, 2006.

[98] Yoav Sagi, Rami Pugatch, Ido Almog, and Nir Davidson. Spectrum of two-level systems with discrete frequency fluctuations. Phys. Rev. Lett., 104:253003, Jun 2010.

[99] E. L. Hahn. Spin echoes. Phys. Rev., 80:580–594, Nov 1950.

[100] Lorenza Viola and Seth Lloyd. Dynamical suppression of decoherence in two-state quantum systems. Phys. Rev. A, 58:2733–2744, Oct 1998.

[101] Lorenza Viola, Emanuel Knill, and Seth Lloyd. Dynamical decoupling of open quantum systems. Phys. Rev. Lett., 82:2417–2421, Mar 1999.

[102] Peter W. Shor. Scheme for reducing decoherence in quantum computer memory. Phys. Rev. A, 52:R2493–R2496, Oct 1995.

[103] Artur Ekert and Chiara Macchiavello. Quantum error correction for communication. Phys. Rev. Lett., 77:2585–2588, Sep 1996.

[104] D.V. Averin, K. Xu, Y. P. Zhong, C. Song, H. Wang, and Siyuan Han. Suppression of dephasing by qubit motion in superconducting circuits. arXiv:1509.00122, 2015.

[105] R. Kubo. Generalized cumulant expansion method. J. Phys. Soc. Japan, 17:1100, 1962.

[106] N. G. van Kampen. Stochastic Processes in Physics and Chemistry. North-Holland Personal Library. North Holland, 2007.

[107] Janez Stepinik. Validity limits of gaussian approximation in cumulant expansion for diffusion attenuation of spin echo. Physica B: Condensed Matter, 270(12):110 – 117, 1999.

[108] M. Nakahara, S. Kanemitsu, M. M. Salomaa, and S. (eds.) Takagi. Physical Realizations of

quantum computing. World Scientific Publishing C0. Pte. Ltd., 2006.
[109] U. Weiss. Quantum dissipative systems. World Scientific Publishing C0. Pte. Ltd., 1999.
[110] N V Prokof'ev and P C E Stamp. Theory of the spin bath. Reports on Progress in Physics, 63(4):669, 2000.
[111] C. Gardiner and P. Zoller. Quantum Noise. Springer-Verlag, 2004.
[112] E. Paladino, L. Faoro, G. Falci, and Rosario Fazio. Decoherence and $1/f$ noise in josephson qubits. Phys. Rev. Lett., 88:228304, May 2002.
[113] Alexander Shnirman, Gerd Schön, Ivar Martin, and Yuriy Makhlin. Low- and high-frequency noise from coherent two-level systems. Phys. Rev. Lett., 94:127002, Apr 2005.
[114] Félix Beaudoin and W. A. Coish. Microscopic models for charge-noise-induced dephasing of solid-state qubits. Phys. Rev. B, 91:165432, Apr 2015.
[115] Sebastian Zanker and Michael Marthaler. Qubit dephasing due to quasiparticle tunneling. Phys. Rev. B, 91:174504, May 2015.
[116] K. Rabenstein, V.A. Sverdlov, and D.V. Averin. Qubit decoherence by gaussian low-frequency noise. JETP Letters, 79(12):646–649, 2004.
[117] Y. Nakamura, Yu. A. Pashkin, T. Yamamoto, and J. S. Tsai. Charge echo in a cooper-pair box. Phys. Rev. Lett., 88:047901, Jan 2002.
[118] F. Yoshihara, K. Harrabi, A. O. Niskanen, Y. Nakamura, and J. S. Tsai. Decoherence of flux qubits due to $1/f$ flux noise. Phys. Rev. Lett., 97:167001, Oct 2006.
[119] J Bergli, Y M Galperin, and B L Altshuler. Decoherence in qubits due to low-frequency noise. New Journal of Physics, 11(2):025002, 2009.
[120] Hanno Gassmann, Florian Marquardt, and C. Bruder. Non-markoffian effects of a simple nonlinear bath. Phys. Rev. E, 66:041111, Oct 2002.
[121] M. I. D'yakonov and V. I. Perel'. Spin relaxation of conduction electrons in noncentrosymmetric semiconductors. Sov. Phys. Solid State, 13:3023–3026, 1972.
[122] R. H. Dicke. The effect of collisions upon the doppler width of spectral lines. Phys. Rev., 89:472–473, Jan 1953.
[123] G. J. Milburn. Quantum zeno effect and motional narrowing in a two-level system. J. Opt. Soc. Am. B, 5(6):1317–1322, Jun 1988.
[124] K. Wódkiewicz, B. W. Shore, and J. H. Eberly. Noise in strong laser-atom interactions: Frequency fluctuations and nonexponential correlations. Phys. Rev. A, 30:2390–2398, Nov 1984.
[125] G. E. Uhlenbeck and L. S. Ornstein. On the theory of the brownian motion. Phys. Rev., 36:823–841, Sep 1930.
[126] Yoav Sagi, Rami Pugatch, Ido Almog, Nir Davidson, and Michael Aizenman. Motional broadening in ensembles with heavy-tail frequency distribution. Phys. Rev. A, 83:043821, Apr 2011.
[127] M. I. Dykman, M. Khasin, J. Portman, and S. W. Shaw. Spectrum of an oscillator with jumping frequency and the interference of partial susceptibilities. Phys. Rev. Lett., 105:230601, Dec 2010.
[128] M. Silveri. Nonlinear stochastic driving of a superconducting qubit. PhD thesis, University of Oulu, 2013.
[129] K. Jensen, Kwanpyo Kim, and A. Zettl. An atomic-resolution nanomechanical mass sensor. Nature Nanotech., 3:533–537, 2008.
[130] Thomas P. Burg, Michel Godin, Scott M. Knudsen, Wenjiang Shen, Greg Carlson, John S. Foster, Ken Babcock, and Scott R. Manalis. Weighing of biomolecules, single cells and single nanoparticles in fluid. Nature, 446(7139):1066–1069, April 2007.
[131] A. K. Naik, M. S. Hanay, W. K. Hiebert, X. L. Feng, and M. L. Roukes. Towards single-molecule nanomechanical mass spectrometry. Nature Nanotechnology, 4(7):445–450, July 2009.
[132] M. S. Hanay, S. Kelber, A. K. Naik, D. Chi, S. Hentz, E. C. Bullard, E. Colinet, L. Duraffourg, and M. L. Roukes. Single-protein nanomechanical mass spectrometry in real time. Nature Nanotechnology, 7(9):602–608, September 2012.
[133] D. Rugar, R. Budakian, H. J. Mamin, and B. W. Chui. Single spin detection by magnetic

resonance force microscopy. Nature, 430(6997):329–332, July 2004.

[134] H. J. Mamin, M. Poggio, C. L. Degen, and D. Rugar. Nuclear magnetic resonance imaging with 90-nm resolution. Nature Nanotechnology, 2(5):301–306, May 2007.

[135] R. Graham. Squeezing and Frequency Changes in Harmonic Oscillations. Journal of Modern Optics, 34(6-7):873–879, June 1987.

[136] T. Kiss, J. Janszky, and P. Adam. Time evolution of harmonic oscillators with time-dependent parameters: A step-function approximation. Physical Review A, 49(6):4935–4942, June 1994.

[137] M. Sebawe Abdalla and R. K. Colegrave. Squeezing induced in a harmonic oscillator by a sudden change in mass or frequency. Physical Review A, 48(2):1526–1531, August 1993.

[138] A. M. Zagoskin, E. Il'ichev, and Franco Nori. Heat cost of parametric generation of microwave squeezed states. Physical Review A, 85(6):063811, June 2012.

[139] J. Janszky and P. Adam. Strong squeezing by repeated frequency jumps. Physical Review A, 46(9):6091–6092, November 1992.

[140] I. Averbukh, B. Sherman, and G. Kurizki. Enhanced squeezing by periodic frequency modulation under parametric instability conditions. Physical Review A, 50(6):5301–5308, December 1994.

[141] A. M. Zagoskin, E. Ilichev, M. W. McCutcheon, Jeff F. Young, and Franco Nori. Controlled Generation of Squeezed States of Microwave Radiation in a Superconducting Resonant Circuit. Physical Review Letters, 101(25):253602, December 2008.

[142] P. D. Nation, J. R. Johansson, M. P. Blencowe, and Franco Nori. *Colloquium* : Stimulating uncertainty: Amplifying the quantum vacuum with superconducting circuits. Rev. Mod. Phys., 84:1–24, Jan 2012.

[143] C. M. Wilson, G. Johansson, A. Pourkabirian, M. Simoen, J. R. Johansson, T. Duty, F. Nori, and P. Delsing. Observation of the dynamical Casimir effect in a superconducting circuit. Nature, 479(7373):376–379, November 2011.

[144] P. Lahteenmaki, G. S. Paraoanu, J. Hassel, and P. J. Hakonen. Dynamical Casimir effect in a Josephson metamaterial. Proceedings of the National Academy of Sciences, 110(11):4234–4238, March 2013.

[145] Pasi Lhteenmki, Visa Vesterinen, Juha Hassel, G.S. Paraoanu, Heikki Sepp, and Pertti Hakonen. Advanced concepts in josephson junction reflection amplifiers. Journal of Low Temperature Physics, 175(5-6):868–876, 2014.

[146] N. Bergeal, F. Schackert, M. Metcalfe, R. Vijay, V. E. Manucharyan, L. Frunzio, D. E. Prober, R. J. Schoelkopf, S. M. Girvin, and M. H. Devoret. Phase-preserving amplification near the quantum limit with a josephson ring modulator. Nature, 465, 2010.

[147] N. Roch, E. Flurin, F. Nguyen, P. Morfin, P. Campagne-Ibarcq, M. H. Devoret, and B. Huard. Widely tunable, nondegenerate three-wave mixing microwave device operating near the quantum limit. Phys. Rev. Lett., 108:147701, Apr 2012.

[148] M. A. Castellanos-Beltran and K. W. Lehnert. Widely tunable parametric amplifier based on a superconducting quantum interference device array resonator. Applied Physics Letters, 91(8), 2007.

[149] M. A. Castellanos-Beltran, K. D. Irwin, G. C. Hilton, L. R. Vale, and K. W. Lehnert. Amplification and squeezing of quantum noise with a tunable josephson metamaterial. Nat. Phys., 4:929 – 931, 2008.

[150] Kevin O'Brien, Chris Macklin, Irfan Siddiqi, and Xiang Zhang. Resonant phase matching of josephson junction traveling wave parametric amplifiers. Phys. Rev. Lett., 113:157001, Oct 2014.

[151] P. W. Anderson and P. R. Weiss. Exchange Narrowing in Paramagnetic Resonance. Reviews of Modern Physics, 25(1):269–276, January 1953.

[152] Jiansong Gao, Jonas Zmuidzinas, Benjamin A. Mazin, Henry G. LeDuc, and Peter K. Day. Noise properties of superconducting coplanar waveguide microwave resonators. Applied Physics Letters, 90(10):102507, March 2007.

[153] M. I. Dykman, M. Khasin, J. Portman, and S. W. Shaw. Spectrum of an Oscillator with

Jumping Frequency and the Interference of Partial Susceptibilities. Physical Review Letters, 105(23):230601, December 2010.

[154] J. Atalaya, A. Isacsson, and M. I. Dykman. Diffusion-induced dephasing in nanomechanical resonators. Physical Review B, 83(4):045419, January 2011.

[155] M. D. LaHaye, J. Suh, P. M. Echternach, K. C. Schwab, and M. L. Roukes. Nanomechanical measurements of a superconducting qubit. Nature, 459(7249):960–964, June 2009.

[156] Matthew Reagor, Wolfgang Pfaff, Christopher Axline, Reinier W. Heeres, Nissim Ofek, Katrina Sliwa, Eric Holland, Chen Wang, Jacob Blumoff, Kevin Chou, Michael J. Hatridge, Luigi Frunzio, Michel H. Devoret, Liang Jiang, and Robert J. Schoelkopf. A quantum memory with near-millisecond coherence in circuit QED. arXiv:1508.05882, August 2015.

[157] Herbert Walther, Benjamin T H Varcoe, Berthold-Georg Englert, and Thomas Becker. Cavity quantum electrodynamics. Reports on Progress in Physics, 69(5):1325, 2006.

[158] R. J. Schoelkopf and S. M. Girvin. Wiring up quantum systems. Nature, 451:664, 2008.

[159] T. Niemczyk, F. Deppe, H. Huebl, E. P. Menzel, F. Hocke, M. J. Schwarz, J. J. Garcia-Ripoll, D. Zueco, T. Hümmer, E. Solano, A. Marx, and R. Gross. Circuit quantum electrodynamics in the ultrastrong-coupling regime. Nat. Phys., 6:772, 2010.

[160] D. Ballester, G. Romero, J. J. García-Ripoll, F. Deppe, and E. Solano. Quantum simulation of the ultrastrong-coupling dynamics in circuit quantum electrodynamics. Phys. Rev. X, 2:021007, May 2012.

[161] C. Cohen-Tannoudji, J. Dupont-Roc, and G. Grynberg. Atom-Photon Interactions: Basic Processes and Applications. Wiley-VCH, 2004.

[162] B. R. Mollow. Power spectrum of light scattered by two-level systems. Phys. Rev., 188:1969–1975, Dec 1969.

[163] J. J. Sanchez-Mondragon, N. B. Narozhny, and J. H. Eberly. Theory of spontaneous-emission line shape in an ideal cavity. Phys. Rev. Lett., 51:550–553, Aug 1983.

[164] G. S. Agarwal. Vacuum-field rabi splittings in microwave absorption by rydberg atoms in a cavity. Phys. Rev. Lett., 53:1732–1734, Oct 1984.

[165] M. G. Raizen, R. J. Thompson, R. J. Brecha, H. J. Kimble, and H. J. Carmichael. Normal-mode splitting and linewidth averaging for two-state atoms in an optical cavity. Phys. Rev. Lett., 63:240–243, Jul 1989.

[166] Yifu Zhu, Daniel J. Gauthier, S. E. Morin, Qilin Wu, H. J. Carmichael, and T. W. Mossberg. Vacuum rabi splitting as a feature of linear-dispersion theory: Analysis and experimental observations. Phys. Rev. Lett., 64:2499–2502, May 1990.

[167] R. J. Thompson, G. Rempe, and H. J. Kimble. Observation of normal-mode splitting for an atom in an optical cavity. Phys. Rev. Lett., 68:1132–1135, Feb 1992.

[168] C. Weisbuch, M. Nishioka, A. Ishikawa, and Y. Arakawa. Observation of the coupled exciton-photon mode splitting in a semiconductor quantum microcavity. Phys. Rev. Lett., 69:3314–3317, Dec 1992.

[169] Hailin Wang, Jagdeep Shah, T. C. Damen, W. Y. Jan, J. E. Cunningham, M. Hong, and J. P. Mannaerts. Coherent oscillations in semiconductor microcavities. Phys. Rev. B, 51:14713–14716, May 1995.

[170] Stanley Pau, Gunnar Björk, Joseph Jacobson, Hui Cao, and Yoshihisa Yamamoto. Microcavity exciton-polariton splitting in the linear regime. Phys. Rev. B, 51:14437–14447, May 1995.

[171] F. Bernardot, P. Nussenzveig, M. Brune, J. M. Raimond, and S. Haroche. Vacuum rabi splitting observed on a microscopic atomic sample in a microwave cavity. EPL (Europhysics Letters), 17(1):33, 1992.

[172] M. Brune, F. Schmidt-Kaler, A. Maali, J. Dreyer, E. Hagley, J. M. Raimond, and S. Haroche. Quantum rabi oscillation: A direct test of field quantization in a cavity. Phys. Rev. Lett., 76:1800–1803, Mar 1996.

[173] A. Wallraff, D. I. Schuster, A. Blais, L. Frunzio, R.-S. Huang, J. Majer, S. Kumar, S. M. Girvin, and R. J. Schoelkopf. Strong coupling of a single photon to a superconducting qubit using

circuit quantum electrodynamics. Nature, 431:162, 2004.

[174] Lev S. Bishop, J. M. Chow, Jens Koch, A. A. Houck, M. H. Devoret, E. Thuneberg, S. M. Girvin, and R. J. Schoelkopf. Nonlinear response of the vacuum rabi resonance. Nat Phys, 5, 2009.

[175] H. J. Carmichael, P. Kochan, and B. C. Sanders. Photon correlation spectroscopy. Phys. Rev. Lett., 77:631–634, Jul 1996.

[176] J. M. Fink, M. Göppl, M. Baur, R. Bianchetti, P. J. Leek, A. Blais, and A. Wallraff. Climbing the jaynes-cummings ladder and observing its $\sqrt{n}$ nonlinearity in a cavity qed system. Nature, 454:315, 2008.

[177] J. Kasprzak, S. Reitzenstein, E. A. Muljarov, C. Kistner, C. Schneider, M. Strauss, and S. Höfling. Up on the jaynes-cummings ladder of a quantum-dot/microcavity system. Nature Materials, 9:304, 2010.

[178] R. P. Feynman. Simulating physics with computers. International Journal of Theoretical Physics, 21(6-7):467–488, 1982.

[179] David Deutsch and Richard Jozsa. Rapid solution of problems by quantum computation. Proceedings of the Royal Society of London A: Mathematical, Physical and Engineering Sciences, 439(1907):553–558, 1992.

[180] Lov K. Grover. A fast quantum mechanical algorithm for database search. In Proceedings of the Twenty-eighth Annual ACM Symposium on Theory of Computing, STOC '96, pages 212–219, New York, NY, USA, 1996. ACM.

[181] Peter W. Shor. Polynomial-time algorithms for prime factorization and discrete logarithms on a quantum computer. SIAM Journal on Computing, 26(5):1484–1509, 1997.

[182] T. D. Ladd, F. Jelezko, R. Laflamme, Y. Nakamura, C. Monroe, and J. L. O'Brien. Quantum computers. Nature, 464:45, 2010.

[183] Alexandre Blais, Jay Gambetta, A. Wallraff, D. I. Schuster, S. M. Girvin, M. H. Devoret, and R. J. Schoelkopf. Quantum-information processing with circuit quantum electrodynamics. Phys. Rev. A, 75:032329, Mar 2007.

[184] Yu-xi Liu, L. F. Wei, J. R. Johansson, J. S. Tsai, and Franco Nori. Superconducting qubits can be coupled and addressed as trapped ions. Phys. Rev. B, 76:144518, Oct 2007.

[185] P. J. Leek, S. Filipp, P. Maurer, M. Baur, R. Bianchetti, J. M. Fink, M. Göppl, L. Steffen, and A. Wallraff. Using sideband transitions for two-qubit operations in superconducting circuits. Phys. Rev. B, 79:180511, May 2009.

[186] I. Chiorescu, P. Bertet, K. Semba, Y. Nakamura, C. J. P. M. Harmans, and J. E. Mooij. Coherent dynamics of a flux qubit coupled to a harmonic oscillator. Nature, 431:159, 2004.

[187] A. Wallraff, D. I. Schuster, A. Blais, J. M. Gambetta, J. Schreier, L. Frunzio, M. H. Devoret, S. M. Girvin, and R. J. Schoelkopf. Sideband transitions and two-tone spectroscopy of a superconducting qubit strongly coupled to an on-chip cavity. Phys. Rev. Lett., 99:050501, Jul 2007.

[188] Jens Koch, Terri M. Yu, Jay Gambetta, A. A. Houck, D. I. Schuster, J. Majer, Alexandre Blais, M. H. Devoret, S. M. Girvin, and R. J. Schoelkopf. Charge-insensitive qubit design derived from the cooper pair box. Phys. Rev. A, 76:042319, Oct 2007.

[189] S. Haroche and J.-M. Raimond. Exploring the Quantum: Atoms, Cavities, and Photons. Oxford University Press, 2006.

[190] Félix Beaudoin, Jay M. Gambetta, and A. Blais. Dissipation and ultrastrong coupling in circuit qed. Phys. Rev. A, 84:043832, Oct 2011.

[191] Shuang-Yuan Xie, Fei Jia, and Ya-Ping Yang. Interactions of a two-level atom and a field with a time-varying frequency without rotating-wave approximation. Optics Communications, 273(2):451 – 459, 2007.

[192] C. K. Law, S.-Y. Zhu, and M. S. Zubairy. Modification of a vacuum rabi splitting via a frequency-modulated cavity mode. Phys. Rev. A, 52:4095–4098, Nov 1995.

[193] Yaping Yang, Jingping Xu, Gaoxiang Li, and Hong Chen. Interactions of a two-level atom and a field with a time-varying frequency. Phys. Rev. A, 69:053406, May 2004.

[194] Maciej Janowicz. Evolution of wave fields and atom-field interactions in a cavity with one oscillating mirror. Phys. Rev. A, 57:4784–4790, Jun 1998.

[195] Li Wang, Jingpin Xu, and Yunfeng Gao. Interaction of a two-level atom and a field with a time-varying frequency in a kerr-like medium. Journal of Physics B: Atomic, Molecular and Optical Physics, 43(9):095102, 2010.

[196] D. I. Schuster, A. Wallraff, A. Blais, L. Frunzio, R.-S. Huang, J. Majer, S. M. Girvin, and R. J. Schoelkopf. ac stark shift and dephasing of a superconducting qubit strongly coupled to a cavity field. Phys. Rev. Lett., 94:123602, Mar 2005.

[197] Jay Gambetta, Alexandre Blais, D. I. Schuster, A. Wallraff, L. Frunzio, J. Majer, M. H. Devoret, S. M. Girvin, and R. J. Schoelkopf. Qubit-photon interactions in a cavity: Measurement-induced dephasing and number splitting. Phys. Rev. A, 74:042318, Oct 2006.

[198] A. P. Sears, A. Petrenko, G. Catelani, L. Sun, Hanhee Paik, G. Kirchmair, L. Frunzio, L. I. Glazman, S. M. Girvin, and R. J. Schoelkopf. Photon shot noise dephasing in the strong-dispersive limit of circuit qed. Phys. Rev. B, 86:180504, Nov 2012.

[199] Markus Aspelmeyer, Tobias J. Kippenberg, and Florian Marquardt. Cavity optomechanics. Rev. Mod. Phys., 86:1391–1452, Dec 2014.

[200] Alessandro Farace and Vittorio Giovannetti. Enhancing quantum effects via periodic modulations in optomechanical systems. Phys. Rev. A, 86:013820, Jul 2012.

[201] Marc Bienert and Pablo Barberis-Blostein. Optomechanical laser cooling with mechanical modulations. Phys. Rev. A, 91:023818, Feb 2015.

[202] Jie-Qiao Liao, C. K. Law, Le-Man Kuang, and Franco Nori. Enhancement of mechanical effects of single photons in modulated two-mode optomechanics. Phys. Rev. A, 92:013822, Jul 2015.

[203] J. Borregaard, M. Zugenmaier, J. M. Petersen, H. Shen, G. Vasilakis, K. Jensen, E. S. Polzik, and A. S. Sø rensen. Room temperature quantum memory and scalable single photon source based on motional averaging. arXiv:1501.03916, 2015.

[204] G. Kurizki, P. Bertet, Y. Kubo, K. Mõlmer, D. Petrosyan, P. Rabl, and J. Schmiedmayer. Quantum technologies with hybrid systems. PNAS, 112:38663873, October 2014.

[205] G.S. Paraoanu. Realism and single-quanta nonlocality. Foundations of Physics, 41(4):734–743, 2011.

[206] M. Baur, S. Filipp, R. Bianchetti, J. M. Fink, M. Gppl, L. Steffen, P. J. Leek, A. Blais, and A. Wallraff. Measurement of autler-townes and mollow transitions in a strongly driven superconducting qubit. Phys. Rev. Lett., 102:243602, 2009.

[207] Mika A. Sillanpää, Jian Li, Katarina Cicak, Fabio Altomare, Jae I. Park, Raymond W. Simmonds, G. S. Paraoanu, and Pertti J. Hakonen. Autler-townes effect in a superconducting three-level system. Phys. Rev. Lett., 103:193601, 2009.

[208] Jian Li, G. S. Paraoanu, Katarina Cicak, Fabio Altomare, Jae I. Park, Raymond W. Simmonds, Mika A. Sillanpää, and Pertti J. Hakonen. Decoherence, autler-townes effect, and dark states in two-tone driving of a three-level superconducting system. Phys. Rev. B, 84:104527, Sep 2011.

[209] Jian Li, G. S. Paraoanu, Katarina Cicak, Fabio Altomare, Jae I. Park, Raymond W. Simmonds, Mika A. Sillanpää, and Pertti J. Hakonen. Dynamical autler-townes control of a phase qubit. Sci. Rep., 2:645, 2012.

[210] William R. Kelly, Zachary Dutton, John Schlafer, Bhaskar Mookerji, Thomas A. Ohki, Jeffrey S. Kline, and David P. Pappas. Direct observation of coherent population trapping in a superconducting artificial atom. Phys. Rev. Lett., 104:163601, 2010.

[211] A. A. Abdumalikov, O. Astafiev, A. M. Zagoskin, Yu. A. Pashkin, Y. Nakamura, and J. S. Tsai. Electromagnetically induced transparency on a single artificial atom. Phys. Rev. Lett., 104:193601, 2010.

[212] K. Bergmann, H. Theuer, and B. W. Shore. Coherent population transfer among quantum states of atoms and molecules. Review of Modern Physics, 70:1003, 1998.

[213] F. D. M. Haldane. Model for a quantum hall effect without landau levels: Condensed-matter realization of the "parity anomaly". Phys. Rev. Lett., 61:2015–2018, Oct 1988.

[214] S. S. Chern. Characteristic classes of hermitian manifolds. The Annals of Mathematics, 57:85–121, 1946.

[215] D. J. Thouless, M. Kohmoto, M. P. Nightingale, and M. den Nijs. Quantized hall conductance in a two-dimensional periodic potential. Phys. Rev. Lett., 49:405–408, Aug 1982.

[216] Mahito Kohmoto. Topological invariant and the quantization of the hall conductance. Annals of Physics, 160(2):343 – 354, 1985.

[217] P. Roushan, C. Neill, Yu Chen, M. Kolodrubetz, C. Quintana, N. Leung, M. Fang, R. Barends, B. Campbell, Z. Chen, B. Chiaro, A. Dunsworth, E. Jeffrey, J. Kelly, A. Megrant, J. Mutus, P. J. J. O/'Malley, D. Sank, A. Vainsencher, J. Wenner, T. White, A. Polkovnikov, A. N. Cleland, and J. M. Martinis. Observation of topological transitions in interacting quantum circuits. Nature, 515:241–244, November 2014.

[218] M. D. Schroer, M. H. Kolodrubetz, W. F. Kindel, M. Sandberg, J. Gao, M. R. Vissers, D. P. Pappas, Anatoli Polkovnikov, and K. W. Lehnert. Measuring a topological transition in an artificial spin-1/2 system. Phys. Rev. Lett., 113:050402, Jul 2014.

[219] V. Gritzev and A. Polkovnikov. Quantized hall conductance in a two-dimensional periodic potential. PNAS, 109:6457–6462, April 2012.

[220] D. Jaksch and P. Zoller. The cold atom hubbard toolbox. Annals of Physics, 315(1):52 – 79, 2005. Special Issue.

[221] Immanuel Bloch, Jean Dalibard, and Wilhelm Zwerger. Many-body physics with ultracold gases. Rev. Mod. Phys., 80:885–964, Jul 2008.

[222] André Eckardt, Christoph Weiss, and Martin Holthaus. Superfluid-insulator transition in a periodically driven optical lattice. Phys. Rev. Lett., 95:260404, Dec 2005.

[223] H. Lignier, C. Sias, D. Ciampini, Y. Singh, A. Zenesini, O. Morsch, and E. Arimondo. Dynamical control of matter-wave tunneling in periodic potentials. Phys. Rev. Lett., 99:220403, Nov 2007.

[224] E. Kierig, U. Schnorrberger, A. Schietinger, J. Tomkovic, and M. K. Oberthaler. Single-particle tunneling in strongly driven double-well potentials. Phys. Rev. Lett., 100:190405, May 2008.

[225] Ennio Arimondo, Donatella Ciampini, André Eckardt, Martin Holthaus, and Oliver Morsch. Chapter 10 - kilohertz-driven bose-einstein condensates in optical lattices. In Ennio Arimondo Paul Berman and Chun Lin, editors, Advances in Atomic, Molecular, and Optical Physics, volume 61 of Advances In Atomic, Molecular, and Optical Physics, pages 515 – 547. Academic Press, 2012.

[226] J. Dalibard. Introduction to the physics of artificial gauge fields. arXiv:1504.05520, 2015.

[227] J. Struck, C. Ölschläger, M. Weinberg, P. Hauke, J. Simonet, A. Eckardt, M. Lewenstein, K. Sengstock, and P. Windpassinger. Tunable gauge potential for neutral and spinless particles in driven optical lattices. Phys. Rev. Lett., 108:225304, May 2012.

[228] J. Struck, M. Weinberg, C. Ölschläger, C. P. Windpassinger, J. Simonet, K. Sengstock, R. Höppner, P. Hauke, A. Eckardt, M. Lewenstein, and L. Mathey. Engineering ising-xy spin-models in a triangular lattice using tunable artificial gauge fields. Nat. Phys., 9:738, 2013.

[229] G. Jotzu, M. Messer, R. Desbuquois, M. Lebrat, T. Uehlinger, D. Greif, and T. Esslinger. Experimental realization of the topological haldane model with ultracold fermions. Nature, 515:237, 2014.

[230] M. Aidelsburger, M. Atala, M. Lohse, J. T. Barreiro, B. Paredes, and I. Bloch. Realization of the hofstadter hamiltonian with ultracold atoms in optical lattices. Phys. Rev. Lett., 111:185301, Oct 2013.

[231] Hirokazu Miyake, Georgios A. Siviloglou, Colin J. Kennedy, William Cody Burton, and Wolfgang Ketterle. Realizing the harper hamiltonian with laser-assisted tunneling in optical lattices. Phys. Rev. Lett., 111:185302, Oct 2013.